



MSc Thesis

Stable Isotopes of Atmospheric Water Vapor in Copenhagen, Denmark

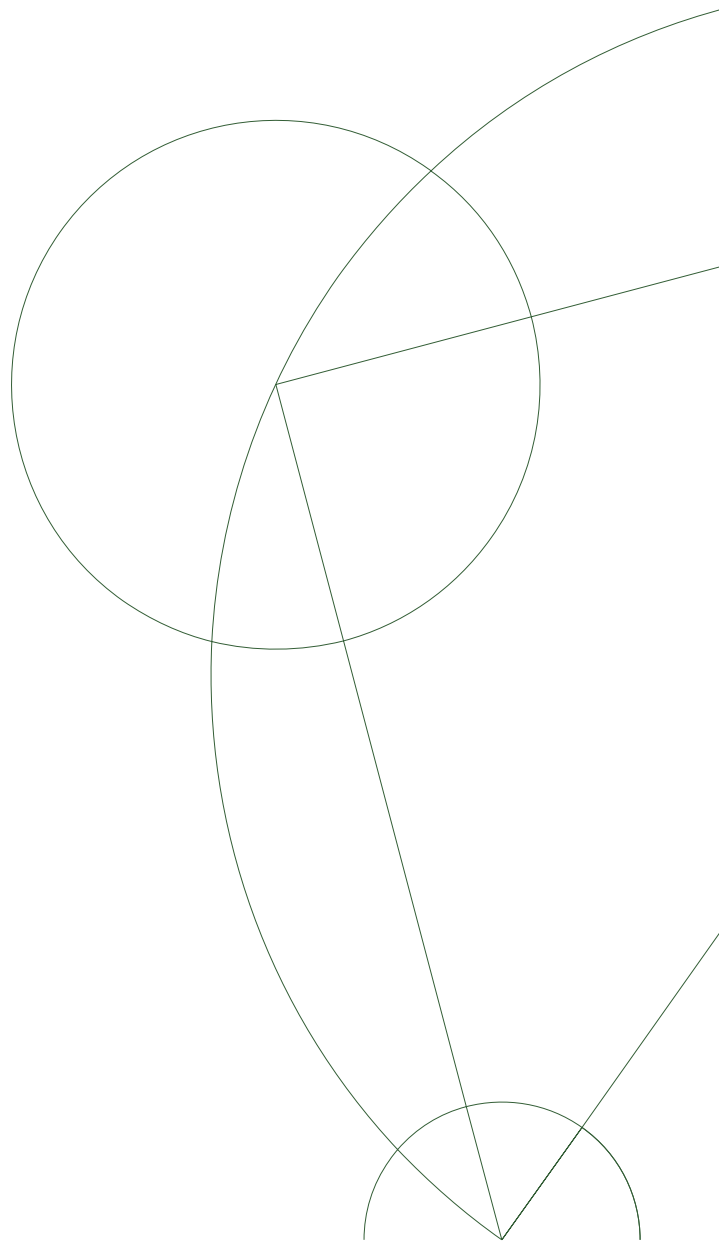
By:

Vasileios Mandrakis

Academic supervisor:
Vasileios Gkinis

Co supervisor:
Bo Møller Vinther

Submitted 17/05/2016



Abstract

This MSc project deals with the stable isotopic composition of atmospheric water vapor. It's main aim is to successfully sample and calibrate the isotopic data of vapor at the Rockefeller complex, Copenhagen. High temporal resolution of the water vapor isotopic values is obtained from a 24-hour sampling scheme using two Picarro-Cavity Ring Down Spectrometers (CRDS). A comparison between the data of the two CRDSs is taking place for a better evaluation of the data series and a more in depth understanding of how the CRDSs perform when they are used for the collection of water vapor. Sampling of meteoric water is done by using a rain collector suitable for storing rain and snow. Data from the vapor phase are combined with sampled precipitation in order to make an interpretation of the links between the isotopic composition of the vapor and the liquid/solid state of water.

Keywords: water, vapor, isotopes, meteoric water, ring down spectrometer

Acknowledgments

First of all, I would like to thank my supervisors Vasileios Gkinis and Bo Møllesøe Vinther that have always shown patience and encouraged me. Vasileios has been a true inspiration for me, always providing the right motivation to search and investigate in more depth, having criticism and never give up, even when things seem difficult and tough. Bo has helped me a lot with his feedback and he was always coming back with new and innovative ideas, helping me to develop critical thought. Their contribution at this study has been of vital importance.

I would also like to thank Trevor James Popp who has been responsible at the isotope lab of the Center for Ice and Climate, University of Copenhagen. He has always been supportive, bringing positive attitude and letting me work in a more independent and autonomous way. Being a member of Center for Ice and Climate and working at the isotope lab has been a great experience since I gained a lot of knowledge on a real research environment. Working conditions are exceptional and people involved there are experienced and motivating. Mika Lanzky is thanked for her advice regarding Matlab and Christian Terkelsen Holme for helping me with his instructive feedback for this project.

My fiends Alex, Stauros, Babis and Nikos have always been there for me, proving that having real friends is one of the greatest gifts in life.

Finally, I would like to conclude with thanking my family. It would be impossible to complete my studies without their support and encourage, despite the fact that are thousands of kilometers away. They are the ones showing me that chasing your dreams is what matter the most.

Contents

Abstract	i
Acknowledgments	ii
Contents	iii
List of figures	v
List of tables	vii
1 Introduction	1
2 Physical background of the water stable isotopes	5
2.1 Structure of the Atomic Nucleus	5
2.2 Water stable isotopes	6
2.2.1 Isotopic ratios and the δ notation	8
2.2.2 Deuterium Excess	9
2.3 Isotope fractionation	10
2.3.1 Isotope fractionation factor	10
2.3.2 Equilibrium Fractionation	11
2.3.3 Kinetic Fractionation	12
2.4 Rayleigh condensation	12
3 Experimental set-up	14
3.1 NIR Cavity Ring Down Spectroscopy	14
3.2 Experimental system set-up	17
3.3 The Rain Collector	20
3.3.1 Design, characteristics and maintenance of the rain collector .	21
3.3.1.1 Replacement of the stainless steel mesh	23
3.3.1.2 Maintenance of the rain collector	24
3.4 Fractionation Experiment	24
3.4.1 Results of the fractionation experiment	25
4 Vapor Data Calibration and Processing	30
4.1 Humidity calibration	30
4.1.1 Data acquisition	30
4.1.2 The linear section of humidity levels	35

4.1.3	Correction of the data for varying humidity levels using a linear regression	37
4.1.4	Correction of the data for varying humidity levels using a 3 rd order polynomial fit	39
4.2	Calibration with standards	45
4.2.1	Run with 3 standards: VSMOW-SLAP calibration (Odo) . . .	46
4.2.2	Run with 2 waters: VSMOW-SLAP calibration (Walter) . . .	51
4.3	Vapor data processing	55
4.4	Intercomparison between the two instruments	63
5	Results	67
5.1	Experimental Results	67
5.1.1	Meteoric water samples	67
5.1.1.1	Method for measuring the meteoric water samples . .	67
5.1.2	Results for the meteoric water samples	68
5.1.3	Vapor data	71
5.2	Correlation between the meteoric water samples and atmospheric water vapor	73
6	Discussion-Conclusions	78
6.1	Discussion	78
6.2	Investigating possible time shifts between the data series of the two spectrometers	80
6.3	Conclusions	84
6.4	Outlook	84
	Bibliography	86
	Appendices	88
A		89
A.0.1	Dates of collected meteoric water samples	89
A.0.2	Full data series acquired from Odo	90

List of Figures

1.1	Location of the Rockefeller Complex	4
2.1	The periodic table of the elements	6
2.2	$\delta^{18}\text{O}$ and δD variations in natural waters. Picture: Craig (1961)	9
2.3	Schematic of the Rayleigh condensation scheme	13
3.1	The optical cavity and cavity ring-down time	16
3.2	System set-up	17
3.3	Realistic image of our experimental set-up	19
3.4	The vapor line and the plastic bottle for sampling atmospheric water vapor	20
3.5	The rain collector	21
3.6	Dimensions and schematics of the rain collector. Picture: Groeningen et al., 2012	23
3.7	Isotopic composition of the fractionation test	29
4.1	Humidity levels of the humidity calibration	32
4.2	Raw mean isotopic values for the various humidity levels	34
4.3	Linear section of humidity calibration - $\delta^{18}\text{O}$ humidity correction factors	36
4.4	Linear section of humidity calibration - δD humidity correction factors	37
4.5	Calibrated mean isotopic values for the various humidity levels	39
4.6	Raw mean isotopic values for the various humidity levels	42
4.7	Linear section of humidity calibration - $\delta^{18}\text{O}$ humidity correction factors	43
4.8	Linear section of humidity calibration - $\delta^{18}\text{O}$ humidity correction factors	44
4.9	Calibrated mean isotopic values for the various humidity levels	45
4.10	Selected areas for calibration with 3 standards (Odo)	47
4.11	Calibration with 3 standards (Odo, 2nd group of selected areas)	50
4.12	Selected areas of two waters for calibration with 2 waters (Odo)	52
4.13	Selected areas of two waters for calibration with 2 waters (Odo)	53
4.14	Calibration with 2 waters (Walter)	53
4.15	Outliers for Odo	56
4.16	Data processing: Separation between data for valve position 1 and valve position 2	59
4.17	Data processing: October humidity calibration for Odo	60
4.18	Data processing: October VSMOW-SLAP calibration for Odo	61

4.19	Data processing: October 3 rd order 1D median filter for Odo	62
4.20	Negative time steps for the two spectrometers	63
4.21	Data processing: Interpolated data based on the linear regression . .	65
4.22	Data processig: Interpolated data based on the 3 rd order polynomial fit	66
5.1	Isotopic composition of the meteoric water samples	70
5.2	Diurnal isotopic variability of vapor for both instruments	72
5.3	Diurnal isotopic variability of vapor for days 190-210	73
5.4	Isotopic variability of meteoric water samples and atmospheric water vapor for late August-early September	75
5.5	Isotopic variability of meteoric water samples and vapor for November	77
6.1	Data processing: Time shift between Odo and Walter	82
6.2	Data processing: Isotopic variability of the two instruments as seen for different time spans	83
A.1	Full period of measurements for Odo	90

List of Tables

3.1	Fractionation Experiment for 30/07/2015	25
3.2	Fractionation Experiment for 04/08/2015	25
3.3	Isotopic values of the standards used for the fractionation experiment	26
3.4	Isotopic composition of the fractionation experiment for 30/07/2015 .	26
3.5	Isotopic composition of the fractionation experiment for 04/08/2015 .	26
3.6	Change in isotopic composition for 30/07/2015	28
3.7	Change in isotopic composition for 04/08/2015	28
4.1	Slopes of the linear fit for the two instruments	35
4.2	Measured and calibrated isotopic values of local standards (1st group of measurements)	48
4.3	Measured and calibrated isotopic values of local standards (2nd group of measurements)	48
4.4	Coefficients of the snow calibration (Odo)	51
4.5	Offset of the NEEM standard for the two calibrations (Odo)	51
4.6	Isotopic values of two waters (Odo)	54
4.7	Coefficients of the snow calibration (Walter)	54
5.1	Standards used for measuring meteoric water samples	68
A.1	Dates of collected meteoric water samples	89

1

Introduction

In recent years climate change has been one of the most discussed topics around the world. According to the Intergovernmental Panel on Climate Change (IPCC, 2014) global warming seems to affect Earth in a multidimensional way, including not only environmental consequences but also economic, health and safety issues, food production, security and many more. Melting of ice sheets, polar ice caps and shrinking of continental glaciers contribute to the observed mean global sea level rise, forcing millions of people to migrate towards safer locations. Extreme events like intense rainfalls and extended heat waves have been more common recently and according to future projections they seem to follow the same or an even more strengthened rhythm of appearance (1).

The climate system is an interactive system consisting of five major components: the atmosphere, the hydrosphere, the cryosphere, the land surface and the biosphere, forced or influenced by various external forcing mechanisms, the most important of which is the Sun. Also the direct effect of human activities on the climate system is considered an external forcing. Each one of these parts can be further divided into sub-systems, all interacting with each other through complicated mechanisms, many of which are still not fully understood.

Circulation of the Earth's water between the different reservoirs is known as the water cycle (also referred to as hydrological cycle) and includes various processes during which water evaporates from the sea and enters into the atmosphere, where it later condenses and falls as rain or snow, returning back to the sea by rivers or back to the atmosphere by evapotranspiration. Between the different phase changes water needs a lot of energy to transform into vapor (taking up energy from its surroundings and thus cooling the environment) and it releases this energy in the form of latent heat when it cools and condenses back into its liquid form from water vapor to create liquid water droplets in the air, forming clouds and fog. This

absorption and release of energy is one of the most effective ways to transfer heat from equatorial areas polewards.

Stable water isotopes can be used as tracers in a large number of hydrological, climatic and ecological applications. Analysis and processing of data that refer to the stable isotopes of hydrogen and oxygen can help us extract useful information about the global water cycle and also reconstruct paleo-climatic conditions with high accuracy. The spatial variation of stable isotopes in precipitation and vapor represents an isotopic signal that we accurately need to map in order to understand meteorological processes and how the climate system functions in more depth. Furthermore, in an upcoming warmer world due to present climate change, understanding the nature of atmospheric water vapor, which acts as one of the strongest greenhouse gases, is of vital importance.

This study focuses on measuring the stable isotopes of atmospheric water vapor in Copenhagen, Denmark. Stable isotopes are variants of a specific element which consist of the same number of protons inside the nucleus but differ in the number of neutrons. Due to the fact that the chemical behavior of an atom is largely determined by the structure of the electrons orbiting around the nucleus, different isotopes exhibit nearly identical chemical behavior but might slightly differ in their physical properties due to differences in their atomic mass (or molecular when we refer to water molecules). The stable isotopes of water are divided into the light (H_2^{16}O) and the heavy ones (H_2^{18}O and HD^{16}O). They occur naturally in the environment, but their natural abundance differs with different environmental conditions.

Water vapor stable isotopes have been measured in this study by using two commercially available Cavity Ring Down Spectrometers (CRDS) of the manufacture company Picarro (model L1102-i). These instruments are capable of measuring the isotopic ratios, D/H and $^{18}\text{O}/^{16}\text{O}$, between the heavy and the light isotopes. For the same period that atmospheric vapor was measured, a rain collector, located close to the building where the two instruments were operating, was used to sample precipitation. Samples were analyzed and measured in the Isotope Laboratory of the Center for Ice and Climate (CIC).

The thesis is structured in 6 different chapters. **Chapter 2** describes the basic physical background of water stable isotopes. Definitions of the isotopic ratios and the δ values are included in this chapter. Rayleigh condensation, equilibrium and kinetic isotope fractionation are also described here.

Chapter 3 includes basic information on how the CRDSs function and description of the experimental set-up used in this study to measure isotopes in atmospheric vapor; technical details regarding the system's different parts are included in this chapter. Also described are the characteristics of the rain collector used to sample meteoric water; the results of testing the collector's ability to store precipitation for some hours and possible isotopic fractionation effects due to evaporation of the sample are also presented in this section.

Chapter 4 describes the methods used to process the acquired vapor data. Data are calibrated in terms of varying atmospheric humidity with respect to a reference value (20 kppm); correction for different humidities is performed using two mathematical approaches, a linear regression and a 3rd order polynomial fit. Comparison and evaluation of the two methods is shown at the end of this chapter. In addition, calibration on the SMOW-SLAP scale of the data acquired from the first spectrometer, is featured at this chapter. Calibration of the second instrument was not performed by directly injecting standards of known isotopic composition but was, instead, performed by calibrating data with respect to the first instrument.

Chapter 5 includes results for both vapor and meteoric water data. Isotopic behavior and correlation between vapor and precipitation is examined and discussed.

Chapter 6 summarizes our results for the data series acquired from the two instruments. Possible improvements of the system are proposed and discussion about limitations arising from different factors are testified in this last chapter. Finally, some basic assumptions regarding the quality of the two data series are presented.

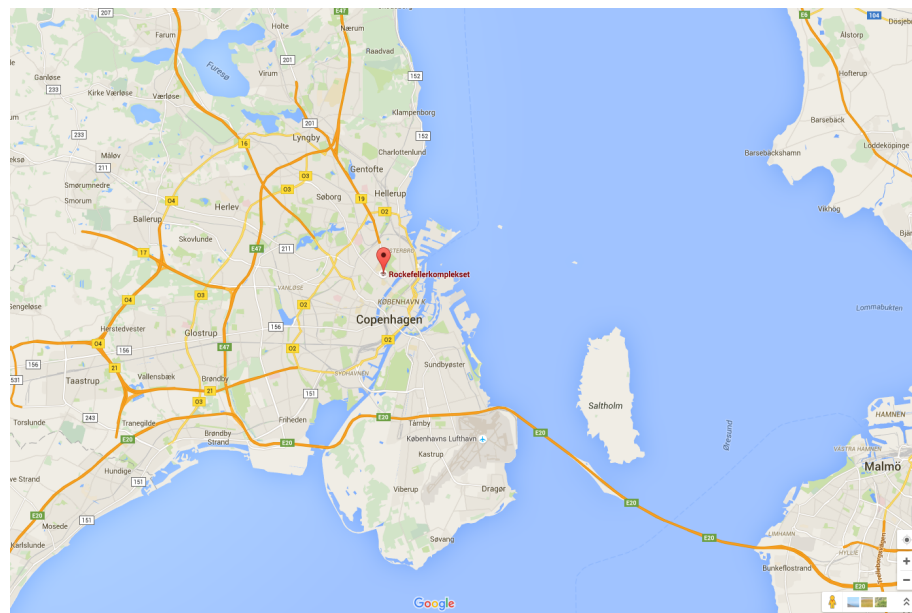


Figure 1.1: Exact location in which this study took place. Sampling, measuring and analysis have been performed at Center for Ice and Climate, at the 2nd floor of the Rockefeller Complex, Copenhagen.

2

Physical background of the water stable isotopes

This chapter overviews the basic concepts and principles of stable isotopes of water. First, a brief introduction referring to the physics behind the isotopes is given, followed by basic definitions such as the isotopic ratios, the δ notation and the isotopic fractionation.

2.1 Structure of the Atomic Nucleus

Atoms consist of a nucleus that is surrounded by electrons. The concentration of matter inside the nucleus is dense and consists of two kind of particles which have approximately the same mass: the positively charged protons and the neutrons which carry no electric charge. The number of protons (Z), the atomic number, is equal to the number of electrons that orbit the nucleus. Electrons have a much smaller mass compared to protons and neutrons ($1/1800$) and they carry a negative electrical charge. Consequently, the atom as a whole is neutrally charged. Protons and neutrons, the fundamental particles that make up the nucleus, are called nucleons. The sum of the number of protons and neutrons in a nucleus is the nuclear mass number, A :

$$A = Z + N \tag{2.1}$$

The notation describing a specific nucleus of the element X is:

$${}^A_ZX \tag{2.2}$$

where Z is the atomic number (number of protons in the nucleus), A is the mass number (sum of protons and neutrons that exist inside the nucleus) and N is the number of neutrons (13). The chemical properties of an element (X) are primarily driven by the number of electrons that are orbiting around the nucleus, the atomic number Z characterizes the element. Electrons are circulating around the nucleus, forming shells that consist of a maximum number of electrons. Especially important is the outer, incomplete shell of electrons which is finally the factor that determines the chemical properties of a specific element. As a result all the elements can be arranged in the Periodic Table of the Elements (2.1).

The Periodic Table of the Elements

1 H Hydrogen 1.01																	2 He Helium 4.00														
3 Li Lithium 6.94	4 Be Beryllium 9.01																	5 B Boron 10.81	6 C Carbon 12.01	7 N Nitrogen 14.01	8 O Oxygen 16.00	9 F Fluorine 19.00	10 Ne Neon 20.18								
11 Na Sodium 22.99	12 Mg Magnesium 24.31																	13 Al Aluminum 26.98	14 Si Silicon 28.09	15 P Phosphorus 30.97	16 S Sulfur 32.07	17 Cl Chlorine 35.45	18 Ar Argon 39.95								
19 K Potassium 39.10	20 Ca Calcium 40.08	21 Sc Scandium 44.96	22 Ti Titanium 47.87	23 V Vanadium 50.94	24 Cr Chromium 52.00	25 Mn Manganese 54.94	26 Fe Iron 55.85	27 Co Cobalt 58.93	28 Ni Nickel 58.69	29 Cu Copper 63.55	30 Zn Zinc 65.39	31 Ga Gallium 69.72	32 Ge Germanium 72.61	33 As Arsenic 74.92	34 Se Selenium 78.96	35 Br Bromine 79.90	36 Kr Krypton 83.80														
37 Rb Rubidium 85.47	38 Sr Strontium 87.62	39 Y Yttrium 88.91	40 Zr Zirconium 91.22	41 Nb Niobium 92.91	42 Mo Molybdenum 95.94	43 Tc Technetium (98)	44 Ru Ruthenium 101.07	45 Rh Rhodium 102.91	46 Pd Palladium 106.42	47 Ag Silver 107.87	48 Cd Cadmium 112.41	49 In Indium 114.82	50 Sn Tin 118.71	51 Sb Antimony 121.76	52 Te Tellurium 127.60	53 I Iodine 126.90	54 Xe Xenon 131.29														
55 Cs Cesium 132.91	56 Ba Barium 137.33	57 La Lanthanum 138.91	72 Hf Hafnium 178.49	73 Ta Tantalum 180.95	74 W Tungsten 183.84	75 Re Rhenium 186.21	76 Os Osmium 190.23	77 Ir Iridium 192.22	78 Pt Platinum 195.08	79 Au Gold 196.97	80 Hg Mercury 200.59	81 Tl Thallium 204.38	82 Pb Lead 207.2	83 Bi Bismuth 208.98	84 Po Polonium (209)	85 At Astatine (210)	86 Rn Radon (222)														
87 Fr Francium (223)	88 Ra Radium (226)	89 Ac Actinium (227)	104 Rf Rutherfordium 178.49	105 Db Dubnium (265)	106 Sg Seaborgium (266)	107 Bh Bohrium (264)	108 Hs Hassium (268)	109 Mt Meitnerium (268)	110 Ds Darmstadtium (281)	111 Rg Roentgenium (272)	112 Cn Copernicium (285)																				
																		58 Ce Cerium 140.12	59 Pr Praseodymium 140.91	60 Nd Neodymium 144.24	61 Pm Promethium (145)	62 Sm Samarium 150.36	63 Eu Europium 151.96	64 Gd Gadolinium 157.25	65 Tb Terbium 158.93	66 Dy Dysprosium 162.50	67 Ho Holmium 164.93	68 Er Erbium 167.26	69 Tm Thulium 168.93	70 Yb Ytterbium 173.04	71 Lu Lutetium 174.97
																		90 Th Thorium 232.04	91 Pa Protactinium 231.04	92 U Uranium 238.03	93 Np Neptunium (237)	94 Pu Plutonium (244)	95 Am Americium (243)	96 Cm Curium (247)	97 Bk Berkelium (247)	98 Cf Californium (251)	99 Es Einsteinium (252)	100 Fm Fermium (257)	101 Md Mendelevium 288.10	102 No Nobelium (289)	103 Lr Lawrencium (260)

Legend for element box (Li):
 - Top: Atomic Number (3)
 - Middle: Element Symbol (Li)
 - Bottom: Element Name (Lithium)
 - Bottom-right: Average Atomic Mass (6.94)

Figure 2.1: The periodic table of the elements ¹

2.2 Water stable isotopes

The term isotopes refers to variants of a specific chemical element that have the same number of protons inside their nucleus but differ in the number of neutrons. As a result, isotopes of a specific element have the same atomic number but not the same mass number. In general nuclei with even number of protons or/and neutrons are more stable. Nuclei of which the number of protons or/and neutrons corresponds to some specific even number (i.e. 2, 8, 20, 28, 50, 82 and 126) are highly stable and thus have a large natural abundance (13).

¹www.middleschoolchemistry.com/multimedia/chapter4/lesson2

The most common isotopes of hydrogen are the light ^1H and the heavy ^2H (also called deuterium and often written as D) with mass abundance in the hydrosphere of 99.985% and 0.015%, respectively. The most common isotopes for oxygen are the light ^{16}O , and the heavy ^{17}O and ^{18}O whose abundances are 99.763%, 0.037% and 0.2%, respectively (13).

Water molecules (H_2O) are composed of two hydrogen atoms and one oxygen atom. Due to the existence of stable hydrogen and oxygen isotopes, water molecules consist of different isotopologues such as H_2^{16}O , H_2^{18}O and HD^{16}O , where the heavier water molecules HD^{16}O [0.032%] and H_2^{18}O [0.200%] are rare compare to the more abundant light water molecule H_2^{16}O [99.768%]. Notice that the square brackets define the relative abundance.

Water isotopologues exhibit different physical and chemical properties due to mass differences of the atomic nuclei of the stable isotopes they consist of. A consequence of the mass difference is that heavier water molecules have a lower mobility. The kinetic energy of a molecule (water molecule or any other molecule) is:

$$\frac{1}{2} \cdot m \cdot \bar{v}^2 = k \cdot T \quad (2.3)$$

where m is the molecular mass, \bar{v} is the average molecular velocity, k is the Boltzmann's constant and T the absolute temperature. Due to the fact that for the same temperature for different isotopic species and in order to keep the product $1/2m\bar{v}^2$ steady, we see that in the case of a larger mass we necessarily have a smaller velocity. As a result, the heavier water molecules H_2^{18}O and HD^{16}O have lower diffusion velocities (13).

In addition, particles are characterized by three different modes of motion: vibrations of the atoms in the molecule with respect to each other, rotation around a molecular axis and translation which corresponds to displacement of the molecule as a whole. These modes have an impact on the binding energy of the molecules with different mass such that isotopically heavier molecules have a higher binding energy. This results in H_2^{18}O and HD^{16}O having a lower vapor pressure than H_2^{16}O and also they evaporate less easily (13).

2.2.1 Isotopic ratios and the δ notation

The isotopic ratio is defined as the ratio between the abundant and rare isotopes of an element:

$$R = \frac{\text{abundance of rare isotope}}{\text{abundance of abundant isotope}} \quad (2.4)$$

The ratio is usually written using a superscript before the ratio symbol R, which refers to the isotope under consideration. Based on this definition, we can express the isotopic ratios of the stable isotopes of the hydrogen and oxygen as:

$${}^2R = \frac{D}{{}_1H}, \quad {}^{17}R = \frac{{}^{17}O}{{}^{16}O}, \quad {}^{18}R = \frac{{}^{18}O}{{}^{16}O} \quad (2.5)$$

In general isotope ratios are not reported as absolute numbers mainly due to the fact that mass spectrometers are not reliable for acquiring absolute ratio numbers and secondly because comparison between different laboratories around the world requires the use of internationally accepted references to which samples have to be related. The δ value is used to report an isotope abundance and is defined as the relative deviation of a measured isotopic ratio (R_i) in a sample with respect to the isotopic ratio of a standard (R_{ST}):

$$\delta_i = \frac{R_i - R_{ST}}{R_{ST}} = \frac{R_i}{R_{ST}} - 1 \quad (2.6)$$

It is common to express the δ value of a sample in per mille (or per mil) which refers to parts per thousand. A δ value of -0.001 is given as $\delta = -1/1000 = -1\text{‰}$.

After taking into account the previous definitions, we can symbolize the different δ values in water as:

$$\delta D = \frac{{}^2R_{(A)} - {}^2R_{(vsmow)}}{{}^2R_{(vsmow)}}, \quad \delta^{17}O = \frac{{}^{17}R - {}^{17}R_{(vsmow)}}{{}^{17}R_{(vsmow)}}, \quad \delta^{18}O = \frac{{}^{18}R - {}^{18}R_{(vsmow)}}{{}^{18}R_{(vsmow)}} \quad (2.7)$$

where VSMOW is the Vienna Standard Mean Ocean Water, the internationally accepted water with reference values defined by the International Atomic Energy Agency (IAEA).

2.2.2 Deuterium Excess

Measurements of freshwater and precipitation worldwide show that there is a strong relationship between $\delta^{18}\text{O}$ and δD due to their observed co-variability. Values are correlated through the relationship:

$$\delta D = 8 \cdot \delta^{18}\text{O} + 10\text{‰} \quad (2.8)$$

Equation 2.8 is a straight line known as the meteoric water line (2).

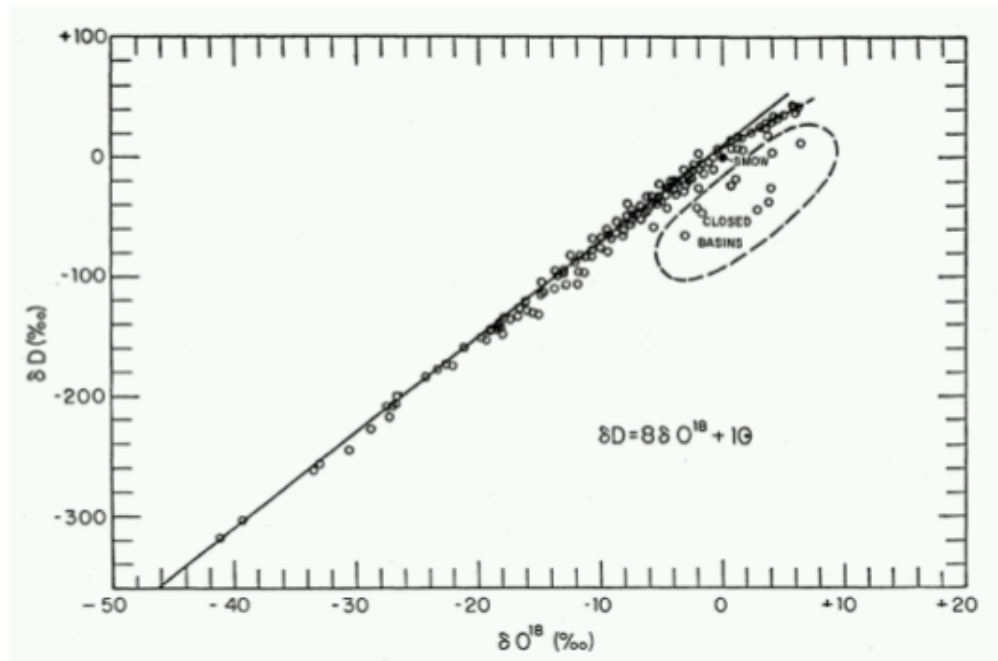


Figure 2.2: $\delta^{18}\text{O}$ and δD variations in natural waters. Picture: Craig (1961)

The slope is the result of the fact that the relative mass difference between D and ^2H is 8 times larger than the difference between ^{18}O and ^{16}O . The deviation of a water sample from the global meteoric water line is defined as deuterium excess (4), given as:

$$d = \delta D - 8 \cdot \delta^{18}\text{O} \quad (2.9)$$

Despite the fact that deuterium excess is not a fundamental property of water, it is a simple way to combine information that comes from oxygen and hydrogen isotopic ratios. Deuterium excess is correlated with the prevailing physical conditions

(relative humidity (RH), air temperature T and sea-surface temperature (SST)) of the oceanic source area of evaporation and the mixing of different air masses along their trajectory all the way to the precipitation site. As a result, a change in relative humidity or sea-surface temperature at the location where evaporation takes place has an impact on the deuterium excess value; this is true not only for the tropical and subtropical precipitation but also for the precipitation all the way to polar ice sheets.

2.3 Isotope fractionation

According to classical chemistry the chemical properties of isotopes or molecules that contain different isotopes of the same element (i.e. H_2^{16}O and H_2^{18}O) are the same. Although this is partially true, if we are capable of making measurements with high accuracy we will find differences in chemical and physical properties between different isotopes of the same element. This phenomenon of existing isotopic differences is due to isotope fractionation which is defined as the change in the isotopic composition of an element in a certain compound driven by the transition of the compound from one physical state or chemical composition to another (13). Isotope fractionation is used to explain how various physical and chemical processes affect the relative abundance of isotopes. It occurs during the phase transition of a compound from one state to another, i.e. liquid water to water vapor, or into another compound (kinetic isotope fractionation) or it can be seen as a difference in isotopic composition between two compounds that are in chemical or physical equilibrium (equilibrium isotope fractionation).

2.3.1 Isotope fractionation factor

Isotope fractionation refers to the relative abundance of isotopes before and after a chemical or physical process is taking place. The isotope fractionation factor is defined as the ratio of the two isotope ratios:

$$\alpha_{B/A} = \frac{R_B}{R_A} \quad (2.10)$$

and describes the isotopic ratio in the phase A relative to the isotopic ratio in

phase B. For the rest of this section we will focus on the equilibrium and kinetic fractionation factors and we will specifically refer to the fractionation factors for the physical processes of evaporation and condensation of water. The fractionation factors related to these processes depend mainly on the isotopic species (heavier or lighter isotopes), the temperature (fractionation factors increase with decreasing temperatures) and whether the condensates liquid or solid (i.e. rain or snow). The corresponding fractionation factors are in this case numbers slightly greater than one and for temperatures that prevail across the Earth's surface, α ranges between 1.008 and 1.025 for $^{18}\text{O}/^{16}\text{O}$ fractionation and between 1.07 and 1.25 for D/H fractionation (3).

2.3.2 Equilibrium Fractionation

The equilibrium (or thermodynamic) isotope fractionation is used to describe the isotope ratios before and after a physical or chemical process that takes place under equilibrium conditions. Equilibrium fractionation involves exchange or redistribution of isotopes of a specific element and can be represented as:



where the asterisk is used to express the presence of the rare isotope. During equilibrium conditions, and from the energy state point of view, the heavier isotope becomes enriched in the compound that has the largest molecular weight (13). The transition between different states of matter (under equilibrium conditions) also affects the isotopic ratio of the two states. If we assume, for example, that condensation of water vapor is taking place under equilibrium, the liquid phase becomes enriched in heavier isotopes (^{18}O and D) while the vapor phase becomes enriched in the lighter isotopes (^{16}O and ^1H). Having a process under equilibrium conditions, we can define the equilibrium fractionation factor as:

$$\alpha_{eq} = \frac{R_B}{R_A} \quad (2.12)$$

where R_A and R_B refer to the isotopic ratios before and after the process.

2.3.3 Kinetic Fractionation

When we have a one-way physical or chemical process taking place, then kinetic isotope fractionation happens. It results from differences in the binding energies so that lighter isotopic species have smaller binding energies and higher velocities (3).

One physical procedure that we are particularly interested in is evaporation of water from the oceans (which is the main source of precipitation) and the condensation that takes place afterwards, when the air mass that contains the vapor gradually cools and precipitates. Due to the fact that the vapor pressure of the waters that contain the isotopically heavier molecules are slightly lower than that of the lighter molecules, the heavier molecules evaporate less rapidly from the ocean surface and condense more readily from the vapor. If we take into account that evaporation usually takes place under non-equilibrium conditions (i.e. slight wind and relative humidity below 100 %), we can define the kinetic fractionation factor:

$$\alpha_k = \frac{1 - k \cdot RH_{SST}}{1 - k} \quad (2.13)$$

where RH_{SST} is the relative humidity with respect to the surface temperature of the sea and k is a constant with values between 0.003 and 0.006 depending on the location where evaporation is taking place. Higher values of k correspond to evaporation from areas located closer to the equator while lower values are used for evaporation in more windy conditions, usually closer to the poles.

Finally we define the effective fractionation factor, α_{ef} , as:

$$\alpha_{ef} = \alpha_{eq} \cdot \alpha_k \quad (2.14)$$

2.4 Rayleigh condensation

When an air parcel is transported from the equatorial toward the arctic, it will progressively cool due to lower temperatures prevailing in higher latitude. This will affect the parcel's ability to hold water vapor and will result in condensation and rain-out. The fact that isotopically heavier molecules condense more readily than the light ones will result in fractionation and the vapor will become slightly depleted

in heavy isotopes denoted by lower δ values. As the air parcel moves further north (or south if we in the southern hemisphere) it will gradually cool and water will be precipitated in the form of rain and snow. Since the heavier isotopes preferentially condensate, the δ value of the air parcel will become lower as it gets colder. This phenomenon is called Rayleigh condensation and can be seen graphically in Figure 2.3. Notice that we define the δ value of the ocean water close to the subtropics to be equal to 0.

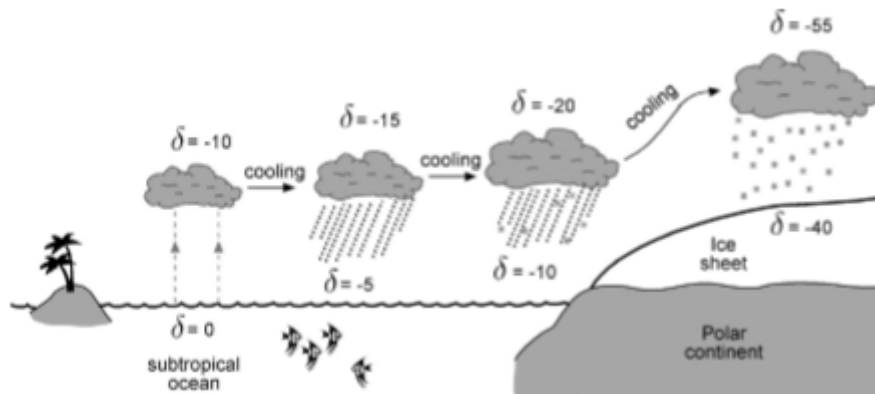


Figure 2.3: Schematic of the Rayleigh condensation scheme. As the air parcel transports to higher latitudes, evaporation and condensation re-distribute water between the atmosphere and the land-oceans; repeated fractionations act cumulatively in the δ values of precipitation and associated vapor. Picture: Cuffey and Paterson (2010)

3

Experimental set-up

3.1 NIR Cavity Ring Down Spectroscopy

Each atmospheric gas has a specific absorption-emission spectrum which acts as its spectral signature. Water molecules have their strongest absorption lines in the mid and near infrared spectra. When water molecules are in gaseous form, three types of transition can cause absorption of electromagnetic radiation: rotational, vibrational and electronic transitions in which a molecule is promoted to an excited electronic state.

We can connect the proportion of absorbed light with the number of molecules that interact with the light, through the Lambert-Beer law, which gives the absorbance, A , of a solution:

$$A = \log\left(\frac{I(t)}{I_0}\right) = \varepsilon l C \quad (3.1)$$

where ε is the molar absorptivity, l is the length of the solution that light goes through and C is the concentration of that solution. Measuring the decay of the intensity allows us to determine the concentration of the absorber molecules.

The absorption of electromagnetic radiation, though, is different for the isotopic variants of water due to different masses which result in slightly different geometrical structures and characteristic dimensions. The individual transitions between the energy states of the isotopic variants of water correspond to the absorption of photons of different wavelengths (i.e. energies) (17). As a result, the relative intensities between the different isotopes of hydrogen and oxygen can be attributed to relative isotopic abundances, providing the necessary information to calculate the isotopic ratios between the light (H_2^{16}O) and heavy (H_2^{18}O , HD^{16}O) water molecules.

Two Near Infrared Cavity Ring-Down Spectrometers (NIR-CRDS) of the manufacture Picarro (L1102-i) are used in this study. The vapor sample flows inside the optical cavity of the instrument where three mirrors of finite reflectivity ($R > 99.999\%$) are facing each other at constant angles. The laser light, coupled into the optical cavity, beams and stays in resonance until a certain intensity builds up to a maximum value. The light source is then turned off and the light intensity starts to decay exponentially as it interacts with the gaseous absorbers while traveling inside the optical cavity and due to successive reflections on the three mirrors ($\approx 10^5$ times resulting in a path of the order of kilometres). This decay, referred to as "ring-down time", depends only on the reflectivity of the mirrors, R , the length of the cavity, l_c , and the absorption coefficient of the selected absorption feature, $\alpha(\nu)$ (7). The ring-down time is given by the equation:

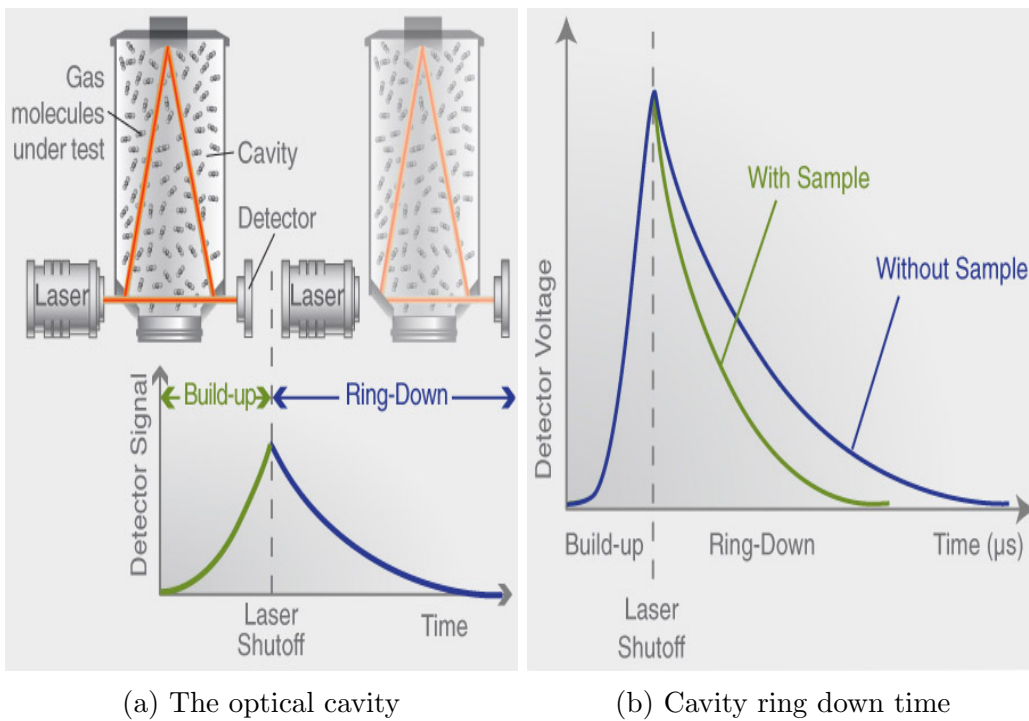
$$\tau(\nu) = \frac{l_c}{c[(1 - R) + \alpha(\nu)l_c]} \quad (3.2)$$

As shown in Figure 3.1, the spectrometer compares the ring-down time when the cavity is empty of vapor to the time when a gas species is introduced in the cavity. This accelerates the exponential decay and the instrument continuously compares and calculates the ring-down time with and without absorption due to the introduced gas species. The light signal measured at the photodetector is given by the equation:

$$I(t, \lambda) = I_0 e^{-t/\tau(\lambda)} \quad (3.3)$$

where I_0 is the transmitted light intensity at the moment when the laser source is turned off and $\tau(\lambda)$ is the ring down time constant.

This method that compares the ring down time when we have a gas that absorbs with the ring-down time without any gas is performed by tuning the laser's wavelength to different values; the range of tuning includes wavelengths where the gas absorbs and wavelengths where the gas does not absorb light from the laser source, resulting, finally, in the comparing the two ring-down times as previously described.



(a) The optical cavity

(b) Cavity ring down time

Figure 3.1: Left image: the optical cavity where the light intensity is measured after successive reflections on the three mirrors; the intensity initially builds up until a certain threshold point and is then shut off, resulting in an exponential decay as a result of the interaction between the light and the gas molecules (absorbers). Light signal is measured at the photodetectors. Right image: comparison of the ring-down time with and without the contribution of the gas to the optical loss inside the cavity.¹

¹http://www.picarro.com/assets/images/content/cavity_figure_large.jpg

3.2 Experimental system set-up

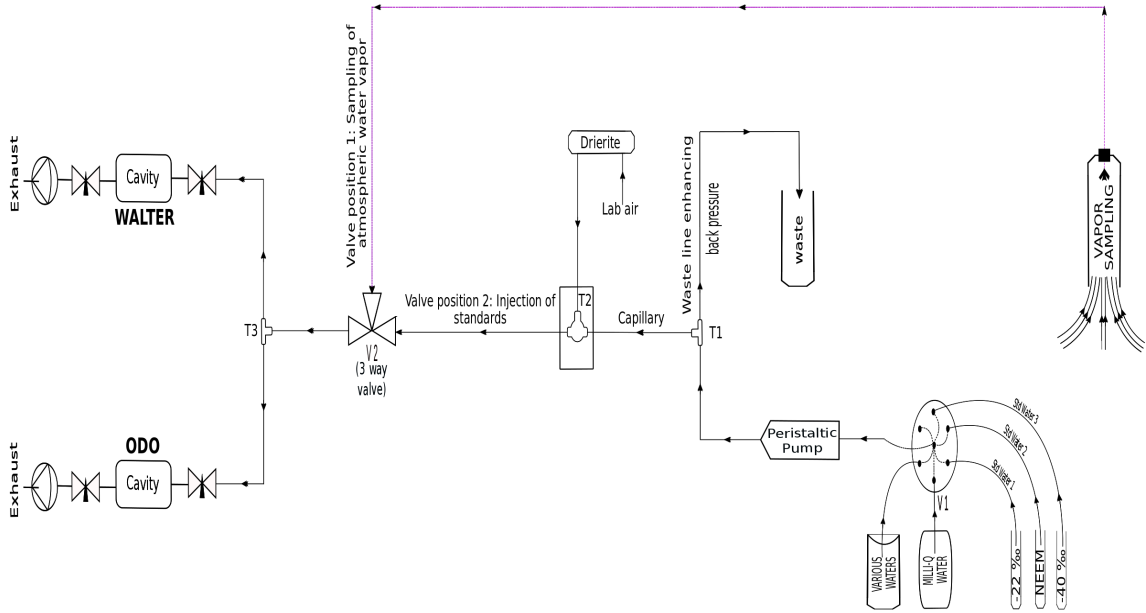


Figure 3.2: Block diagram of the system

Figure 3.2 shows the block diagram of our experimental set-up. The system is adjusted to operate in two basic modes, controlled by the 3-way valve (V2): the first one is sampling of atmospheric water vapor via the vapor line (valve position 1), shown as the pink colored line at the block diagram, and the second one is when standards of known isotopic composition or Milli-Q water (in general, liquid water samples) are injected inside the optical cavity of the spectrometers (valve position 2). Switching between the two positions of the 3-way valve (V2) allows us to choose between the two modes easily and fast. For the rest of this study, valve position 1 corresponds to measurements of atmospheric vapor and valve position 2 when we inject and measure water that does not correspond to atmospheric vapor.

When the system is switched to valve position 2, different liquid water samples and standards can be selected via a six-port selection valve, shown as V1 in the diagram. Sample is transferred using a peristaltic flexible pump that allows us to regulate the flow rate according to our needs. Usual flow rates are between 0.1 and 0.4 ml/min, but this can be set lower or higher depending on the application. High-purity Perfluoroalkoxy tubing (PFA) with an ID of 0.5 mm is used in this part of the system, exhibiting less stronger, concentration-dependent, memory effects than other materials (16).

After the liquid sample exits the peristaltic pump, it reaches the PEEK Tee split (T1) which also has an ID of 0.5 mm. Connected to the one side of the split is a fused silica capillary of an ID between 30 and 50 μm . The capillary is used to control the quantity of sample that enters the oven. The smaller diameter of the capillary, though, compared to that of the PFA tubing initiates a back pressure at T1 that restricts our desired direction of flow. This problem can be solved by using tubing with ID smaller than that of the capillary, referred to as waste line in our block diagram. This way the imposed back pressure at T1 is balanced and by adjusting the length and the inner diameter of the waste line and the capillary we can tune each time the flow rate through the capillary (7). Taking as a fixed value for the length of the capillary, L_c , around 20 cm, the flow through it, (Q_c), will be given by the equation:

$$Q_c = Q_w \frac{L_w r_c^4}{L_c r_w^4} \approx Q_m \frac{L_w r_c^4}{L_c r_w^4} \quad (3.4)$$

where Q_w and Q_m are the flow of sample at the waste line and the main line, respectively, and $2r$ correspond to the inner diameter.

We notice that the dependence of the flow through the capillary is in the 4th power of the inner radius of the capillary and the waste line tubing, while the dependence on the length of the waste line and the capillary is in the 1st power. This allows us to control the flow through the capillary by choosing tubings (capillary and waste line tubing) of different inner diameter.

The next step when using the liquid water sampling line is to evaporate the sample inside the oven. The important thing during evaporation is that this should take place immediately in order to avoid isotopic fractionation effects. The evaporation oven consists of a stainless steel Valco Tee-split (Valco ZT1M), showed as (T2) in the block diagram. The oven's walls are covered with fabric glass suitable for insulating the oven and keeping the temperature steady around 170 °C. Temperature is regulated via a proportional-integral-controlled (PID) heater. The Valco Tee split is placed on top of an aluminium block to avoid direct contact with the insulating material. Dry air is driven in the oven and gets mixed with the sample to get the desired water vapor concentrations. Air is dried while it goes through a DrieriteTM canister CaSO_4 . Stainless steel of 1/16" is used to transfer atmospheric dried air inside the evaporation chamber.

The sample is transferred afterwards through the 3-way valve to the next Tee-split

(T3), where it splits and gets transferred in the optical cavity of the two spectrometers, that are named as Odo and Walter, in order to distinguish them (these names will be used hereafter in this study to refer to the two spectrometers). We use for this section copper tubing of 1/8" diameter.

Valve position 1 corresponds to a more simple part of the system, since a copper tube of 1/8" is connected to the 3-way valve; the copper tube is directed outside of the room's window in order to sample atmospheric water vapor. The edge of the tube is sealed with a plastic bottle assuring that no precipitated water will enter into the copper tube and alter our measurements or inside the optical cavity of the instruments and create problems in their functionality.

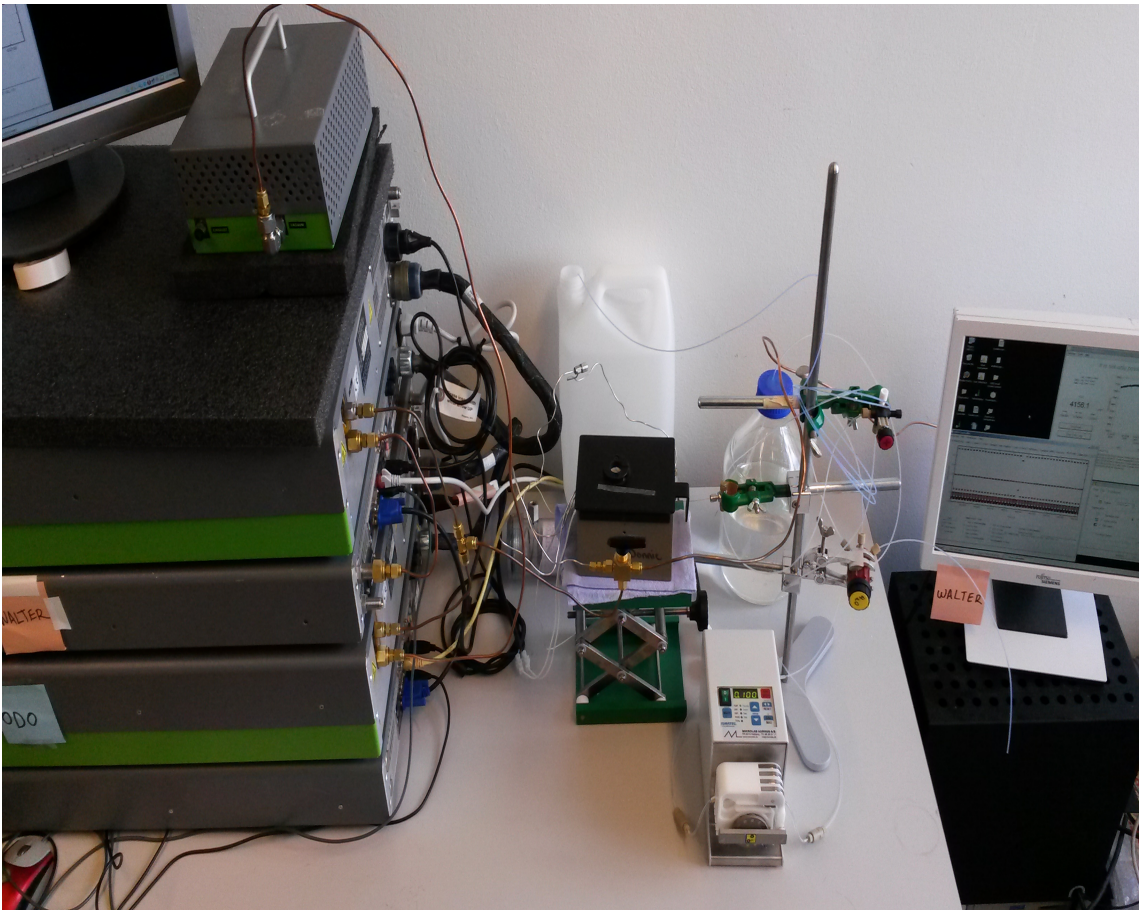


Figure 3.3: Experimental set-up.



Figure 3.4: Left image: the copper tube of the vapor line that exits out of the room to collect atmospheric vapor. Right image: the plastic bottle for sampling atmospheric water vapor. Its top is sealed with expandable polystyrene in order to ensure that we are only sampling vapor and no precipitation is entering to the vapor sampling line through the plastic bottle.

3.3 The Rain Collector

The main purpose of this project is to measure the isotopic composition of atmospheric water vapor. Due to the strong interrelationship between the different phases of water, it is of great interest to compare the stable isotopes measured in vapor and those measured in precipitation (rain or snow). For this reason, a rain collector is used to gather and sample precipitation. The collector is placed on top of a ship container, approximately 2 meters above ground, at the side building of the Rockefeller complex. The location was chosen based on its proximity to the point where vapor collection took place and due to the absence of obstacles that could affect the

direct and easy collection of the precipitation.

3.3.1 Design, characteristics and maintenance of the rain collector

The collector used for the aims of this project belongs to Geological Survey of Denmark and Greenland (GEUS) and was used throughout the whole period that vapor collection was taking place. The manufacturer is the company PALMEX, Zagreb, Croatia and the sampling device is primarily designed in a way that aims to minimize any possible evaporation of the collected sample and thus avoid fractionation. Another characteristic of the collector is the use of easily available parts which results in relatively low cost and ease in replacing different parts of the device.



Figure 3.5: The rain collector. ²

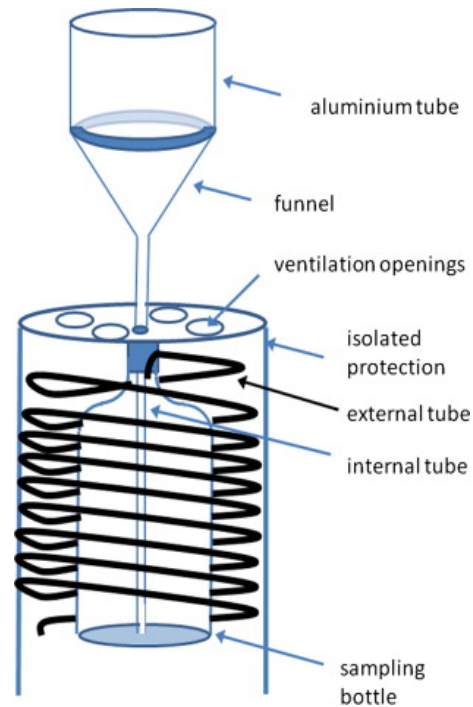
The collector consists of two cylinders of different diameters (220mm and 150mm respectively), both made of PVC hard plastic. The outer cylinder is overspread with silver paint and transparent lacquer. The inner cylinder is a 3 liter bottle and is

²<http://www.rainsampler.com/portfolio-page/rain-sampler-rs1/>

used as the sampling area of the collector. It is easily accessible from the bottom and can be easily changed since only its top thread is mounted on the sampler. The precipitated water is entering the collector through the funnel which is located at the top of the device. The funnel is equipped with a removable stainless steel mesh to prevent dirt entering the bottle. Its upper end is equipped with metal needles to reduce sample contamination by bird droppings. Precipitation enters the funnel and flows through the 15m long soft polypropylene external plastic tube which is mounted to the collector on the fixed screw cap for holding the bottle. Changes in atmospheric pressure will result in movements of the air inside this plastic tube; for this reason its total volume is approximately 10% of the bottle volume and is sufficient for pressure fluctuations of $\pm 50\text{hPa}$ to cause only minor air and moisture exchange between the bottle's head space and the free atmosphere while making sure that there is pressure equilibration (the air pressure in the bottle is always the same as the outside atmospheric pressure) (8). Another important thing one should take into consideration is the best possible thermal insulation needed for the plastic bottle where water is collected. In fact, this is achieved by using a double container construction around the bottle and due to the fact that air can move vertically between the inner container and the outer silver painted container through drilled ventilation openings at the upper side. Last but not least, there is no oil used to prevent evaporation, as opposed to most conventional precipitation collectors. As a result, the maintenance and cleaning of the collector becomes simpler and is necessary less frequently.



(a) Dimensions of the different parts of the rain collector



(b) Schematics of the rain collector. Marked in black is the external plastic tube which covers the sampling bottle and helps pressure equilibration

Figure 3.6: Dimensions and schematics of the rain collector. Picture: Groeningen et al., 2012

3.3.1.1 Replacement of the stainless steel mesh

Despite the fact that the rain collector's construction can be characterized as quite solid and strong and its net weight (without any precipitated water inside the sampling area of the plastic bottle) is approximately 3.8 kg, exceptionally strong winds prevailed during the night between 8 and 9 November, 2015, resulting in displacement of the collector and removal of its stainless steel mesh. In order to replace this part of the collector, we contacted the workshop of Niels Bohr institute and a new mesh was constructed. The material used was again stainless steel, but this time an improvement in the filtration of impurities was made: instead of having one level of sieve, the new mesh included two. The upper one having a larger diameter of holes and the lower one having holes of smaller diameter. This way, impurities such as leaves from trees or macroscopic particles that manage to penetrate through the holes of the first sieve can be filtered in a more successful way due to the presence of the second one.

3.3.1.2 Maintenance of the rain collector

The maintenance of the rain collector is quite simple and was performed only every two or three weeks or when impurities were clearly accumulated at the funnel. In order to remove these impurities, a weak solution of citric acid was injected through the external tube ending up at the sampling bottle; impurities were dissolved and at the same time the low acidity of our solution protected the plastic internal tube and the sampling bottle from being damaged through a possible deformation of its PVC plastic material. Remnants of the citric acid were cleaned in a second step by using MQ water. Finally, the rain collector was left at room temperature for a period of 48 - 72 hours in order to completely dry it out from the Milli-Q water (trademark created by the manufacture Millipore Corporation to describe ultrapure water of "Type 1"-highly purified water).

3.4 Fractionation Experiment

The most important aspect one should take into account when measuring water stable isotopes in samples collected from a rain collector is to make sure that it can successfully prevent water re-evaporation. Evaporation of water that is stored inside the sampling plastic bottle will inevitably alter the isotopic composition of the sample due to fractionation. This section describes a simple experiment that took place on 30/07/2015 and 04/08/2015 and its purpose was to identify any possible change in the isotopic composition of sampled precipitation that stays for some hours inside the rain collector.

Both days that the experiment took place were dry (i.e. no precipitated water) and Milli-Q water used instead of precipitation as the sample under examination. Sampling took place approximately every two hours and the number of samples for each one of the two dates is four (Table 3.1 and 3.2). The fourth column of the tables refers to whether there were clear skies or not at the period between the different sampling times. This may be important because higher temperatures can prevail inside the rain collector if it is directly heated by sunlight (in case of clear skies).

Table 3.1: Fractionation Experiment for
30/07/2015

Number of Sample	Date	Time	Weather Conditions
Baseline Water	30/07	12:00	Cloudy
01	30/07	14:11	Partly Cloudy
02	30/07	16:09	Sunny
03	30/07	18:04	Sunny
04	30/07	20:05	Partly Cloudy

Table 3.2: Fractionation Experiment for
04/08/2015

Number of Sample	Date	Time	Weather Conditions
Baseline Water	04/08	09:20	Sunny
01	04/08	11:18	Sunny
02	04/08	13:18	Sunny
03	04/08	15:23	Partly Cloudy
04	04/08	17:22	Partly Cloudy

The collected samples were placed in KAUTEX narrow neck plastic bottles of 10ml (of the manufacture KAUTEX TEXTRON) and sealed with parafilm tape to avoid any possible fractionation. Finally, they were stored in the Michelsen deep freezer (located at the Rockefeller complex and used for storing ice cores from Greenland and Antarctica) at a temperature of -25°C .

3.4.1 Results of the fractionation experiment

The measurement of the isotopic composition of the Milli-Q water samples took place at 10/08/2015 and the analysis was performed using a Picarro Cavity Ring Down Spectrometer (CRDS) (model L2120-i). The instrument is on the second floor of the Rockefeller complex, where the isotope lab of the Center for Ice and Climate is located. Each sample was measured three times and the mean value is used as the final one. Standards used for the calibration are -15‰ , -22‰ and NEEM (-33.5‰). Precise values of the standards are shown in Table 3.3 and the values of the isotopic composition for the two dates can be found at Tables 3.4 and 3.5.

Table 3.3: Isotopic values of the standards used for the fractionation experiment

Standard	$\delta^{18}O$ (‰)	δD (‰)
-22	-21.88 ± 0.06	-168.45 ± 0.09
NEEM	-33.50 ± 0.03	-257.45 ± 0.20
-40	-39.98 ± 0.08	-311.11 ± 0.35

Table 3.4: Isotopic composition of the fractionation experiment for 30/07/2015

Number of Sample	$\delta^{18}O$ (‰)	δD (‰)	dexcess (‰)
Baseline Water	-9.18 ± 0.08	-62.53 ± 0.21	10.87 ± 0.75
01	-9.18 ± 0.03	-62.03 ± 0.12	11.43 ± 0.32
02	-9.11 ± 0.07	-61.80 ± 0.20	11.07 ± 0.67
03	-9.09 ± 0.03	-61.63 ± 0.15	11.10 ± 0.46
04	-9.07 ± 0.04	-61.50 ± 0.20	11.03 ± 0.21

Table 3.5: Isotopic composition of the fractionation experiment for 04/08/2015

Number of Sample	$\delta^{18}O$ (‰)	δD (‰)	dexcess (‰)
Baseline Water	-9.07 ± 0.06	-61.63 ± 0.15	10.93 ± 0.61
01	-9.08 ± 0.08	-61.53 ± 0.29	11.13 ± 0.40
02	-9.10 ± 0.06	-61.57 ± 0.23	11.23 ± 0.07
03	-9.06 ± 0.06	-61.33 ± 0.06	11.20 ± 0.44
04	-9.18 ± 0.06	-61.03 ± 0.12	12.43 ± 0.35

For the first day of the sampling (30/07/2015) we can see a change for both $\delta^{18}O$ and δD between the baseline water and the collected samples towards less negative values (isotopically heavier collected samples), clearly shown in Figure 2.3a (blue and red line). This could originate from the cumulative effect of possible repeated evaporations of the water located in the sampling plastic bottle of the rain collector, a process mainly driven by high temperatures and resulting in fractionation: heavier molecules evaporate less rapidly and condense more readily leading to isotopically heavier condensate and lighter vapor (3). On the other hand, despite the trend of

gradually measuring higher isotopic values and the indication of possible fractionation, it is of great importance to check the values of Table 3.6, which illustrates the difference in the isotopic content between the first sample (considered as the baseline water) and the samples collected afterwards and compare them with the values that refer to the instrument's precision. We see that the greatest isotopic difference ($+0.11\text{‰}$ for $\delta^{18}\text{O}$ and $+1.03\text{‰}$ for δD) is between the initial (baseline) water and the last sample collected approximately 8 hours later (i.e. the fourth collected sample) and this is valid for both isotopic species. The instrument's acceptable precision of measuring is approximately $\pm 0.1\text{‰}$ for $\delta^{18}\text{O}$ and $\pm 0.7\text{‰}$ for δD . In that sense, none of the previous two values can be considered being inside the instrumental precision and can therefore likely be attributed to fractionation. The rest of the values of Table 3.6 that refer to $\delta^{18}\text{O}$ are smaller than $\pm 0.1\text{‰}$ and hence no fractionation can be directly linked to these values. For δD , the situation is more complicated since only the sample collected after two hours (i.e. the first sample) has a value that is close enough to the value measured for the baseline water. In case that fractionation does actually took place, the values measured by the spectrometer seem to agree well with the fact that fractionation factor for $^{18}\text{O}/^{16}\text{O}$ is smaller than for D/H and, thus, hydrogen isotopes fractionate much more strongly than the oxygen isotopes (3); the stronger fractionation of hydrogen shows the large effect on molecular vibration frequencies when a D atom replaces an H atom in a water molecule.

The results for the second date that the fractionation experiment took place (04/08/2015) show similar behavior as the first date only for δD , with only the value for $\delta^{18}\text{O}$ of the fourth sample (-0.11‰) being larger than the instrument's measuring precision. Furthermore, the isotopic content of the samples measured this time by the CRDS show a tendency towards isotopically lighter values for three out of four samples for $\delta^{18}\text{O}$. The isotopic values for δD are higher (less negative) for all samples and stay well below the instrumental precision, indicating no significant fractionation of the baseline water.

Taking into account the values of Tables 3.6 and 3.7 we could say that no clear assumption can be drawn from the two days, since they do not show the same trend in terms of change in their isotopic values. The first experiment shows a sign of fractionation since both isotopic species become isotopically lighter; such behavior is not repeated in the second time the experiment took place. This shows that the meteoric water samples that will be later collected should stay inside the plastic sampling box of the rain collector not too long to make sure that fractionation is

kept to a minimum. The rain collector has been tested again (Gröning et al., 2012) when similar experiments took place for longer periods using the same collector; the shift versus the original isotopic composition of the sample in that experiment showed no traceable fractionation effects. Last but not least, weather conditions for most of the period that precipitation would be collected could strengthen our confidence that any problems associated with fractionation of the collected meteoric samples would be minimized since lower temperatures would be recorded as autumn and winter followed.

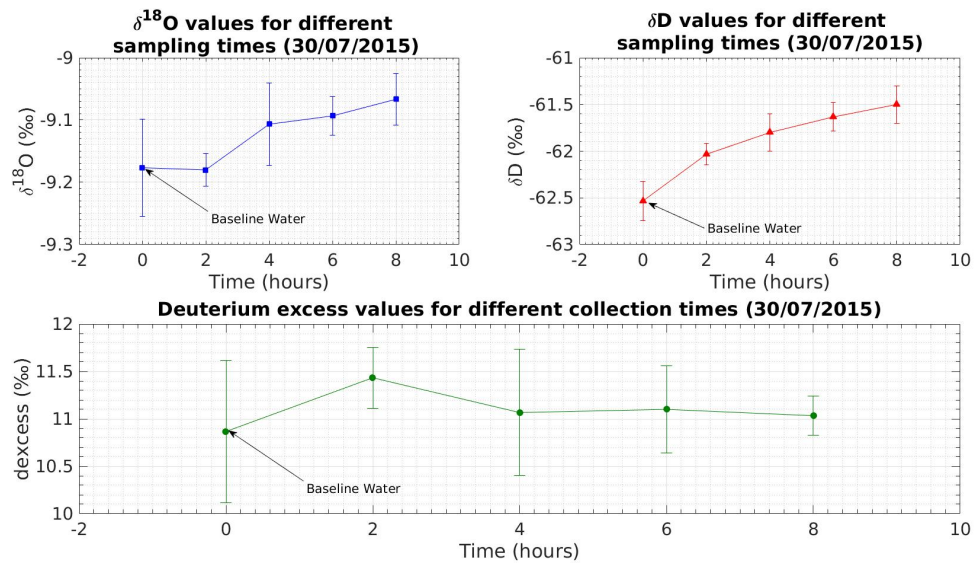
Certainly the two fractionation experiments demonstrate that fractionation effects are not significantly larger than the measurement uncertainties and much smaller than the naturally occurring isotopic differences in precipitation.

Table 3.6: Change in the isotopic composition between baseline water and collected samples (30/07/2015)

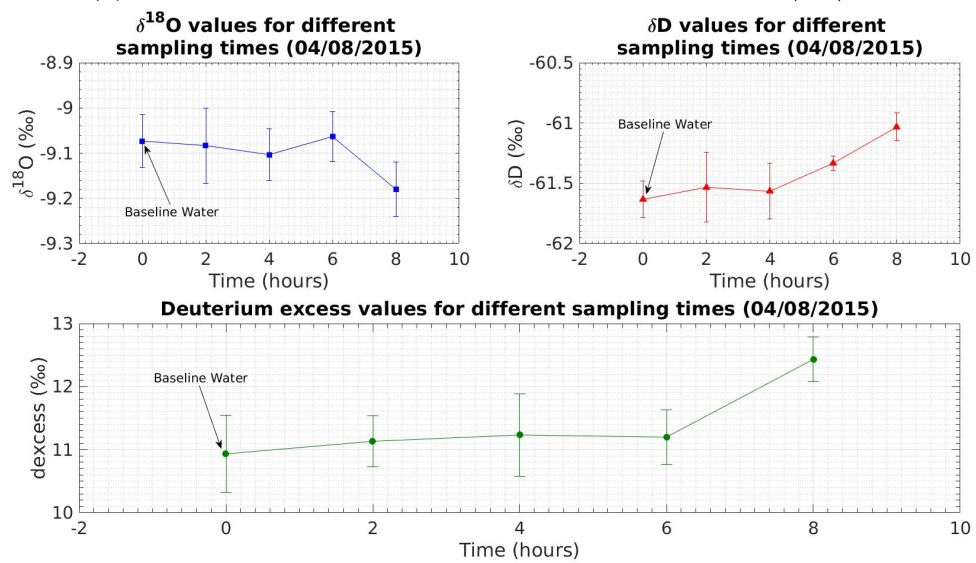
$\delta^{18}O_{(i)} - \delta^{18}O_{baseline}$ (‰)	$\delta D_{(i)} - \delta D_{baseline}$ (‰)
-0.01 ± 0.08	$+0.50 \pm 0.24$
$+0.07 \pm 0.10$	$+0.73 \pm 0.29$
$+0.08 \pm 0.08$	$+0.90 \pm 0.26$
$+0.11 \pm 0.09$	$+1.03 \pm 0.29$

Table 3.7: Change in the isotopic composition between baseline water and collected samples (04/08/2015)

$\delta^{18}O_{(i)} - \delta^{18}O_{baseline}$ (‰)	$\delta D_{(i)} - \delta D_{baseline}$ (‰)
-0.01 ± 0.10	$+0.10 \pm 0.33$
-0.03 ± 0.08	$+0.07 \pm 0.28$
$+0.01 \pm 0.08$	$+0.30 \pm 0.16$
-0.11 ± 0.08	$+0.60 \pm 0.19$



(a) Isotopic composition of the fractionation test for 30/07/2015



(b) Isotopic composition of the fractionation test for 04/08/2015

Figure 3.7: Fractionation test for two different dates using MQ water. Blue color corresponds to $\delta^{18}\text{O}$, red color to δD and green color to dexcess. Sampling took place approximately every two hours

4

Vapor Data Calibration and Processing

4.1 Humidity calibration

Humidity calibration refers to the investigation of the instrument's response and behavior when different concentrations of injected sample flow inside the optical cavity of a NIR-CRDS spectrometer. A water level of 17000-22000 ppm results in optimum performance of the instrument (7) and is the desired concentration one should try to inject with when using a NIR-CRDS for the isotopic analysis of a water sample. The aim of this project, though, is measuring the stable isotopes of atmospheric water vapor and this implies varying levels of humidity, ranging from 5000 ppm or lower during winter months until 25000 ppm or even higher during summer, depending on the prevailing weather system and whether it brings moist or drier air. It is important, therefore, always to correct our measurements for possible fluctuations of injected sample and avoid instrumental drifts due to variability in atmospheric humidity.

4.1.1 Data acquisition

The humidity calibration is performed by injecting water of different humidity levels inside the optical cavity of the spectrometer. The sample used for this purpose is Milli-Q water injected from a 2 liter glass bottle by tuning a peristaltic pump and thus forcing the injected sample that enters the optical cavity to change in terms of water concentration.

As described in section 3.2, the sample flows through the 40 μm silica capillary into the oven where it is instantly vaporized (immediate evaporation is of high importance if we want to avoid isotopic fractionation effects). Finally, the sample (vapor)

enters into the optical cavity of the two instruments and its isotopic composition is measured.

Investigation of the system's response to different humidity levels is made by changing the water concentration in 14 steps, ranging from 5 to 23 kppm. Total experiment time is approximately 120 minutes and subsections of these intervals (≈ 10 min) are chosen according to their quality and stability (Figure 4.1). The basic criterion for the selection of these subsections is the stability of water concentration for each one of the steps. We see, though, that water concentration for the 12th step (≈ 21300 ppm) is not so stable, a situation most likely related with the capillary and how well it is connected to the oven.

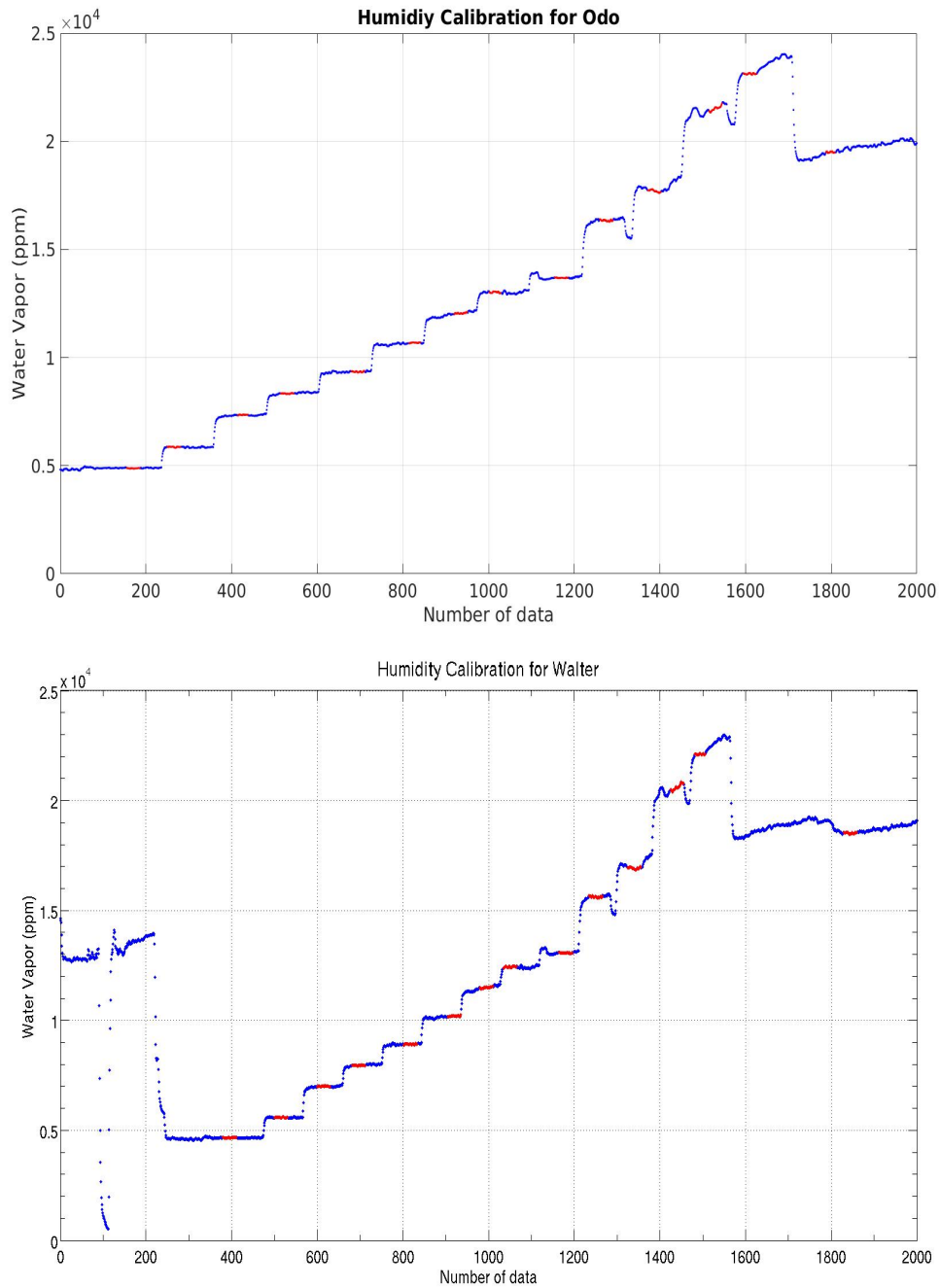


Figure 4.1: Water concentration for the humidity calibration of the two spectrometers (Odo and Walter). Red color corresponds to the selected intervals of each humidity step.

Differences in the mean isotopic composition of the different steps are revealed if we plot the mean δ values of the selected sections as a function of the different humidity levels. Calculation of the difference between the mean values for the lower and higher levels of injected water gives the following results:

$$\begin{aligned}\delta^{18}O_{Odo(13-1)} &= +0.79 \pm 0.56\text{‰} & \delta^{18}O_{Walter(13-1)} &= +1.50 \pm 0.35\text{‰} \\ \delta D_{Odo(13-1)} &= +2.92 \pm 8.09\text{‰} & \delta D_{Walter(13-1)} &= +8.88 \pm 2.01\text{‰}\end{aligned}$$

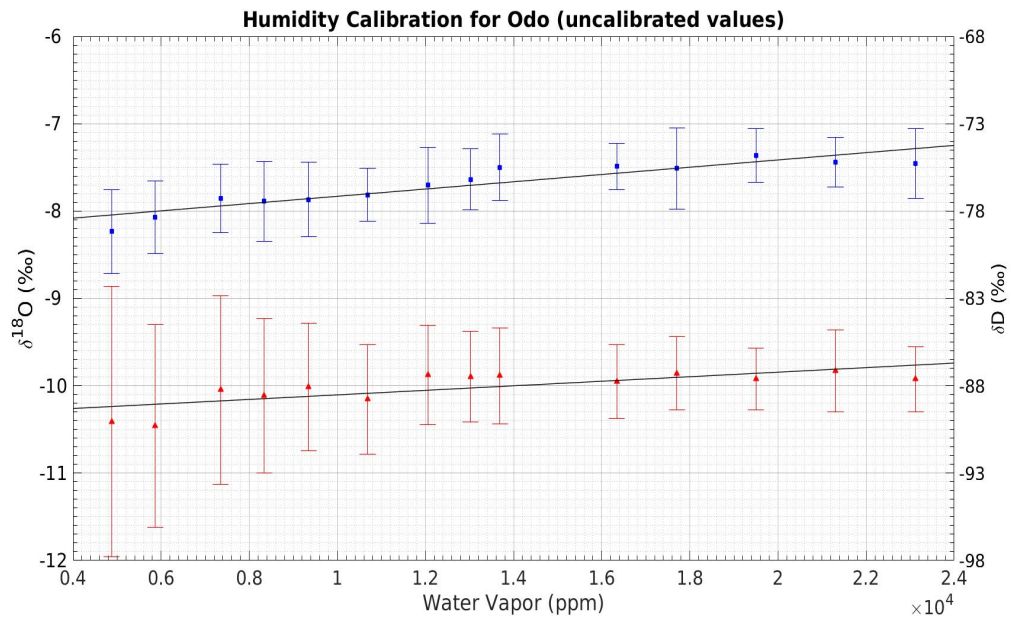
where the subscripts in the equations refer to the two different instruments (Odo or Walter) and the numbers (1 and 13) correspond to the two steps with the lower and higher humidity concentrations, respectively.

During this humidity calibration there were taken 14 different steps and the highest humidity corresponds to step 13 (Figure 4.1). This happened due to the over tuning of the peristaltic pump from step 11 and while trying to reach the next humidity level (step 14 in the plot), resulting in a flow higher than the desired vapor concentration inside the optical cavity (step 12 in the plot). Finally, concentration corresponding to step 14 was achieved by reducing the flow through the peristaltic pump from step 13 to step 14 as seen in Figure 4.1.

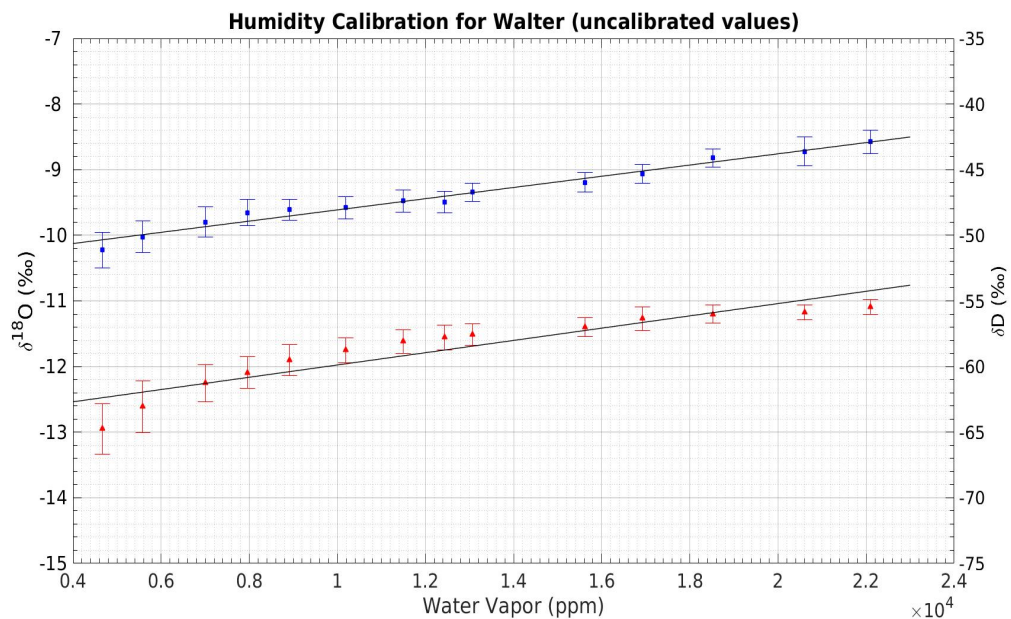
Based on these values, we can see the instruments' different response in terms of mean isotopic values when different concentrations of water sample are injected in the optical cavity. This behavior is present not only for the lower and higher humidity levels, but for all different humidity steps. Looking at Figure 4.2 this becomes obvious since the mean isotopic values for $\delta^{18}O$ and δD measured for lower humidities are isotopically lighter and they gradually become heavier as humidity increases. From the fitted curves at the same figure, we observe an overall linear response of $\delta^{18}O$ for Odo to different water levels and a linear response of δD for the mid-high humidity area. Linearity breaks for the low humidity area for this instrument (below ≈ 7 kppm). On the other hand, Walter displays a generally more non-linear behavior and this can be clearly seen for the low humidity levels for both $\delta^{18}O$ and δD . Nonlinearity is also present for δD at the mid humidity area (8-15kppm).

One thing that is worth paying attention to, is the difference of the mean isotopic values between the two instruments and the standard deviations we get between the lowest and highest humidity level. Odo measures 0.79‰ higher value for $\delta^{18}O$ and 2.92‰ for δD while Walter measures 1.50‰ and 8.88‰ higher values for $\delta^{18}O$ and δD , respectively. From this point of view, Odo appears to be less affected than Walter when humidity levels change; on the other hand Walter depicts smaller standard deviations for all humidity levels and for both isotopic species, as seen from the error bars of the two plots of figure 4.2. Results from Aemisegger et al. (2012) (although experiments performed with a model L1115-i which corresponds to a more recent

and advanced spectrometer) show that the inherent precision of the instrument is dependent on water vapor mixing ratio. Higher measurement uncertainties are found for lower water vapor levels inside the optical cavity, a conclusion consistent with our results.



(a) Mean isotopic values for the different humidity levels (Odo)



(b) Mean isotopic values for the different humidity levels (Walter)

Figure 4.2: Averages of the mean raw values of isotopic composition for the two instruments. Squares correspond to $\delta^{18}\text{O}$ and triangles to δD . Data are fitted with a first-order polynomial fit (solid black lines). The error bars represent $\pm 1\sigma$.

4.1.2 The linear section of humidity levels

As mentioned in the previous section, possible fluctuations of the atmospheric vapor levels will inevitably affect our measurements. In order to correct the measured isotopic composition of the atmospheric vapor we select the relatively linear area between 12 and 24 kppmv and we apply a linear fit on the data, as shown in Figure 4.3 and 4.4 for $\delta^{18}\text{O}$ and δD , respectively. For each humidity level we can calculate the humidity correction term, $\Delta\delta_{\text{hum}}$, which will be derived from the equation (7):

$$\Delta\delta_{\text{hum}} = \lambda(R_{20} - 1) \quad (4.1)$$

where $R_{20} = ([\text{H}_2\text{O}]_{\text{ppmv}})/(20.000_{\text{ppmv}})$ and λ is the slope of the linear fit applied on the data points between 12 and 24 kppmv. The values of the estimated slopes are shown in the following Table 4.1.

Table 4.1: Slopes of the linear fit for the two instruments

	λ_{18}	λ_D
Odo	0.4244	-0.0165
Walter	1.7891	+4.9491

We notice that the slopes for the two instruments are different, with Odo having a slightly negative slope for deuterium. Calculated slopes for Walter are comparable with the values from a previous study (1.94 ‰ and 3.77 ‰ for λ_{18} and λ_D respectively) (7). From Figures 4.3 and 4.4 we also notice that measured values for both isotopologues for Odo exhibit a smaller range compared to the ones for Walter. Uncertainties on the measurements are much smaller for Walter (almost half or even lower for both isotopic species) for all humidity steps (both in the linear and the non linear section of the humidity area).

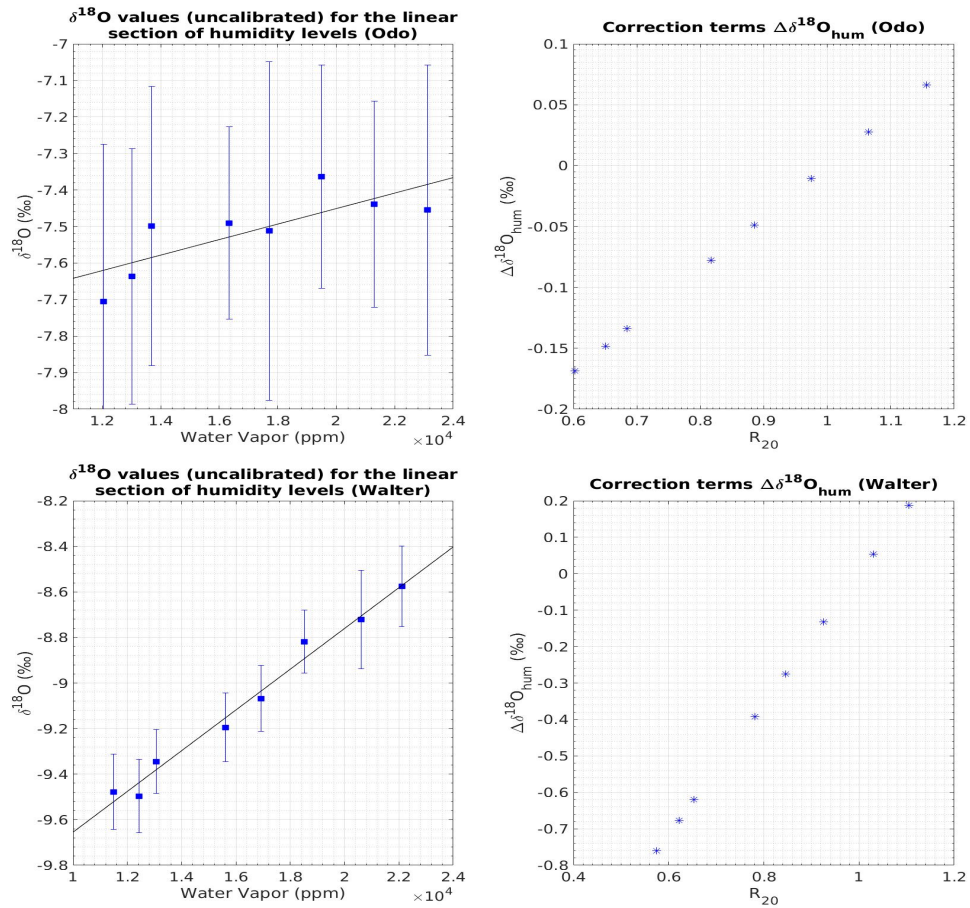


Figure 4.3: Linear section of humidity calibration for the two instruments, Odo (top) and Walter (bottom). Mean values of $\delta^{18}\text{O}$ are plotted as squares for each humidity level. Linear fit is shown as solid black line. Error bars represent $\pm 1\sigma$ for each section. Correction terms are shown as stars.

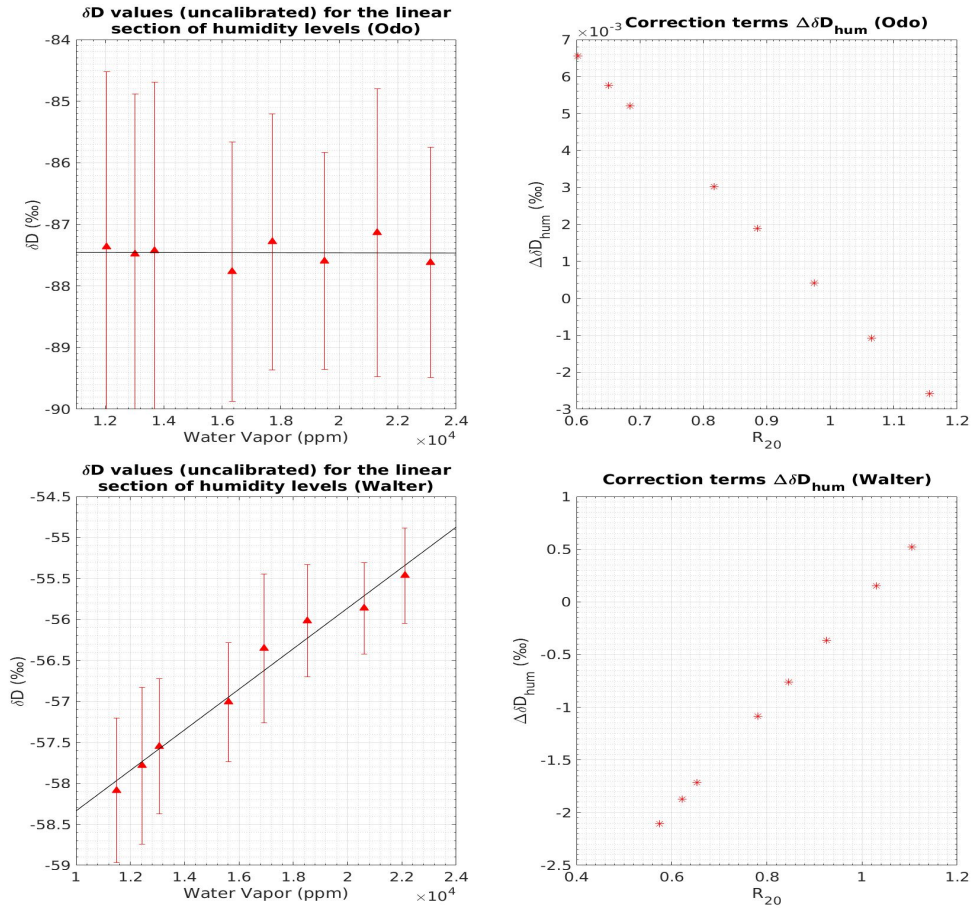


Figure 4.4: Linear section of humidity calibration for the two instruments, Odo (top) and Walter (bottom). Mean values of δD are plotted as triangles for each humidity level. Linear fit is shown as solid black line. Error bars represent $\pm 1\sigma$ for each section. Correction terms are shown as stars. Notice the different magnitude for the correction factors of δD for Odo.

4.1.3 Correction of the data for varying humidity levels using a linear regression

Correction of the raw values can take place if we take into account the humidity correction factors that correspond to the various levels of water concentration. We have to mention that our reference values for $\delta^{18}\text{O}$ and δD correspond to the mean values measured for water concentration of approximately 20 kppm. The following equations are used to calculate the calibrated values of the two isotopic species:

$$\begin{aligned}\delta^{18}O_{humcal(i)} &= \delta^{18}O_{raw(i)} - \Delta\delta^{18}O_{hum(i)} \\ \delta D_{humcal(i)} &= \delta D_{raw(i)} - \Delta\delta D_{hum(i)}\end{aligned}\tag{4.2}$$

where $\delta^{18}\text{O}_{\text{humcal}}$ and $\delta\text{D}_{\text{humcal}}$ are the calibrated values, $\delta^{18}\text{O}_{\text{raw}}$ and $\delta\text{D}_{\text{raw}}$ are the raw (measured) values and subscript (i) refers to one of the humidity steps taken into the linear section of water concentration. Notice that the humidity correction factors, according to the way they were calculated, are lower than zero for water concentration lower than the reference value of 20 kppm and higher than zero for water concentration higher than the reference value (see Figure 4.3 and 4.4) and this is why we are subtracting them from the raw values when we use equations 4.2. This way, for water concentration lower than the reference value we are subtracting a negative quantity (moving the raw isotopic measurements towards the less negative reference isotopic values) and for water concentration higher than the reference value we end up subtracting a positive quantity (thus moving the raw isotopic measurements towards the more negative reference isotopic values).

Corrected values for the linear section of the different humidity steps are shown in Figures 4.3 and 4.4. We observe that the calibrated isotopic values of the two instruments are now closer to the reference values of $\delta^{18}\text{O}$ and δD for the 20 kppm (reference humidity) and the correction is more obvious for both isotopic species when calibration is performed for Walter.

Using equations 4.2 for calculating the humidity factors for the whole range of humidity levels, results in correction of the values for all 14 different steps, as shown in Figure 4.5. Comparison between the values before (Figure 4.2) and after the calibration shows that corrections related with the instruments' response in different levels of injected water should always be taken into account. The correction seems to work better for the higher humidity levels (above $\approx 12\text{kppm}$) and especially for $\delta^{18}\text{O}$; linearity seems to break for the lower humidity levels and becomes quite obvious especially for δD . Further investigation is needed and a possible correction that works better for the low humidities might be necessary in order to correct the raw values for this section.

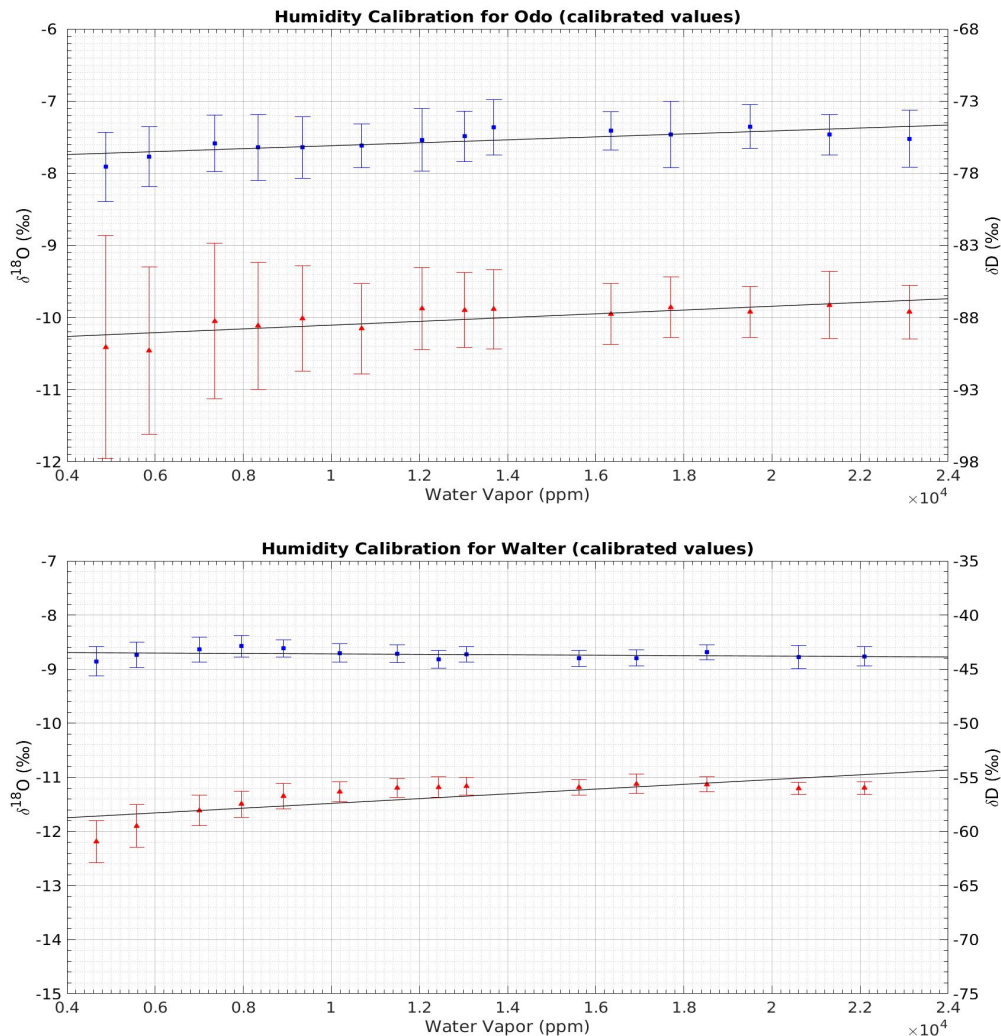


Figure 4.5: Averages of the mean calibrated values for the two instruments after taking into account the humidity correction factors. Squares correspond to $\delta^{18}\text{O}$ and triangles to δD . Data are fitted with a first-order polynomial fit (solid black lines). The error bars represent $\pm 1\sigma$.

4.1.4 Correction of the data for varying humidity levels using a 3rd order polynomial fit

In order to correct our instruments' response at the non-linear area of the low humidity levels and compare the correction with the one performed based on the linear fit, we apply a 3rd order polynomial fit on our data, as shown in Figure 4.6. We choose again 20 kppm as the reference value of water concentration due to the fact that this value lies deep inside the linear area and because the ability of the spectrometers to measure the isotopic composition of the injected sample becomes optimal around

this concentration. The method used this time is similar to the one followed for the correction based on the linear fit, but now we do not calculate the slope and intercept of a straight line but the coefficients of a third order polynomial fitting applied to the whole range of humidities (all 14 different steps). The reason that we do not choose a specific region of humidities, as we did for the linear fitting before, is that now our 3rd order fitting works better when applied to all data compared to the linear fitting that worked satisfying only if we took the higher water vapor values. The general form of the polynomial fitting is:

$$P(x) = ax^3 + bx^2 + cx + d \quad (4.3)$$

where a, b, c and d are the coefficients of the polynomial.

Based on this equation we get for our data the following set of equations:

$$\begin{aligned} \delta^{18}O_{(i)} &= a_1X_{(i)}^3 + b_1X_{(i)}^2 + c_1X_{(i)} + d_1 \\ \delta D_{(i)} &= a_2X_{(i)}^3 + b_2X_{(i)}^2 + c_2X_{(i)} + d_2 \end{aligned} \quad (4.4)$$

where the subscript i refers to one of the 14 humidity steps and X to the mean water vapor for the i section. Equation 4.4 applies for both instruments.

The humidity correction factors are now calculated from the equation:

$$\Delta\delta_{hum} = a(X_{(i)}^3 - X_{(ref)}^3) + b(X_{(i)}^2 - X_{(ref)}^2) + c(X_{(i)} - X_{(ref)}) \quad (4.5)$$

where $X_{(i)}$ refers to the mean water vapor concentration for each one of the 14 humidity steps and $X_{(ref)}$ is equal to 20 kppm.

The humidity correction factors calculated for both instruments and for all 14 steps are shown in the following Figures 4.7 and 4.8. In order to correct our raw data we now use the following system of equations:

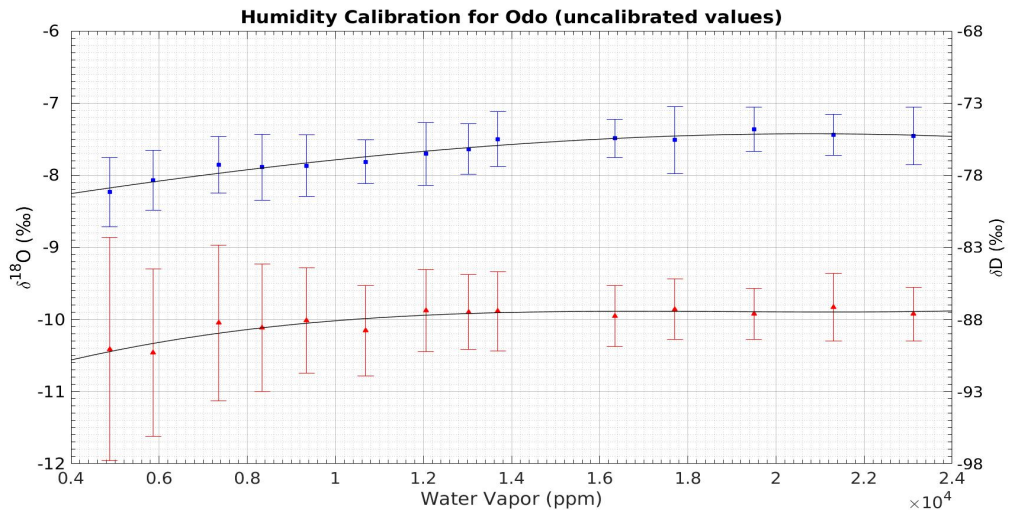
$$\begin{aligned} \delta^{18}O_{humcal(i)} &= \delta^{18}O_{raw(i)} + \Delta\delta^{18}O_{hum(i)} \\ \delta D_{humcal(i)} &= \delta D_{raw(i)} + \Delta\delta D_{hum(i)} \end{aligned} \quad (4.6)$$

where $\delta^{18}O_{humcal}$ and δD_{humcal} are the calibrated values, $\delta^{18}O_{raw}$ and δD_{raw} are the raw (measured) values and subscript (i) refers to the number of the humidity step.

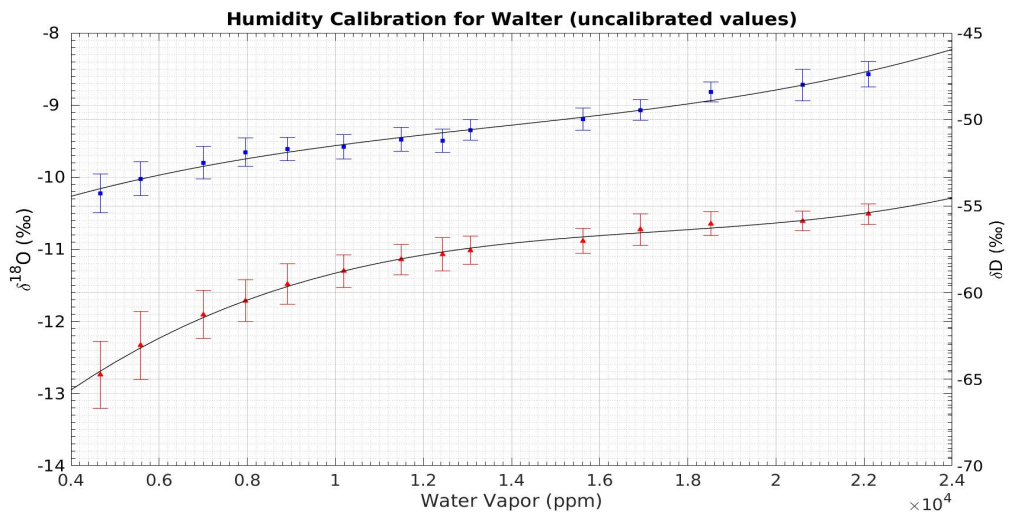
Notice that based on equation 4.5, $\Delta\delta_{\text{hum}}$ are positive for most of the humidity levels (see Figures 4.7 and 4.8) and as a result they need to be added at the raw values.

Our corrected raw data and results are shown in Figures 4.7 and 4.8. Overview of the humidity calibration for both isotopic species of the two instruments with the 3rd order polynomial fit is presented in Figure 4.9.

We see that the fitting is now better than before and the correction for the lower humidity levels seems to improve our calibrated values, bringing them closer to the isotopic values that correspond to the optimal concentration of 20 kppm. Comparison between the two methods of humidity calibration and the effect they have when applied on the raw measurements of the vapor will be given in next chapter.



(a) Mean isotopic values for the different humidity levels (Odo)



(b) Mean isotopic values for the different humidity levels (Walter)

Figure 4.6: Averages of the mean isotopic values (raw) as measured for the same water by the two instruments. Squares correspond to $\delta^{18}\text{O}$ and triangles to δD . Data are fitted with a third-order polynomial fit (solid black lines). The error bars represent $\pm 1\sigma$.

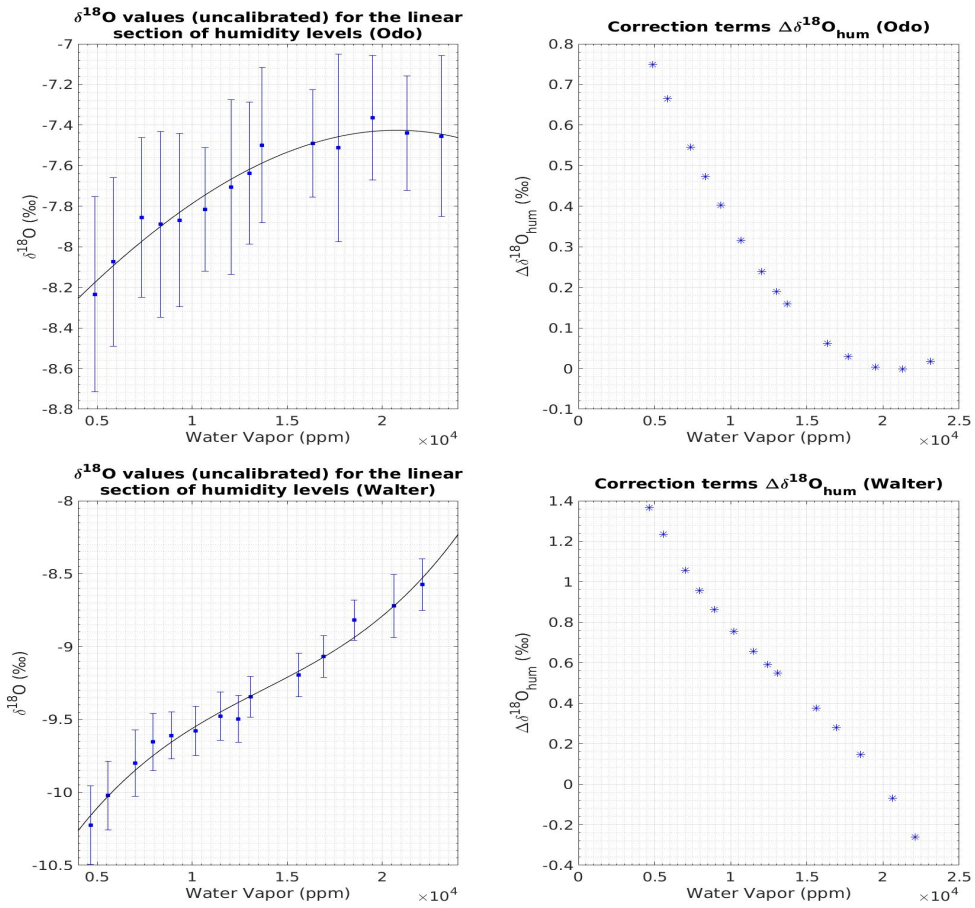


Figure 4.7: Humidity correction factors for the two instruments, Odo (top) and Walter (bottom), calculated with the 3rd order polynomial fitting shown as solid black line. Mean values of $\delta^{18}\text{O}$ are plotted as squares for each humidity level. Error bars represent $\pm 1\sigma$ for each section. Correction terms are shown as stars.

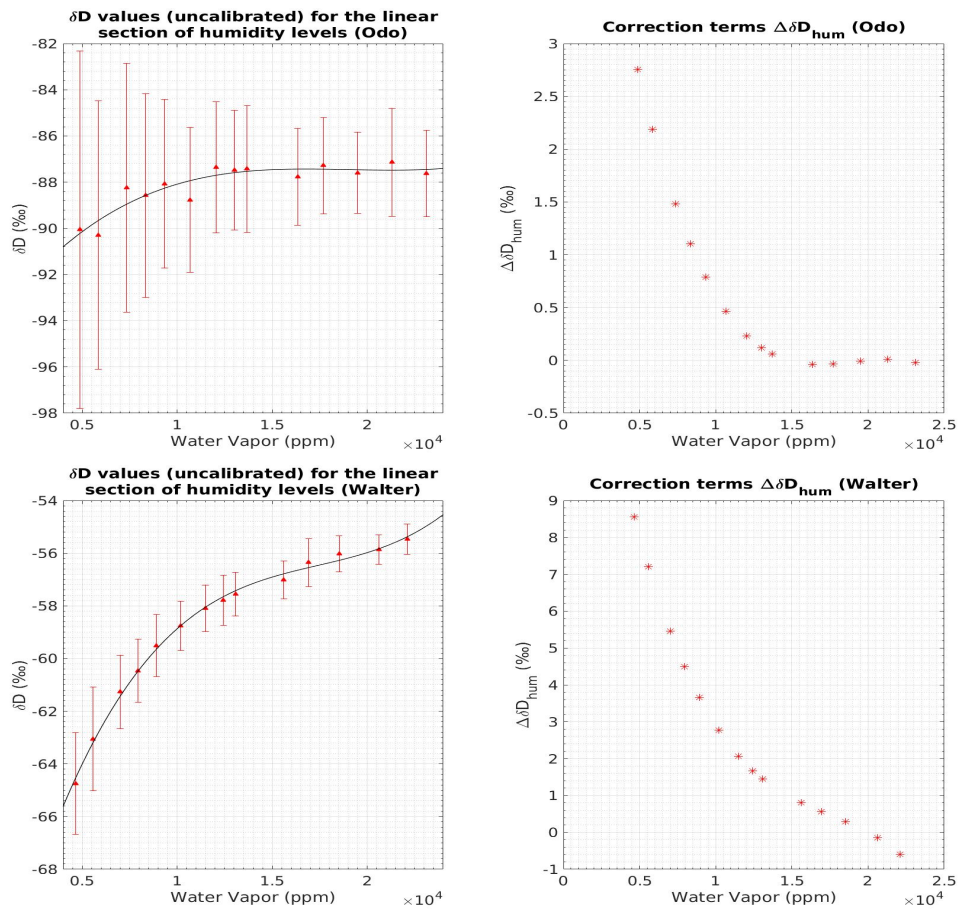


Figure 4.8: Humidity correction factors for the two instruments, Odo (top) and Walter (bottom), calculated with the 3rd order polynomial fitting shown as solid black line. Mean values of δD are plotted as triangles for each humidity level. Error bars represent $\pm 1\sigma$ for each section. Correction terms are shown as stars.

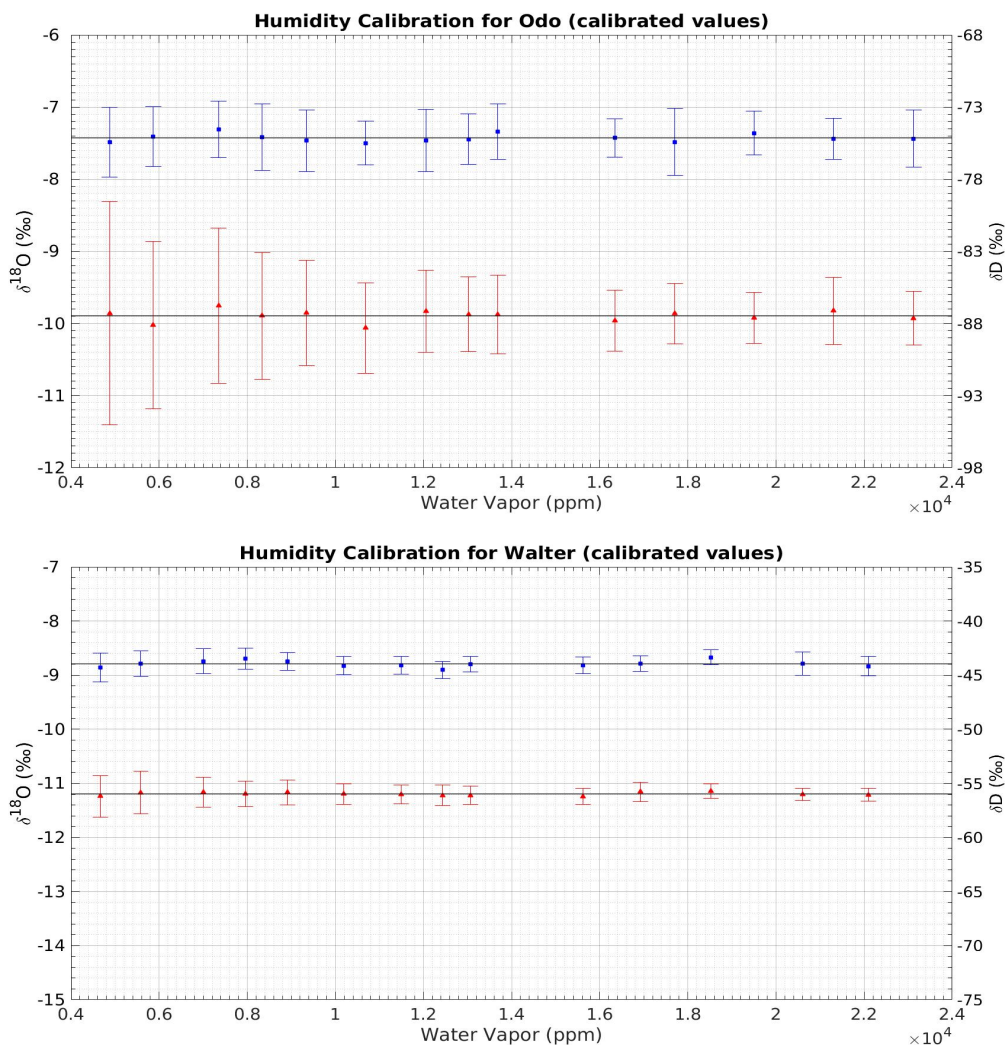


Figure 4.9: Averages of the mean isotopic values (calibrated) after taking into account the 3rd order humidity correction factors. Squares correspond to $\delta^{18}\text{O}$ and triangles to δD . Data are fitted with a first-order polynomial fit (solid black lines). The error bars represent $\pm 1\sigma$.

4.2 Calibration with standards

Reporting of water isotopic measurements requires a proper calibration based on international standards. Calibrating the results using a globally accepted water standard secures that all laboratories are using the same scale and this helps eliminate any possible instrumental drift that may exist due to intrinsic variabilities of the instrument's function.

The International Atomic Energy Agency (IAEA) distributes worldwide the Vi-

enna Standard Mean Ocean Water (VSMOW) and the Standard Light Antarctic Precipitation (SLAP); these are the standard waters used to calibrate the results and based on these waters laboratories around the world can produce their own local standards according to the needs of their measurements.

4.2.1 Run with 3 standards: VSMOW-SLAP calibration (Odo)

In the following experiment we used a set of 3 local standards of different isotopic composition that have been precisely measured at Center for Ice and Climate, University of Copenhagen, with respect to the VSMOW-SLAP scale. We chose sections of approximately 30 data points ($\approx 3\text{min}$) for each one of the standards. Our first choice of sections is based on the quality (stability of vapor concentration for each standard and small fluctuation of the $\delta^{18}\text{O}$ and δD values); the second group of selected sections takes into account also the fact that we want to avoid any possible memory effects that might appear when we change the valve and inject different waters. This is why we chose data points that lie at the end of the corresponding measured standard the second time. Sections that were selected and used for the two calibrations are shown in Figure 4.10. The NEEM standard is used to check the offset between the fit and the measured value for each one of the two calibrations (6). If the offset is less than the spectrometer's precision, the calibration is valid. The mean values of the selected sections are presented in Tables 4.2 and 4.3.

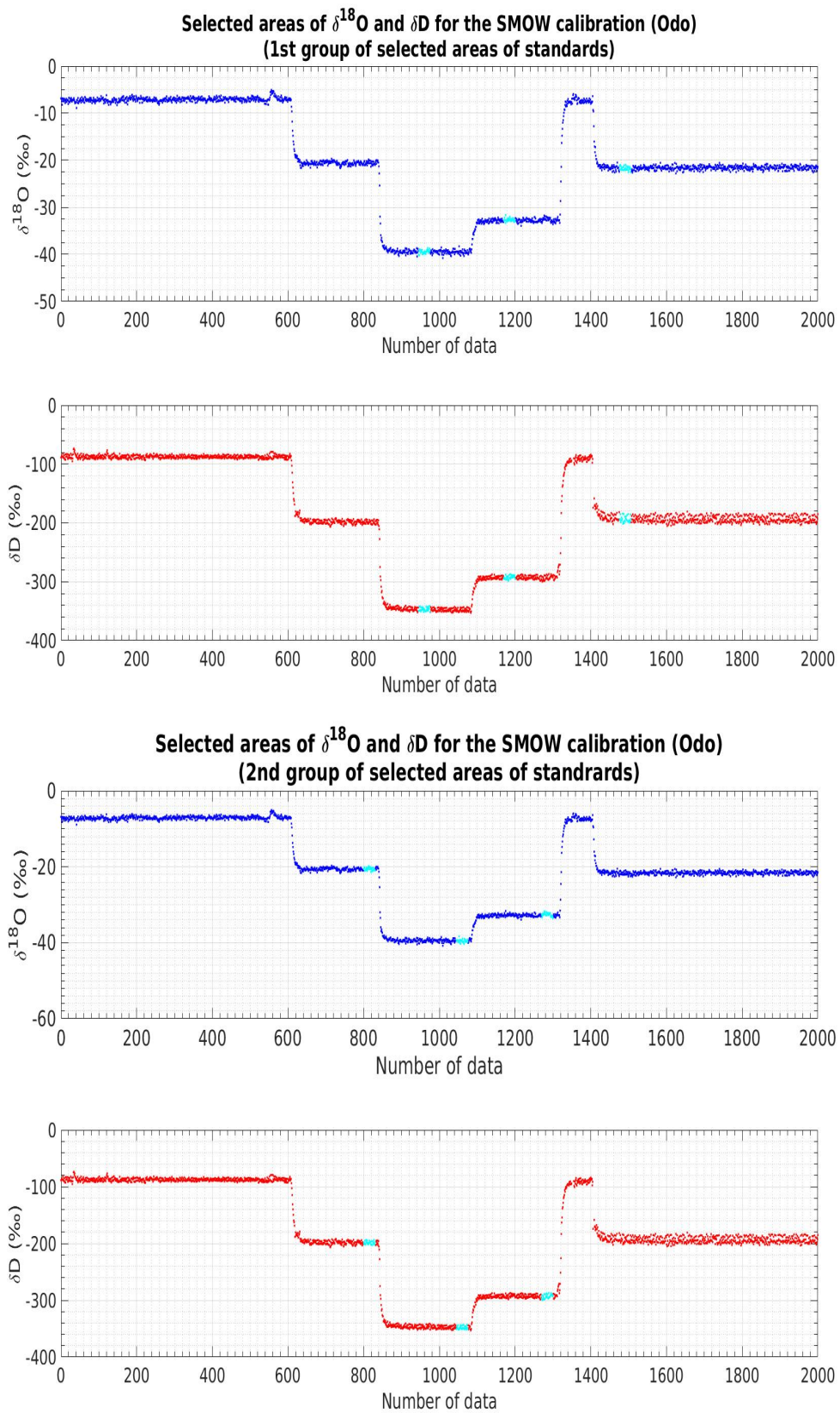


Figure 4.10: Comparison between the selected areas for calibration with 3 standards. Blue color corresponds to $\delta^{18}\text{O}$ and red color to δD . Cyan highlighted areas refer to the selected sections of $\delta^{18}\text{O}$ and δD .

Table 4.2: Isotopic values of the local standards as measured by Odo (1st group of selected areas)

Standard ID	$\delta^{18}O_{real}$ (‰)	$\delta^{18}O_{meas}$ (‰)	δD_{real} (‰)	δD_{meas} (‰)
-22	-21.88 ± 0.06	-21.19 ± 0.41	-168.45 ± 0.09	-192.38 ± 5.03
NEEM	-33.50 ± 0.03	-32.51 ± 0.44	-257.45 ± 0.20	-293.26 ± 3.57
-40	-39.98 ± 0.08	-39.51 ± 0.40	-311.11 ± 0.35	-348.16 ± 2.72

Table 4.3: Isotopic values of the local standards as measured by Odo (2nd group of selected areas)

Standard ID	$\delta^{18}O_{real}$ (‰)	$\delta^{18}O_{meas}$ (‰)	δD_{real} (‰)	δD_{meas} (‰)
-22	-21.88 ± 0.06	-20.67 ± 0.38	-168.45 ± 0.09	-198.60 ± 3.17
NEEM	-33.50 ± 0.03	-32.66 ± 0.33	-257.45 ± 0.20	-292.45 ± 2.88
-40	-39.98 ± 0.08	-39.43 ± 0.38	-311.11 ± 0.35	-347.01 ± 2.99

If we plot the real against the raw (measured) values (Figure 4.18), we can calculate the slope and intercept found by linear regression and described by the equation:

$$\delta_{vsmow(Odo)} = \alpha_{vsmow(Odo)} \cdot \delta_{measured(Odo)} + b_{vsmow(Odo)} \quad (4.7)$$

where $\alpha_{vsmow(Odo)}$ is the slope of the straight line and for our experiment is equal to:

$$\alpha_{vsmow(Odo)} = \frac{\delta_{real(-22)} - \delta_{real(-40)}}{\delta_{measured(-22)} - \delta_{measured(-40)}} \quad (4.8)$$

and $b_{vsmow(Odo)}$ is the intercept of the straight line.

The calculated VSMOW-SLAP coefficients are shown in Table 4.4. Notice that a humidity calibration has been performed (as described in previous section) before any other data processing in order to correct instrumental drifts related with the water concentration inside the optical cavity.

Comparison between the two groups of selected areas reveals the importance of always carefully selecting sections that take into account the memory effect on the

measured isotopic composition when we inject different standards. This can be seen from the offsets of $\delta^{18}\text{O}$ and δD (Table 4.5) that are calculated for the middle (NEEM) standard the two calibrations. We see that for the first case of selected areas which refers to data points pretty much found in the middle of the 3 measured standards (Figure 4.11, 1st and 2nd plot from the top) the offset is -0.43‰ and $+3.38\text{‰}$ for $\delta^{18}\text{O}$ and δD , respectively. These values are much higher than the precision of the spectrometer and the calibration curve can not be considered valid. When the selected sections of data points are located towards the end of each measured standard (Figure 4.11, 3rd and 4th plot from the top) we see that the offset is now -0.06‰ and $+1.21\text{‰}$ for $\delta^{18}\text{O}$ and δD , respectively. Although the value for δD is higher again than the instrumental precision, it is clearly better than the previous one; for $\delta^{18}\text{O}$ the value of the offset is now below the precision of the spectrometer. As a result, the coefficients calculated for the 2nd case will be used for the rest of this project to calibrate our data with respect to the SMOW-SLAP scale.

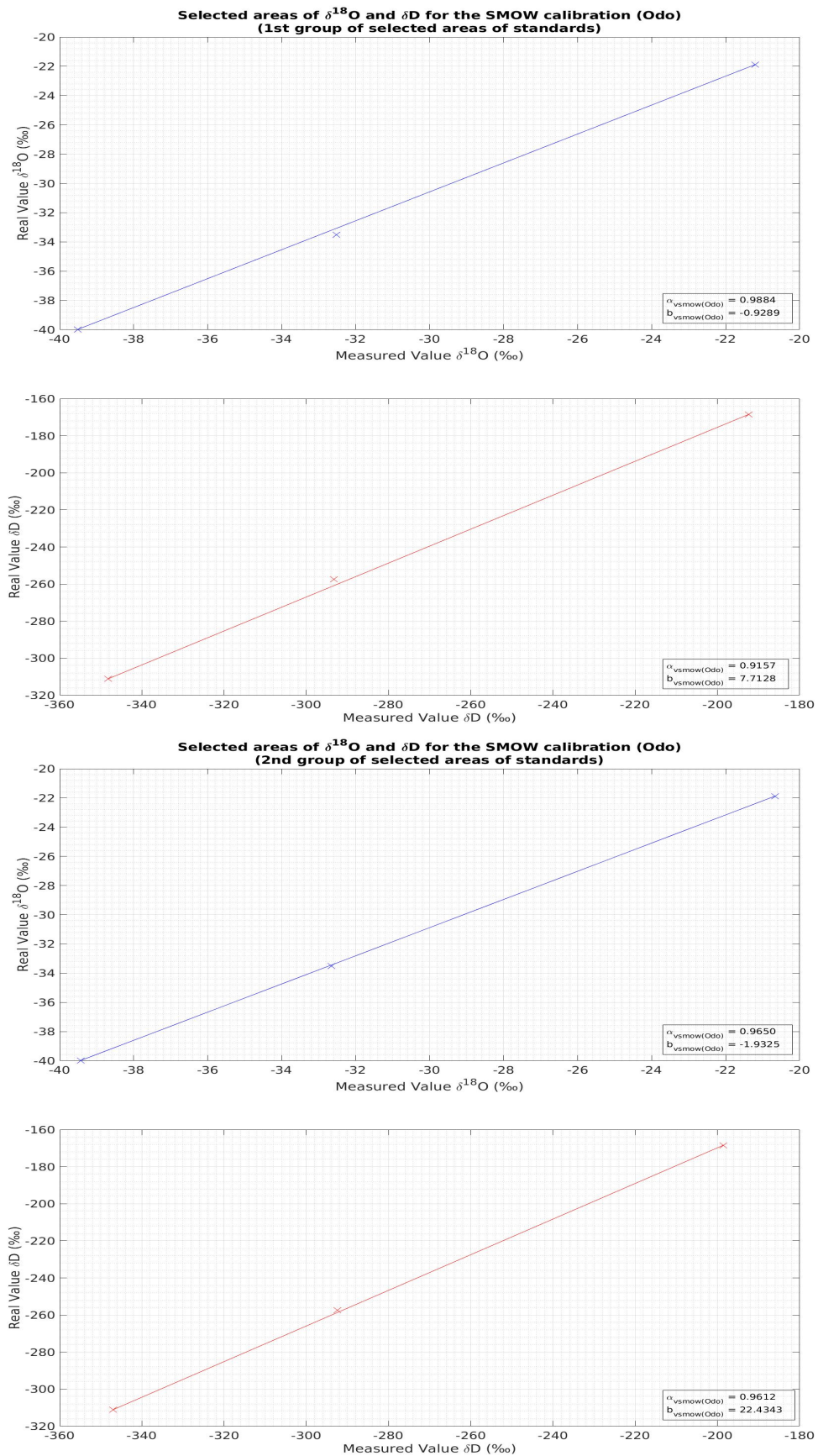


Figure 4.11: Calibration with 3 standards for Odo. Blue color corresponds to $\delta^{18}\text{O}$ and red color to δD . The Xs mark the value of the three standards.

Table 4.4: Coefficients of the SMOW calibration for Odo

	Number of Calibration	Slope	Intercept
$\delta^{18}O$	01	0.99	-0.93
	02	0.97	-1.93
δD	01	0.92	7.71
	02	0.96	22.43

Table 4.5: Offset of the NEEM standard for the two calibrations for Odo

NEEM	Number of Calibration	Offset (%)
$\delta^{18}O$	01	-0.43
	02	-0.06
δD	01	+3.38
	02	+1.21

4.2.2 Run with 2 waters: VSMOW-SLAP calibration (Walter)

Calibration of Walter on the VSMOW-SLAP scale differs from the one that was made for Odo and in some way can be characterized as "indirect". The method used for calibrating Walter's raw measurements is similar to the procedure followed for producing local standards that are calibrated based on the small quantity of the Vienna Standard Mean Ocean Water and the Standard Antarctic Light Precipitation distributed by IAEA. The absence of more than one directly measured and locally produced standards of known isotopic composition, as used for calibrating the raw data of Odo (i.e. -22, NEEM and -40), restricts our capability of performing a direct calibration of Walter's raw measurements based on these standards. The basic idea of calibrating data for Walter can be summarized on the following two steps: first we use the slope and intercept from the previous experiment (see Table 4.4) to calibrate two different waters (injected simultaneously for both instruments) for Odo. At the second step these calibrated values will be used as the real ones in order to correct Walter's raw measurements on the VSMOW-SLAP scale.

The values for the samples of different isotopic composition that were measured are shown in Table 4.6. Each sample was measured simultaneously by the two

spectrometers, the first one at 01/09/2015 and the second at 09/09/2015. Areas of ≈ 20 minutes were selected for each sample in order to perform the correction at the VSMOW-SLAP scale for Odo, as previously described as the first step. Selected areas are shown in Figure 4.12 and their mean values in Table 4.6.

The next step is to plot at the same graph the raw values as measured by Walter (X-axis of the plot) and the VSMOW-SLAP calibrated values of Odo as the real ones (Y-axis of the plot) as seen at the following Figure 4.14.

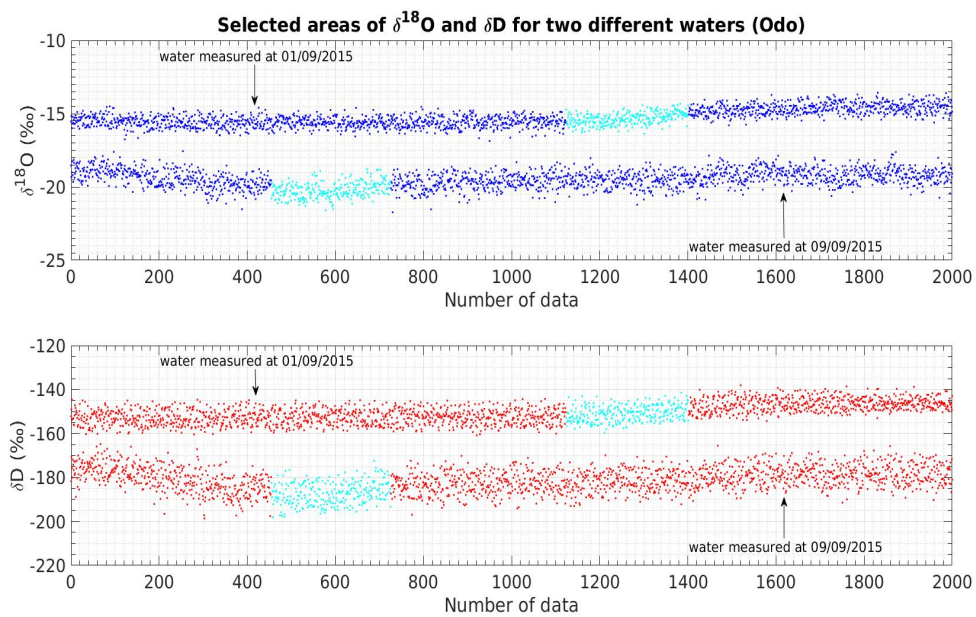


Figure 4.12: Selected areas for calibration of Walter using two different waters. Blue color corresponds to $\delta^{18}\text{O}$ and red color to δD . Cyan highlighted areas refer to the selected sections of $\delta^{18}\text{O}$ and δD as chosen for Odo for the two different dates.

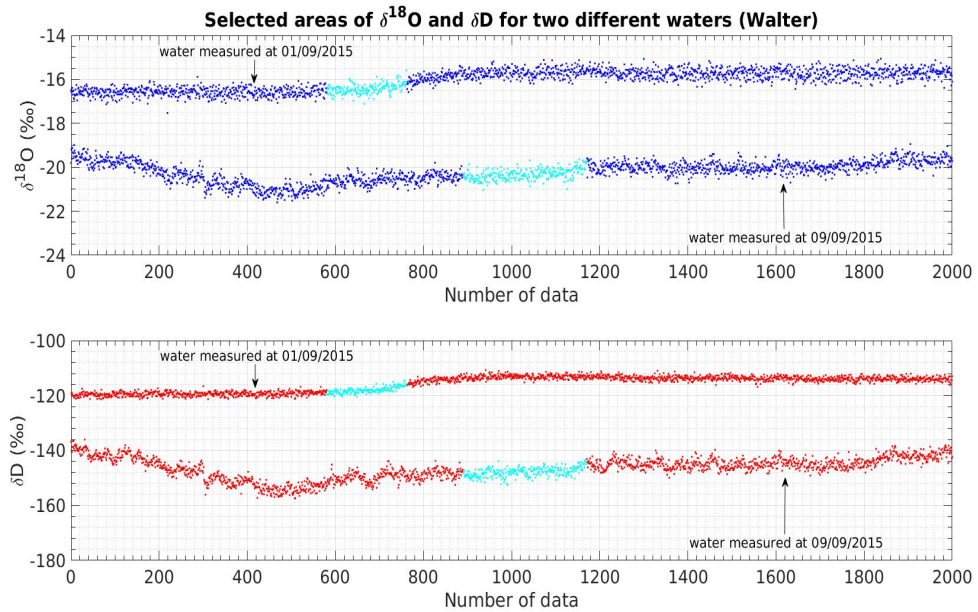


Figure 4.13: Selected areas for calibration of Walter using two different waters. Blue color corresponds to $\delta^{18}\text{O}$ and red color to δD . Cyan highlighted areas refer to the selected sections of $\delta^{18}\text{O}$ and δD as chosen for Walter for the two different dates.

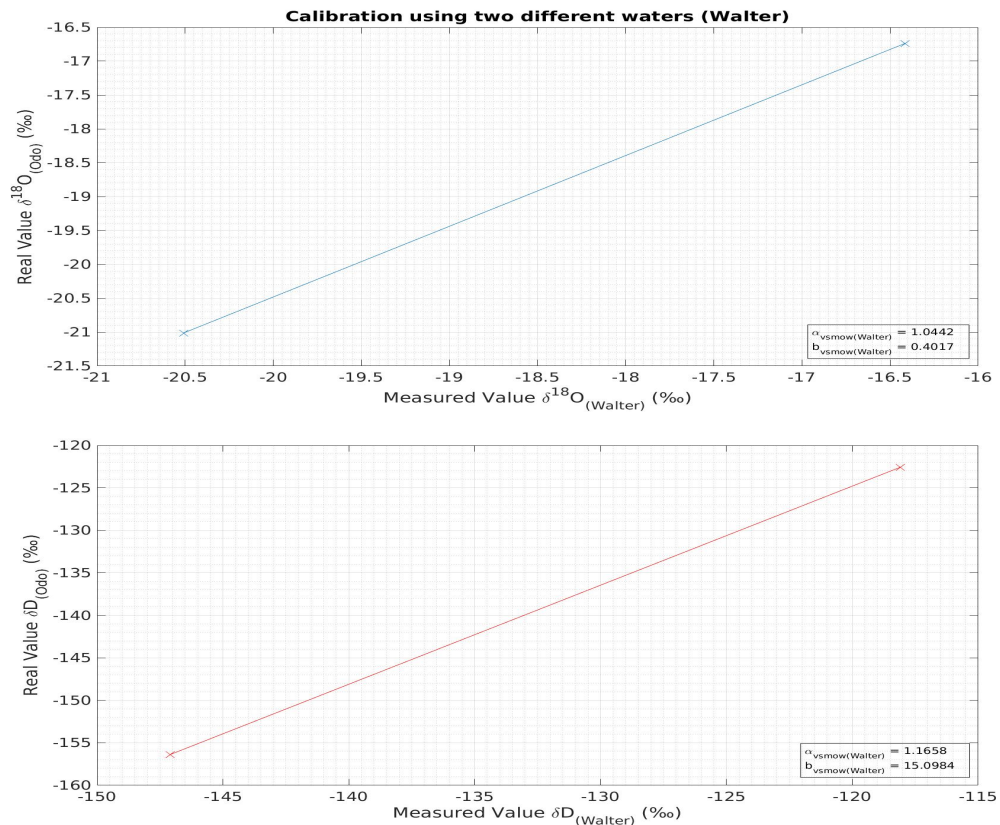


Figure 4.14: Calibration with 2 different waters for Walter. Blue color corresponds to $\delta^{18}\text{O}$ and red color to δD . Marked with X are the values for the two samples.

Values on the VSMOW-SLAP scale for Odo are calculated using the equation 4.3, now written as:

$$\delta_{vsmow(Odo)} = \alpha_{vsmow(Odo)} \cdot \delta_{meas(Odo)} + b_{vsmow(Odo)} \quad (4.9)$$

where $\alpha_{vsmow(Odo)}$ and $b_{vsmow(Odo)}$ are again the slope and intercept for $\delta^{18}O$ and δD and their values can be found in Table 4.4.

The coefficients for Walter can be derived by the equation:

$$\delta_{vsmow(Walter)} = \alpha_{vsmow(Walter)} \cdot \delta_{meas(Walter)} + b_{vsmow(Walter)} \quad (4.10)$$

where

$$\alpha_{vsmow(Walter)} = \frac{\delta_{real(sample2)} - \delta_{real(sample1)}}{\delta_{measured(sample2)} - \delta_{measured(sample1)}} \quad (4.11)$$

and $b_{vsmow(Walter)}$ is the intercept of the straight line. The values of the slope and intercept for Walter are shown at Table 4.7.

Table 4.6: Isotopic values of the samples used to calibrate Walter as measured by Odo.

Sample	$\delta^{18}O_{real(Odo)}$ (‰)	$\delta^{18}O_{meas(Odo)}$ (‰)	$\delta D_{real(Odo)}$ (‰)	$\delta D_{meas(Odo)}$ (‰)	$\delta^{18}O_{meas(Walter)}$ (‰)	$\delta D_{meas(Walter)}$ (‰)
Sample 1	-16.74	-15.34 ± 0.40	-122.58	-150.85 ± 3.55	-16.42 ± 0.22	-118.09 ± 1.12
Sample 2	-21.01	-19.78 ± 0.35	-156.38	-187.01 ± 4.90	-20.51 ± 0.22	-147.09 ± 1.52

Table 4.7: Coefficients of the SMOW calibration for Walter

	Slope	Intercept
$\delta^{18}O$	1.04	0.40
δD	1.17	15.10

4.3 Vapor data processing

Processing of vapor data was a quite demanding issue and it was made in 5 steps, as described in the following paragraphs. Total number of data points for Odo were (2905802) and for Walter (1523209). Difference in the number of data points acquired by the two instruments is primarily due to the fact that Odo measured for 45 days more than Walter and secondly because the two spectrometers are characterized by different acquisition times, approximately 4s and 6s for Odo and Walter, respectively. The data points were processed and the final data include the same number of points but less values: outliers, bad values and data that do not correspond to vapor measurements were excluded during the various steps of data processing and they were replaced by NaNs (stands for *Not a Number* in Matlab). During the various steps figures that correspond to Odo are shown; data processing for Walter is identical.

01: Filtering of the outliers

Acquisition of original raw data included some extreme isotopic values of $\delta^{18}\text{O}$ and δD , probably a result of bad connection in one or more of the system's parts. The silica capillary was quite sensitive and had to be carefully connected to the oven, which sometimes created problems with the stability of the water vapor concentration injected into the spectrometers. Fluctuation of the pressure inside the optical cavity may also result in extremely low or high isotopic values and is a problem that might be attributed to a loose or tight connection between the 3-way valve (check block diagram) and the copper tubes that lead the vapor sample to the two instruments. Figure 4.15 shows a day that problems were recorded with respect to the cavity pressure and the water vapor concentration inside the optical cavity.

Outliers were detected for the whole period of measurements and their values were removed and replaced by NaNs. Extreme measurements were chosen based on whether they were lying outside a range of acceptable values for each of the parameters under investigation; if the value of the parameter was out of this range it was discarded (replaced by NaN). For this specific data point, which corresponded to a certain time, all other measured quantities for this time were also replaced by NaN. First quantity that was taken into account to filter data based on the above description was the measured isotopic values. Next one was the water concentration inside the optical cavity and then the cavity pressure. Hereafter, 1st step filtered data refer to data resulting after excluding the outliers.

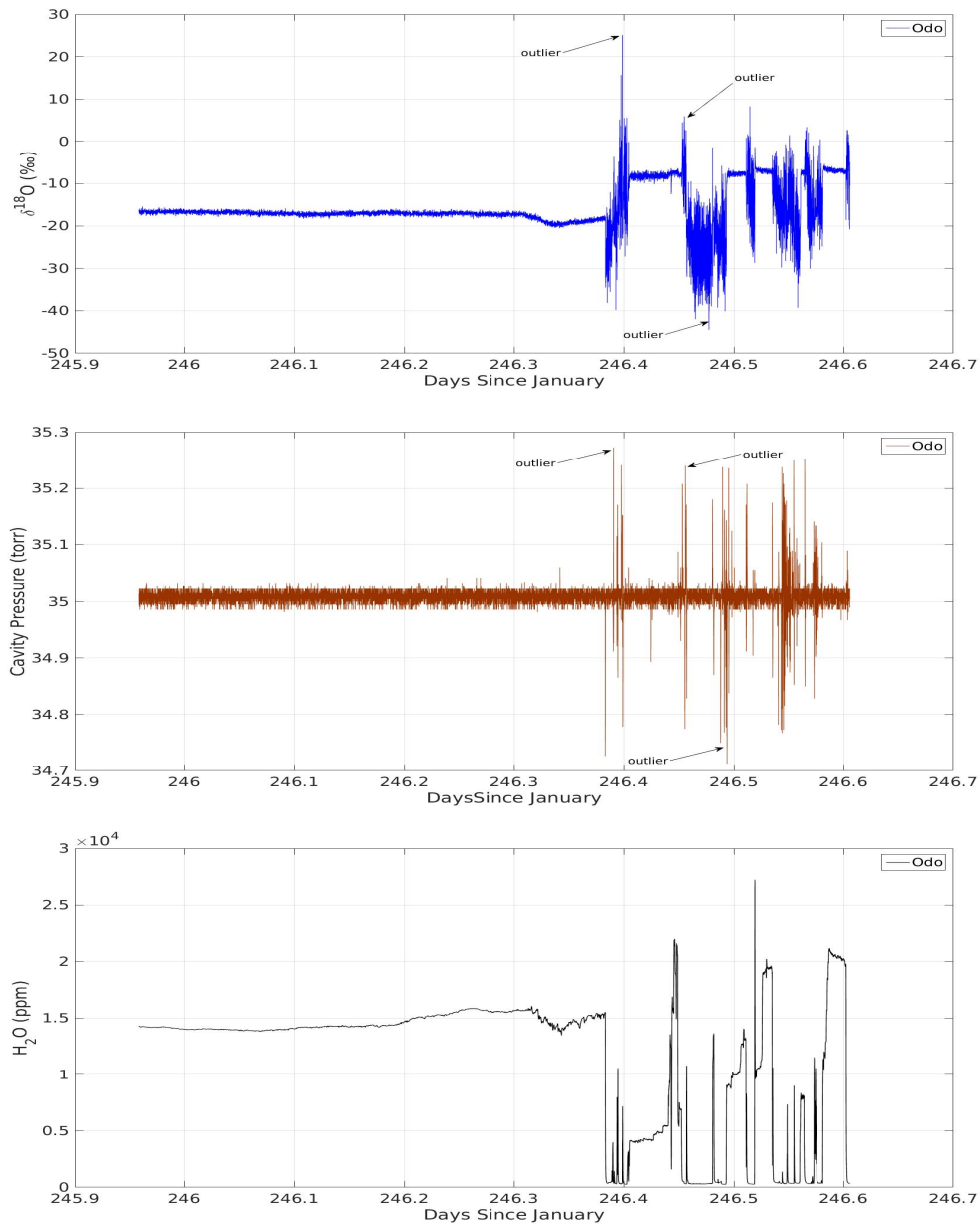


Figure 4.15: Extreme values of $\delta^{18}\text{O}$ measured by Odo at 04/09/2015. Top plot: $\delta^{18}\text{O}$ values (blue color). Middle plot: optical cavity pressure (brown color). Bottom plot: water vapor concentration in the optical cavity (black color). Three of the many outliers of this section are indicated.

02: Selection of atmospheric vapor data

As already mentioned, valve position 1 corresponds to atmospheric vapor measurements while position 2 to all other measurements. This might refer to injection of locally produced standards in order to perform the VSMOW-SLAP calibration or when investigating whether the new oven operates in an optimal way (immediate

evaporation of the injected water) or not. These values needed to be excluded from our final results in order to get the net isotopic signal of the atmospheric water vapor. Selection of the sections corresponding to these measurements took place by manually defining regions (based on notes with the exact dates that valve was switched at position 2) that do not correspond to vapor measurements and by substituting them with NaNs. Notice that values in Figure 4.16 correspond to calibrated data (atmospheric vapor and non atmospheric vapor) for varying humidities and with respect to the VSMOW-SLAP scale.

03: Calibrating the values for the different humidity levels

The next step in our data processing was to correct the measured isotopic values in terms of varying water concentration inside the optical cavity. As already described, a 3rd order polynomial fit was applied in order to calculate the humidity correction factors that correspond to different humidity levels in the optical cavity of the spectrometers. Calibrated values for October are shown in Figure 4.17. Equations 4.3 - 4.6 were used to calibrate data at this step. Notice the isotopic difference of $\delta^{18}\text{O}$ before and after performing the humidity calibration for the periods 280-285 and 300-304 days since January. Humidity correction factors for these days have higher values due to the lower humidity in the atmosphere for these two periods.

04: Calibrating the values with respect to the VSMOW-SLAP scale

During this step data were calibrated with respect to the VSMOW-SLAP scale. Equation 4.7 was used to process data and the values for the slope and the intercept can be found at Table 4.4 (2nd group of selected sections). Results for October can be seen in Figure 4.18. Notice that isotopic values for $\delta^{18}\text{O}$ are lower after the calibration while values for δD are heavier. Importance of calibrating on the VSMOW-SLAP scale is also depicted on the dexcess since the whole data series got positive isotopic values after performing the calibration.

05: Median Filter

After calibrating the values on the VSMOW-SLAP scale, a 3rd order 1D median filter was used to smooth data and perform noise reduction. The window size for filtering was set at 10^3 data points. This means that each entry on our code was replaced with the median of the neighboring 10^3 data points. Median of the segments including NaNs was set to return the filtered signal without taking into account these NaNs. Median filter was chosen due to its non-linearity when filtering. Results before

and after using the median filter are shown at Figure 4.19.

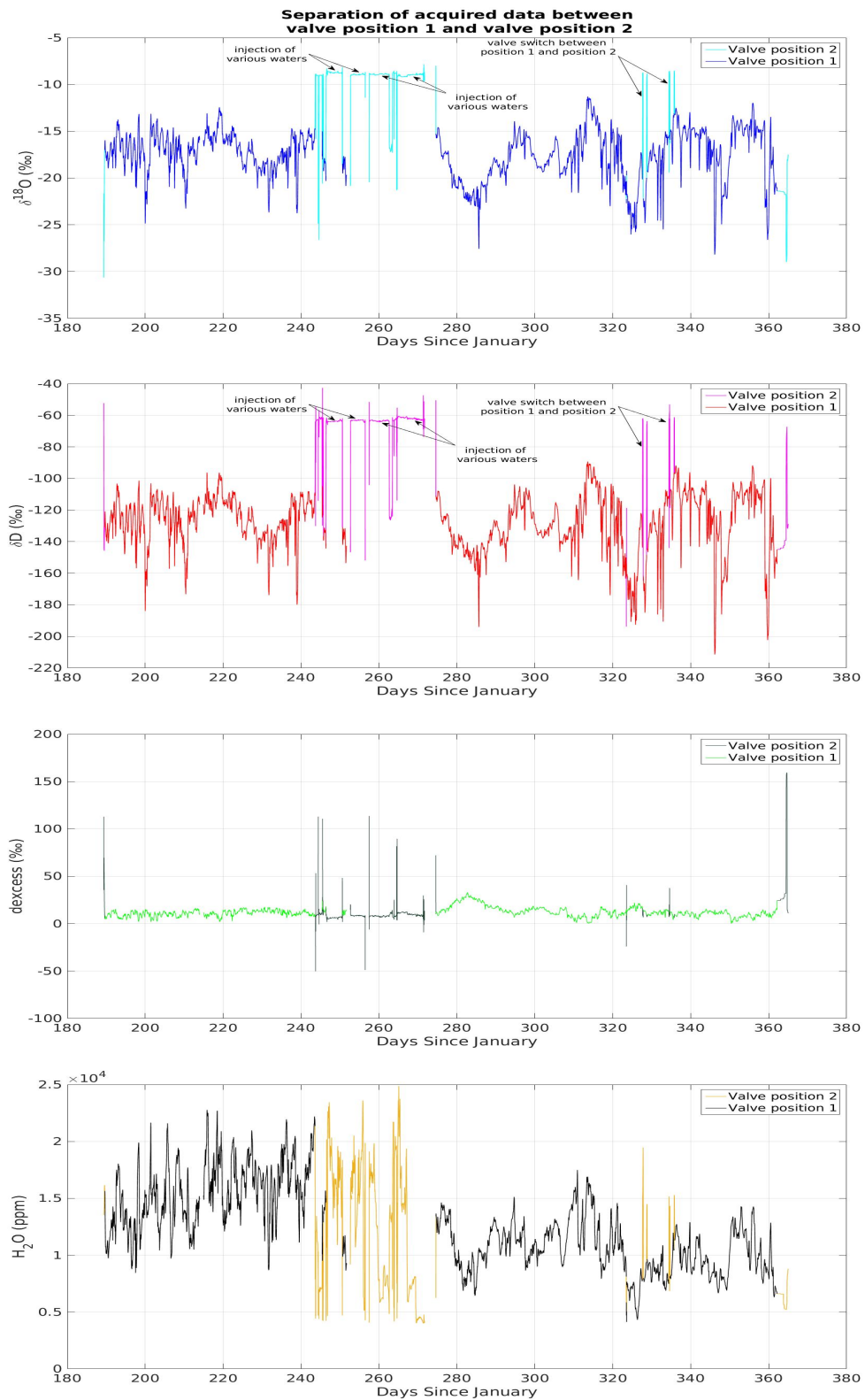


Figure 4.16: Separation of acquired data for the two different valve positions. Valve position 1 refers to vapor sampling and valve position 2 to standards and Milli-Q water. From top to bottom plots: $\delta^{18}\text{O}$, δD , dexcess and H_2O concentration. Data shown correspond to the whole period of measurements for Odo (July-December).

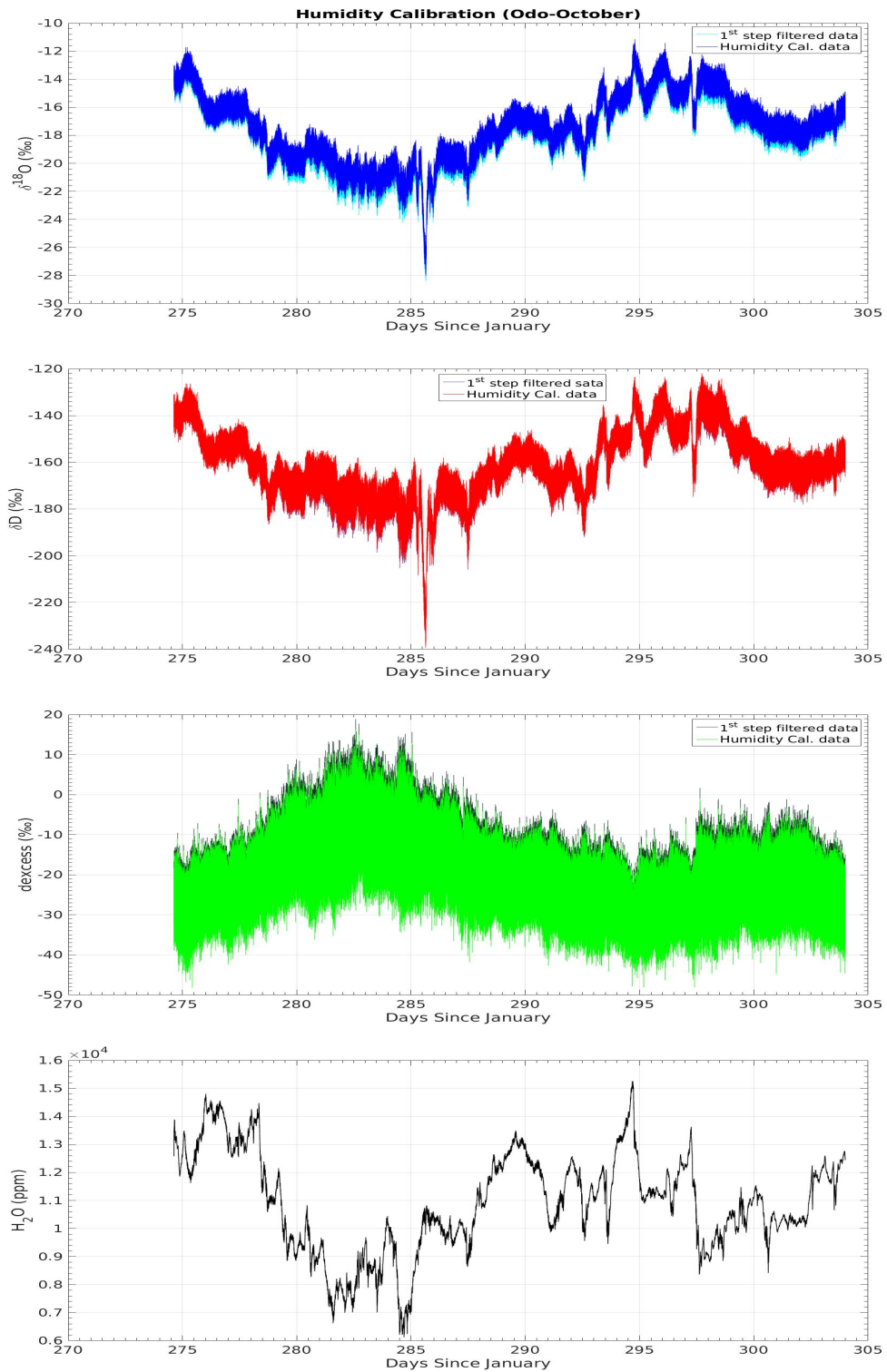


Figure 4.17: Humidity calibration for Odo (October). 1st step filtered data correspond to the data after getting rid of the extreme values of the measured variables. Top plot: $\delta^{18}\text{O}$ values before (cyan) and after the humidity calibration (blue color). Middle plot: similar for δD before (purple) and after the calibration (red). Bottom plot: dexcess before (light green) and after (dark green) the calibration.

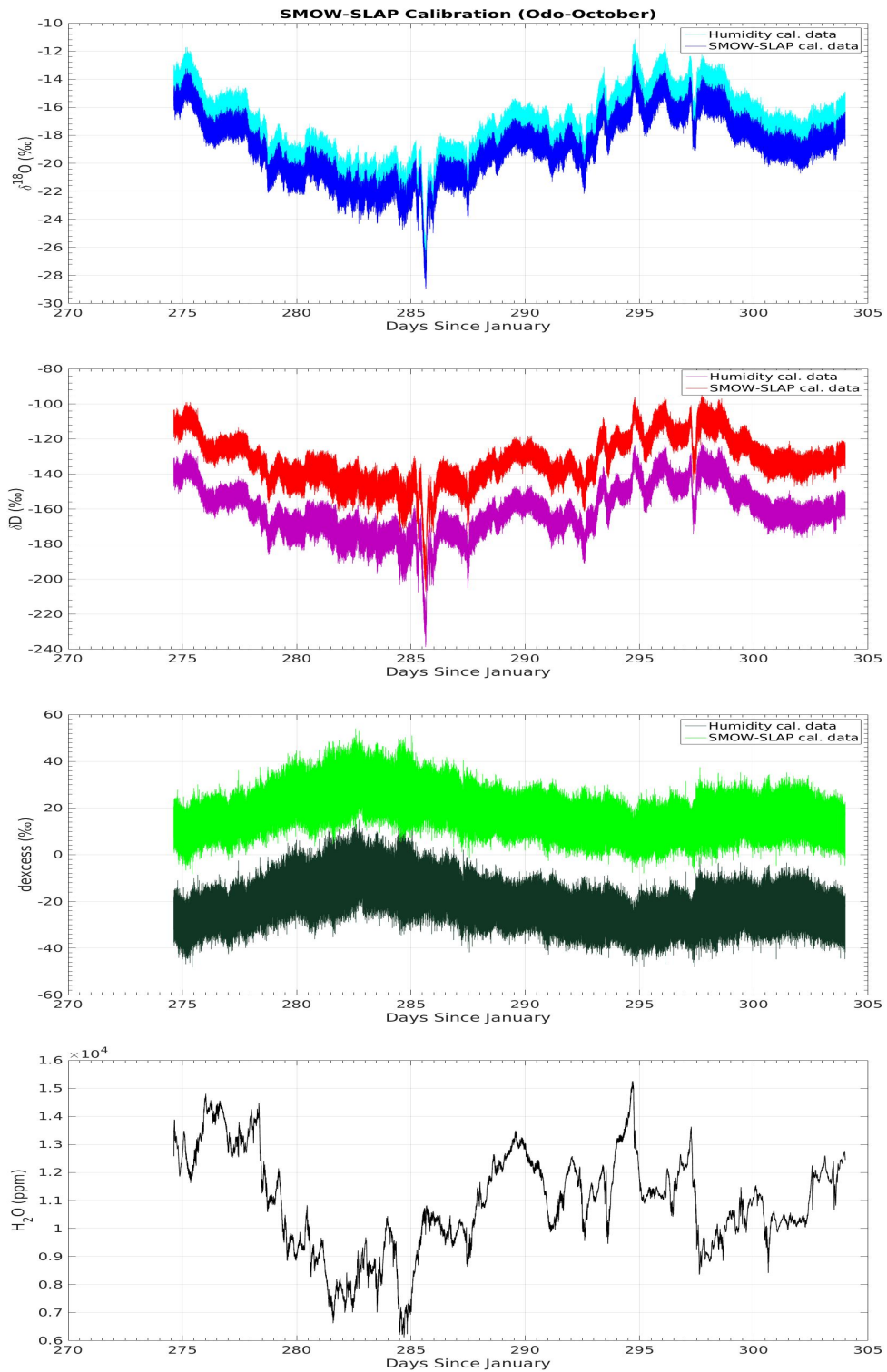


Figure 4.18: Calibration for Odo (October) with respect to the VSMOW-SLAP scale. Data after performing only the humidity calibration are also shown in each plot. From top to bottom plots: $\delta^{18}\text{O}$, δD dexcess and H_2O concentration in the optical cavity.

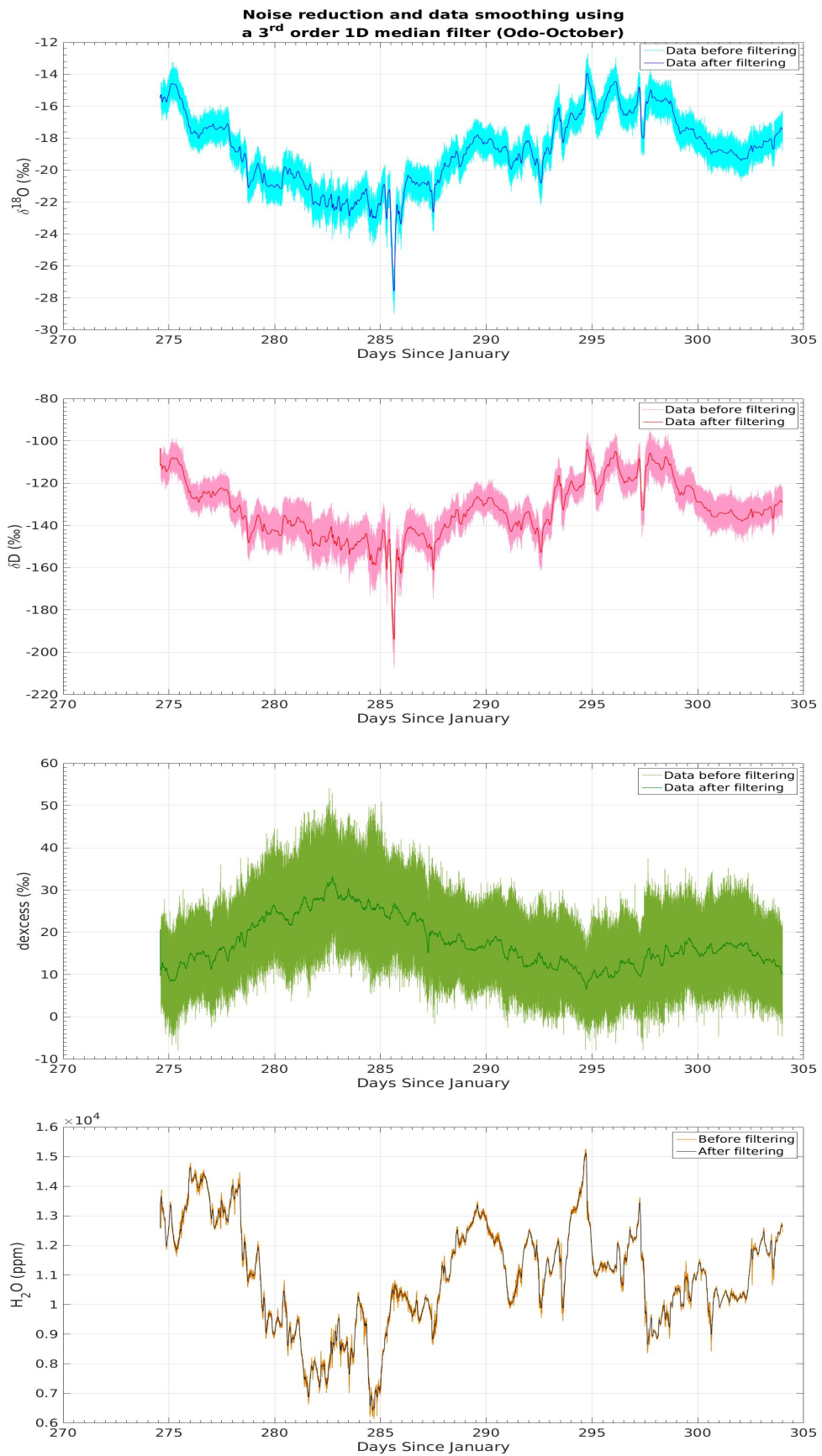


Figure 4.19: Smoothing data using a 3rd order 1D median filter. From top to bottom plots: $\delta^{18}\text{O}$, δD , dexcess and H_2O concentration.

4.4 Intercomparison between the two instruments

Sections 4.1.3 and 4.1.4 describe two different approaches (from a mathematical point of view) in order to correct our data when samples of different humidity levels are injected into the two spectrometers. Difference in acquisition time between the instruments (difference in the number of data points) forces us to interpolate our data in order to produce data series with exactly the same amount of data points for intercomparison. Difficulties performing the interpolation were related to the fact that negative time steps were recorded from the two instruments. These steps were specified and replaced with NaNs, after using the following equation:

$$Time\ Step_{(n+1)} - Time\ Step_{(n)} < 0 \quad (4.12)$$

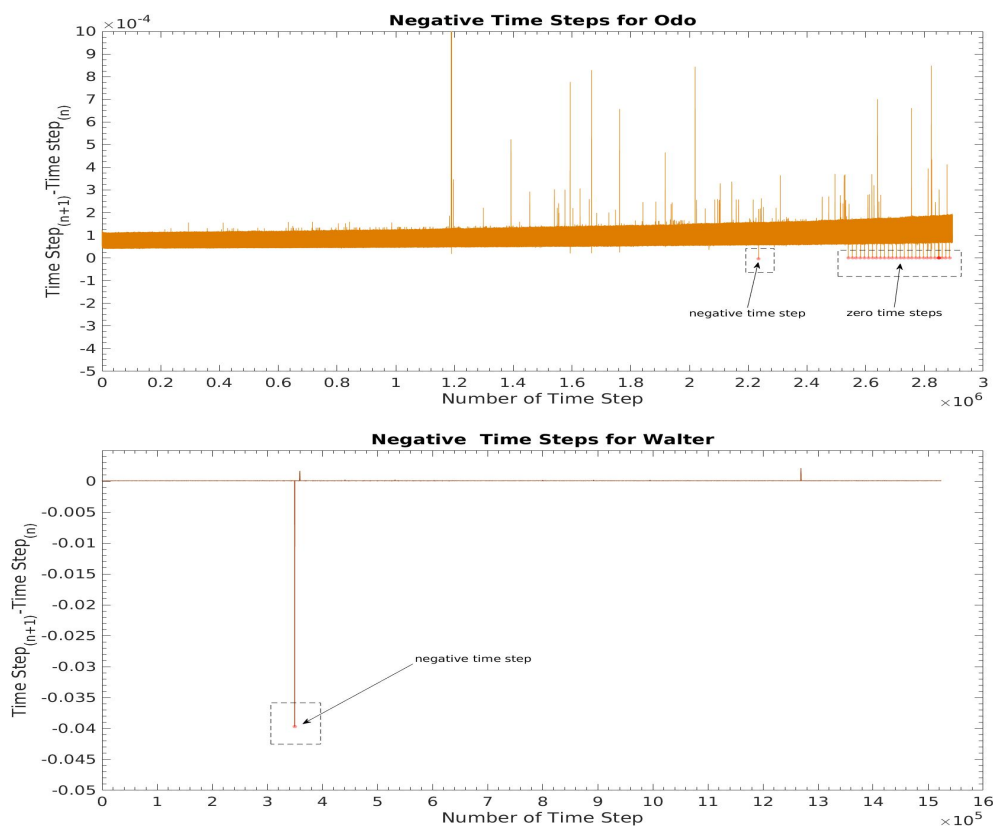


Figure 4.20: Negative time steps for the two spectrometers.

Linear interpolation of data was performed by setting the time step to 15 minutes and of course including data acquired the period 10/07/2015 - 10/11/2015, when

both instruments were still sampling atmospheric water vapor (Walter broke down at 11th of November). Segments of the data series that included bad measurements for one of the two instruments were also excluded from the second instrument because they would later have an impact on the calculation of the root mean square (RMS) difference as well as the correlation coefficient between the interpolated data series.

In the case of a set of n values, RMS for the δ is given by the equation (5):

$$\delta_{rms} = \sqrt{\frac{1}{n}(\delta_1^2 + \delta_2^2 + \dots + \delta_n^2)} \quad (4.13)$$

The correlation coefficient, ρ , of two variables A and B is a measure of their linear dependence. If each variable has N scalar observations, then the correlation coefficient is defined as (11), (14):

$$\rho(A, B) = \frac{1}{N-1} \sum_{i=1}^N \left(\frac{A_i - \mu_A}{\sigma_A} \right) \left(\frac{B_i - \mu_B}{\sigma_B} \right) \quad (4.14)$$

where μ_A and σ_A are the mean and standard deviation of A, respectively, and μ_B and σ_B are the mean and standard deviation of B.

Results of the interpolated values are shown in Figures 4.21 and 4.22. Comparison of the RMS values derived from the two different methods for humidity correction, shows the importance of fitting our data with the 3rd order polynomial fit when we want to calculate the humidity correction factors. Performing a linear regression underestimates the area of low and mid humidity levels, especially for δD values measured by Walter (see also Figure 4.5). Correlation coefficient between the data series of the two instruments remains the same for the two different methods (for $\delta^{18}O$ and δD). Although it decreases for deuterium excess from 0.94 for the linear regression to 0.75 for the higher order fitting, it still indicates a strong relationship between the two data series.

Figure 4.22 includes the daily mean offset between the two instruments, shown as stars. Minimum and maximum offset values for $\delta^{18}O$ are -0.002‰ and $+0.49\text{‰}$, respectively; minimum and maximum offset for δD are $+0.02\text{‰}$ and -4.16‰ , respectively. For dexcess the values range between $+1.60\text{‰}$ and -5.60‰ .

In order to realize the relative magnitude of these values, we can compare it with the observed atmospheric isotopic variability for one day (see Figure 5.4, between

238-239 days since January). The range for this specific day is $\approx 10\text{‰}$ and $\approx 60\text{‰}$ for $\delta^{18}\text{O}$ and δD , respectively. Of course bigger ranges can be seen when, for example, we have transition between rainy and snowy days, reflected by higher isotopic variability. We, thus, conclude, that the two instruments agree well.

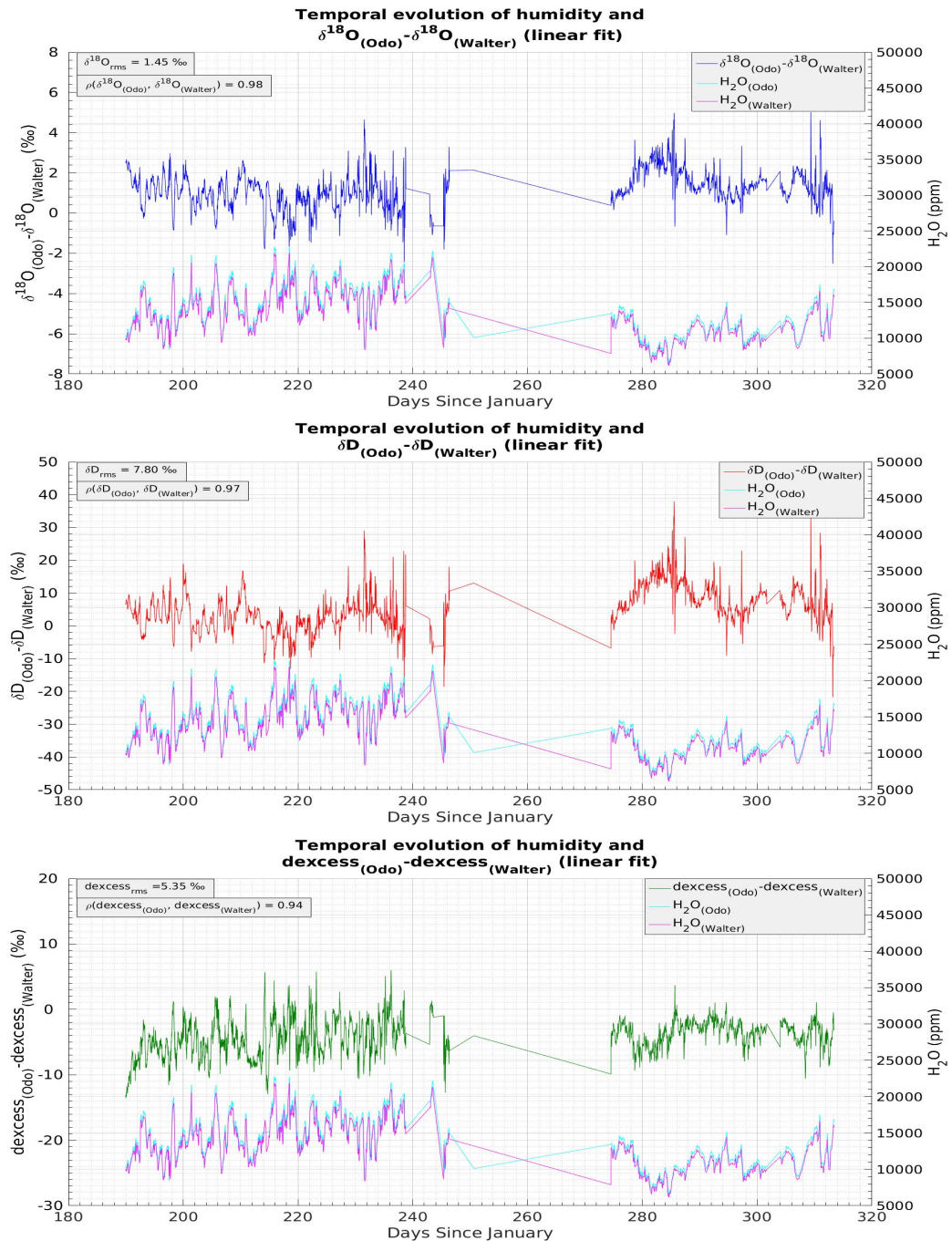


Figure 4.21: Interpolated data after using the linear regression to calculate the humidity correction factors.

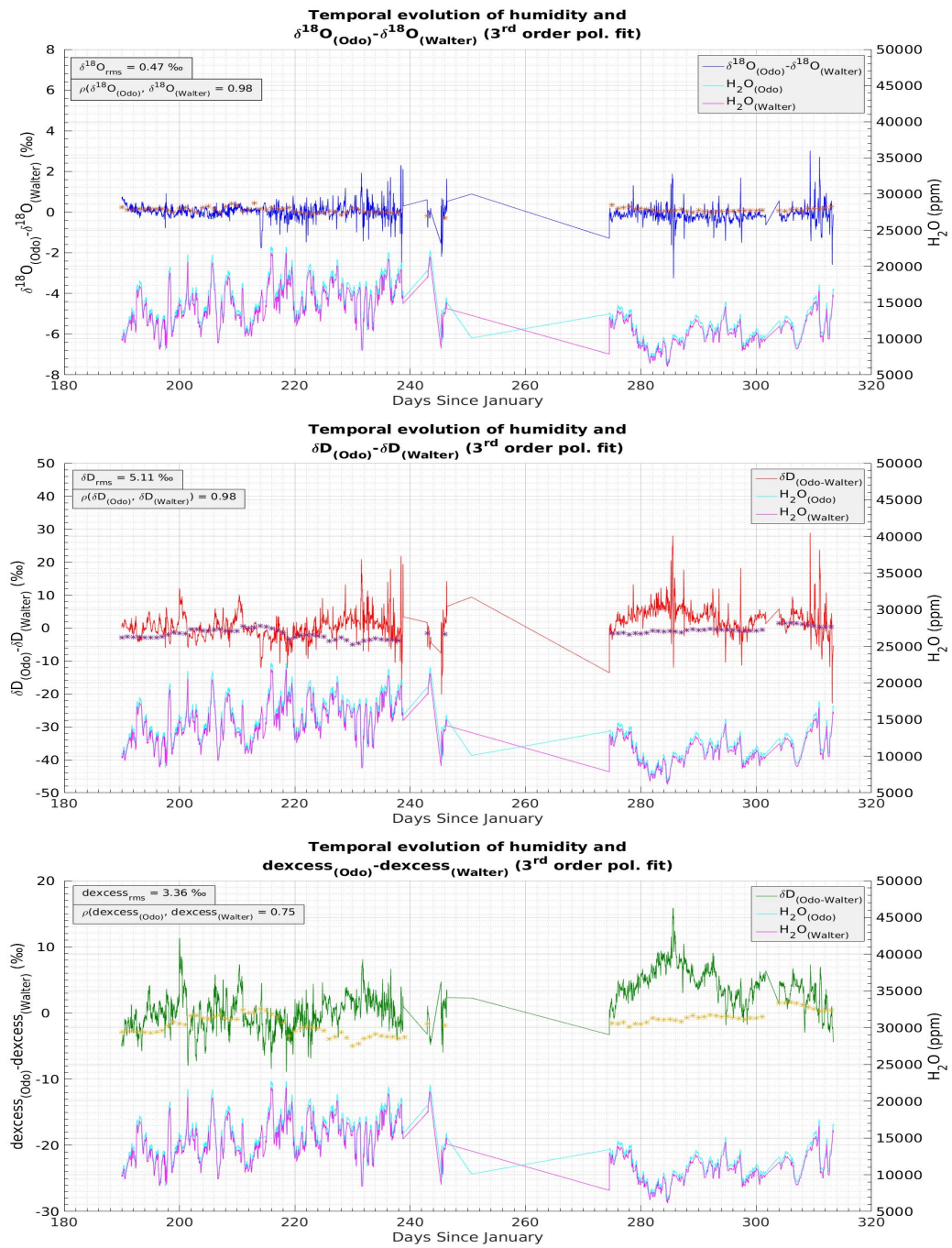


Figure 4.22: Interpolated data based on the 3rd order polynomial fit to calculate the humidity correction factors. Stars in every subplot represent the daily mean offset between the two instruments.

5

Results

5.1 Experimental Results

5.1.1 Meteoric water samples

As already mentioned in Chapter 4, meteoric water samples were collected from August, 2015 until the end of January, 2016. Samples have been maintained frozen inside the Michelsen deep freezer, located at the Rockefeller complex, in order to preserve the isotopic composition they had the moment of collection. They were measured 3 times at the Isotope Lab of the Center for Ice and Climate, each time using different, locally produced standards (Table 5.1). The reason for changing standards each time was to make sure that the isotopic values of $\delta^{18}\text{O}$ and δD of the meteoric water samples were lying inside the area defined by the values of the standards with the highest and lowest isotopic values, resulting this way in a better VSMOW-SLAP calibration. A Picarro Cavity Ring Down Spectrometer (model L2130-i) was used all 3 times to get the results of the isotopic composition of the samples. Total number of samples is 27, corresponding to 25 days when meteoric water samples were collected (for 2 of these dates sampling took place twice a day due to the fact that different systems affected Copenhagen at the same day). Details for the exact date and time of sampling can be found in Appendix A.0.1.

5.1.1.1 Method for measuring the meteoric water samples

The method used to measure our meteoric water samples is identical to the method used at the Isotope Lab of the Center for Ice and Climate to measure ice core samples from Greenland. Samples are prepped into 2 mL glass vials using a pipette with changeable tip. The tip is replaced for every water sample in order to avoid

water residues contaminate the next sample that will be prepped. Vials are sealed with PTFE (polytetrafluoroethylene, a synthetic fluoropolymer of tetrafluoroethylene that has numerous applications) short thread caps in order to avoid any exchange between the samples and the atmosphere.

Table 5.1: Standards used for measuring meteoric water samples. Uncertainties for some of the standards shown in table are not known.

Date	$\delta^{18}O$ (‰)	δD (‰)
06/12/2015	-21.88 ± 0.06	-168.45 ± 0.09
	-33.50 ± 0.03	-257.45 ± 0.20
	-39.98 ± 0.08	-311.11 ± 0.35
15/02/2016	-14.84	-111.10
	-21.88 ± 0.06	-168.45 ± 0.09
	-33.50 ± 0.03	-257.45 ± 0.20
16/02/2016	-8.31	-58.30
	-14.84	-111.10
	-21.88 ± 0.06	-168.45 ± 0.09

Each sample is injected and measured 4 times, but only the last 3 injections are taken into account to obtain the mean isotopic value of the sample and calibrate it on the VSMOW-SLAP scale. Water concentration inside the optical cavity of the spectrometer is around 20 kppm, the optimum concentration for the absorption in the infrared spectrum area. For every run with meteoric water samples that is measured, the isotopic composition of a set of locally produced standards is also measured; the acquired isotopic values of the standards are used to calibrate the samples on the VSMOW-SLAP scale.

5.1.2 Results for the meteoric water samples

The isotopic composition of the collected meteoric water samples is shown in Figure 5.1. We see that precipitation is not distributed uniformly for the whole period of collection. Notice the period between 247-314 (04/09/2015-10/11/2015) days when only one sample was collected (corresponding to 14/10/2015). This of course does not correspond to a period with only one day of precipitation, since our capability of collection was sometimes restricted (i.e. not being in Copenhagen to sample), but

characterizes a relatively dry period. On the other hand, 13 samples were collected for the period between 314-329 (10/11/2015 - 25/11/2015), a number which is almost half of all the selected samples (27 in total). Thus, we could say that November was a wet month and also included the first snow of the year, for the period 324-326 days since January (22-24/11/2015). The isotopic imprint of these two days is clearly depicted as the lowest values of $\delta^{18}\text{O}$ and δD in Figure 5.1. Deuterium excess for these days increases. As an overall trend, we can see that precipitation becomes isotopically lighter while transitioning from warm to colder conditions.

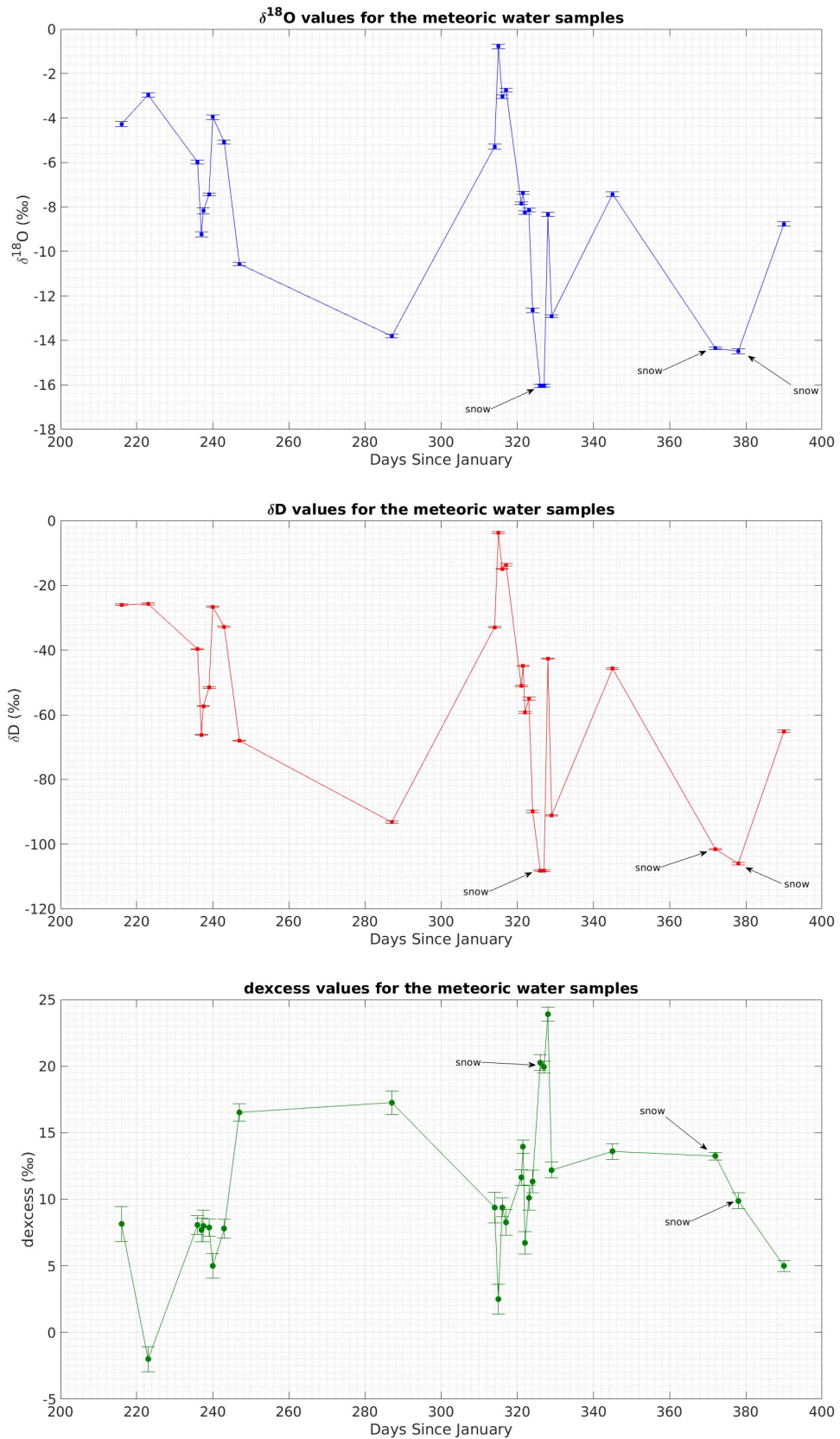


Figure 5.1: Isotopic composition of the meteoric water samples. Blue color corresponds to $\delta^{18}\text{O}$, red color to δD and green color to dexcess. Error bars represent $\pm 1\sigma$ for each sample. Collection took place between August, 2015 and January, 2016.

5.1.3 Vapor data

Figure 5.2 shows the final data for both instruments between 10/07/2015 -10/11/2015. From top to bottom the subplots refer to $\delta^{18}\text{O}$, δD , deuterium excess and humidity in the atmosphere. Data from the two instruments, in general, capture the same isotopic variability in the atmospheric water vapor. The agreement between the two data series is quite good for most of the period and differences between the isotopic values of only δD seem to appear for the period 280 – 290 days since January; this is also depicted in the values of deuterium excess between the two instruments for the same days. No profound explanation for this difference can be given. Testing for pressure inside the optical cavity during these 10 days showed no significant problems.

Diurnal variability of isotopic values can be easily seen, especially for the period 190-240 days (10th of July until the end of August), with maximum values recorded around the first morning hours and minimum values around noon. A possible explanation for this behavior could be the fact that during day-time hours and especially for this period of year, when maximum temperatures are recorded, tropospheric vertical mixing becomes more intense during day when the Sun heats Earth's surface. Exchange of water vapor between layers of the troposphere in higher altitude and the boundary layer, where our sampling takes place, becomes more intense during day. A more well-stratified troposphere during night limits vertical mixing. Minimum and maximum isotopic values for this period also correlate with the minimum and maximum humidity in the atmosphere. Figure 5.3 shows half of the period in order to be easier for the reader to distinguish the diurnal isotopic variability.

Last but not least, period between 250-270 days since January does not include any data due to the fact that both instruments were facing functional problems. Due to the fact that we are interested in checking data that cover the period when both instruments were measuring in order to make intercomparison between the two data series, measurements for Odo that correspond to the period after 10th of November can be found in Appendix A.0.2.

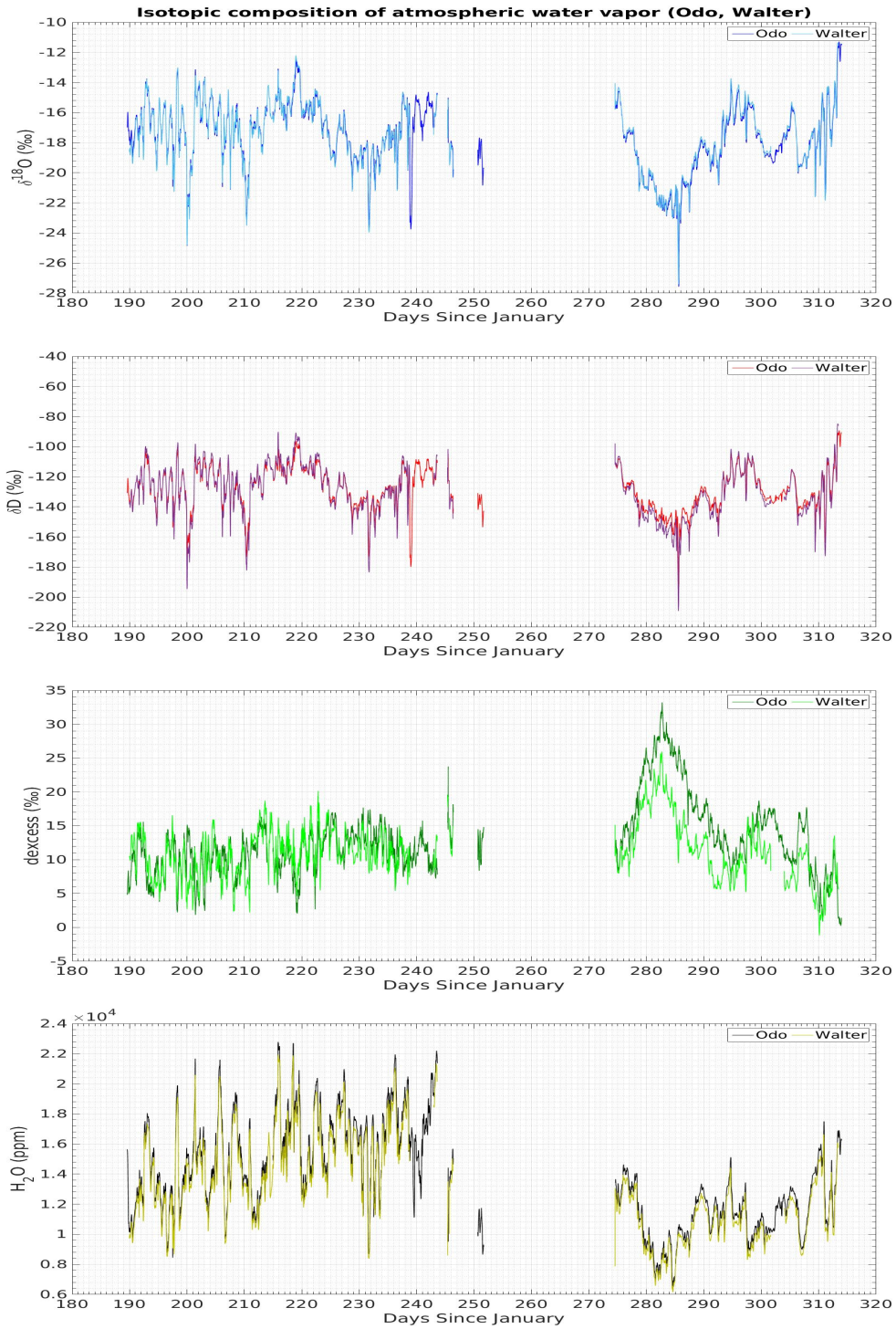


Figure 5.2: Diurnal variability of vapor $\delta^{18}\text{O}$ (blue color), δD (red color), dexcess (green color) and humidity in the atmosphere (black color) for the period between 10th of July and 10th of November.

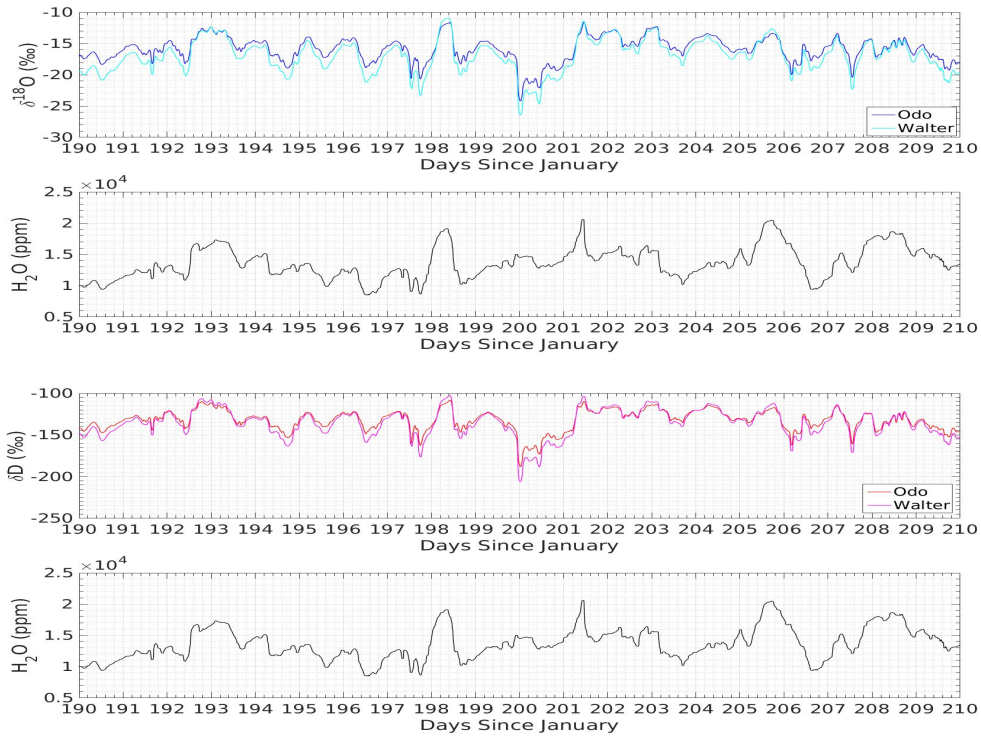


Figure 5.3: Diurnal isotopic variability of vapor $\delta^{18}\text{O}$ (blue color), δD (red color), decess (green color) and humidity in the atmosphere (black color) between 10th of July until the end of the same month. Humidity levels correspond to measurements acquired from Odo.

5.2 Correlation between the meteoric water samples and atmospheric water vapor

This section describes and investigates the isotopic behavior of meteoric water and atmospheric water vapor. We focused on two periods: the first one corresponding to 235-243 days since January (24/08/2015-04/09/2015, Figure 5.4) and the second one covering the period 310-328 days since January (10/11/2015 - 25/11/2015, Figure 5.5). Criterion for our choice was primarily the fact that there was a satisfying number of collected precipitation samples; investigation of the isotopic behavior before, while and after two consecutive weather systems (for the first period) that affected Copenhagen was of course worth paying attention to. Transition between days with rain and snow as well as the number of successive days with precipitation (and not only the total number of days with precipitation for the specific period) also played an important role for choosing the second period.

Figure 5.4 consists of 2 subplots. The top one shows the isotopic values of both isotopic species for meteoric water samples and atmospheric vapor for the specific period; deuterium excess for meteoric water and vapor is presented in the bottom subplot. Numbers in parenthesis correspond to different collected precipitation samples. Samples (3) and (4) correspond to the two different weather systems that affected Copenhagen at 236-237 days since January (25/08/2015). Although no meteorological data are shown in this study, the two systems passed over the city were separated by several hours of clear skies and plenty of sunshine. We notice that an anti-correlation between the isotopic behavior of precipitation and vapor exists: notice that the afternoon system corresponds to vapor that is more depleted in heavy isotopes than the morning one, clearly depicted in the lower values of both isotopic species (around 2 and 12‰ for $\delta^{18}\text{O}$ and δD , respectively). Note also that the hydrogen isotopes fractionate much more strongly than the oxygen isotopes. According to Cuffey and Paterson (2010) “this is not attributed to the relative mass differences of HD^{16}O to H_2^{16}O and H_2^{18}O and H_2^{18}O and H_2^{16}O . Instead, the stronger fractionation of hydrogen reflects the comparatively large effect on molecular vibration frequencies when a D atom replaces an H atom in a water molecule ”.

Isotopic composition of meteoric water, on the other hand, follows the opposite trend: both isotopic values become progressively higher during the transition between the morning and afternoon system. In general, the stable isotope values for water vapor are more depleted compared to precipitation since the heavy isotopic species are preferentially distributed in the condensate phase in agreement with the expected behavior. The same conclusion arises from another study which measured the stable isotopes in vapor and precipitation in Patras, Greece (15).

Notice also the same anti-correlation between the minimum in the isotopic values of vapor and the maximum isotopic values of precipitation for the 9-days period. This picture is in total agreement with the fact that heavier molecules evaporate less rapidly and condense more readily from the vapor, as a result of the lower vapor pressures of the heavier waters when compared to that of the light ones (3). Fractionation, thus, plays a major role in the isotopic imprint of precipitation and associated vapor. Deuterium excess values between vapor and precipitation do not exhibit the same anti-correlation like $\delta^{18}\text{O}$ and δD since isotopic maximum and minimum for this period do not coincide.

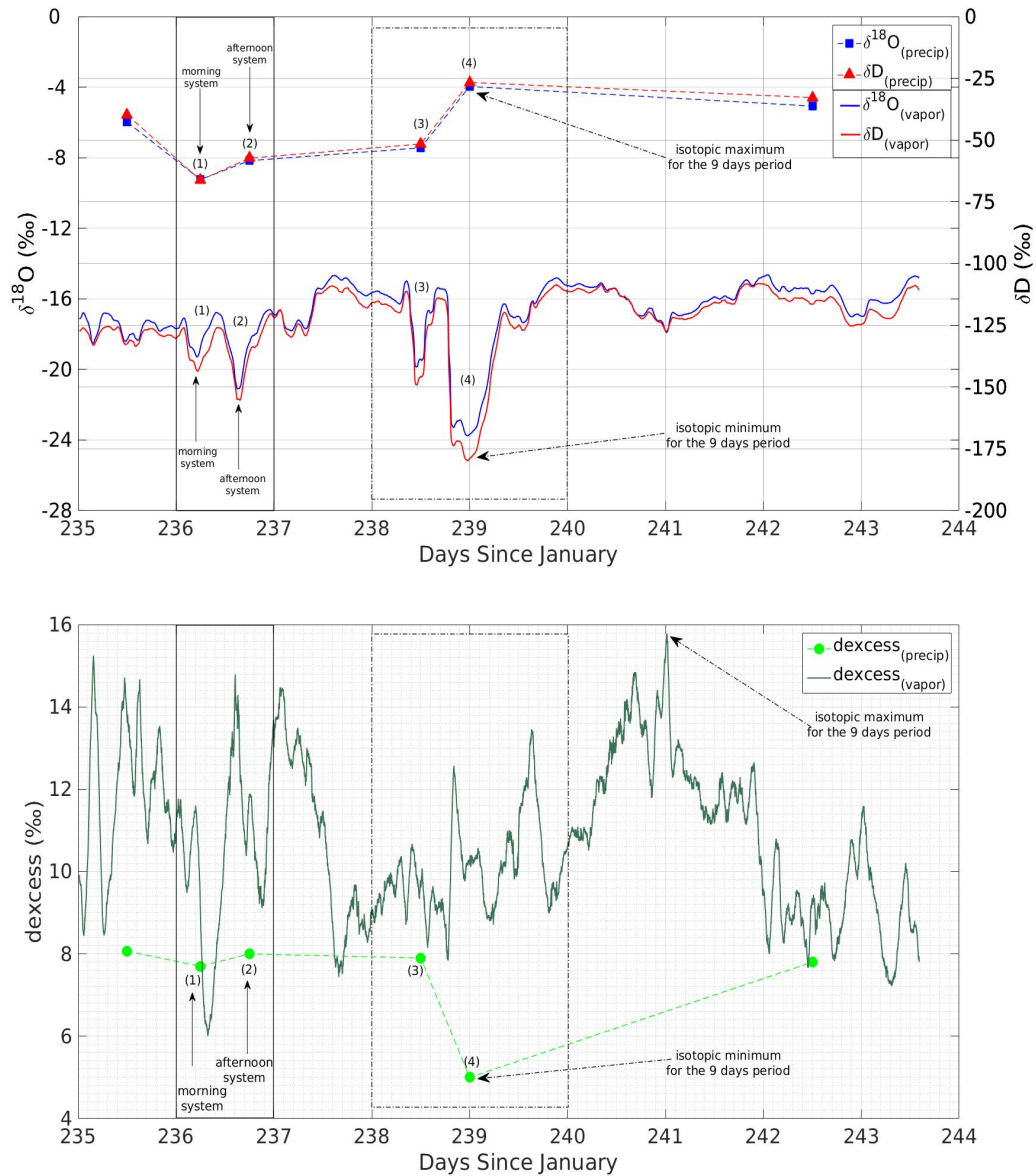


Figure 5.4: Isotopic variability of meteoric water samples and atmospheric water vapor for late August-early September. Vapor data shown in the plots correspond to measurements from Odo.

Figure 5.5 shows the second period, as previously described. Top subplot depicts $\delta^{18}\text{O}$ and δD for precipitation and vapor and the bottom subplot deuterium excess for precipitation and vapor. Clearly depicted is the progressively lower values for both isotopic species for meteoric water and vapor as we transit from liquid (rain) to solid precipitation (snow). Notice the exceptionally low isotopic values for both vapor and precipitation between days 324-326 that correspond to snow and lower temperatures. W. Dansgaard (1964) emphasizes and connects this behavior with

decreasing temperatures and seasonality of the precipitation (4).

Fractionation factor depends on whether the condensate is in liquid (rain) or solid (snow) form. Fractionation factors increase in both cases as temperature fall (12), (9), but the fractionation for ice crystal becomes even stronger as kinetic fractionation takes place during the growth of ice crystals (10). Isotopic values increase after day 326, a behavior explained by the fact that condensate now is in the form of liquid droplets and not ice, probably a result of another system affecting Copenhagen accompanied by higher temperatures. Again, isotopic variability between precipitation and vapor seem to correlate quite good, with vapor being more depleted in heavy isotopes than the associated precipitation. Deuterium excess values for precipitation and vapor seem to follow the same increasing trend.

Based on the measured values of atmospheric water vapor and precipitation we conclude that our data are realistic, since we constantly measure higher isotopic values for both $\delta^{18}\text{O}$ and δD in precipitation compared to atmospheric vapor. The observed co-variability between the solid, liquid and vapor phase is in agreement with what theory and observations predict: precipitation depletes the atmosphere of heavy isotopes.

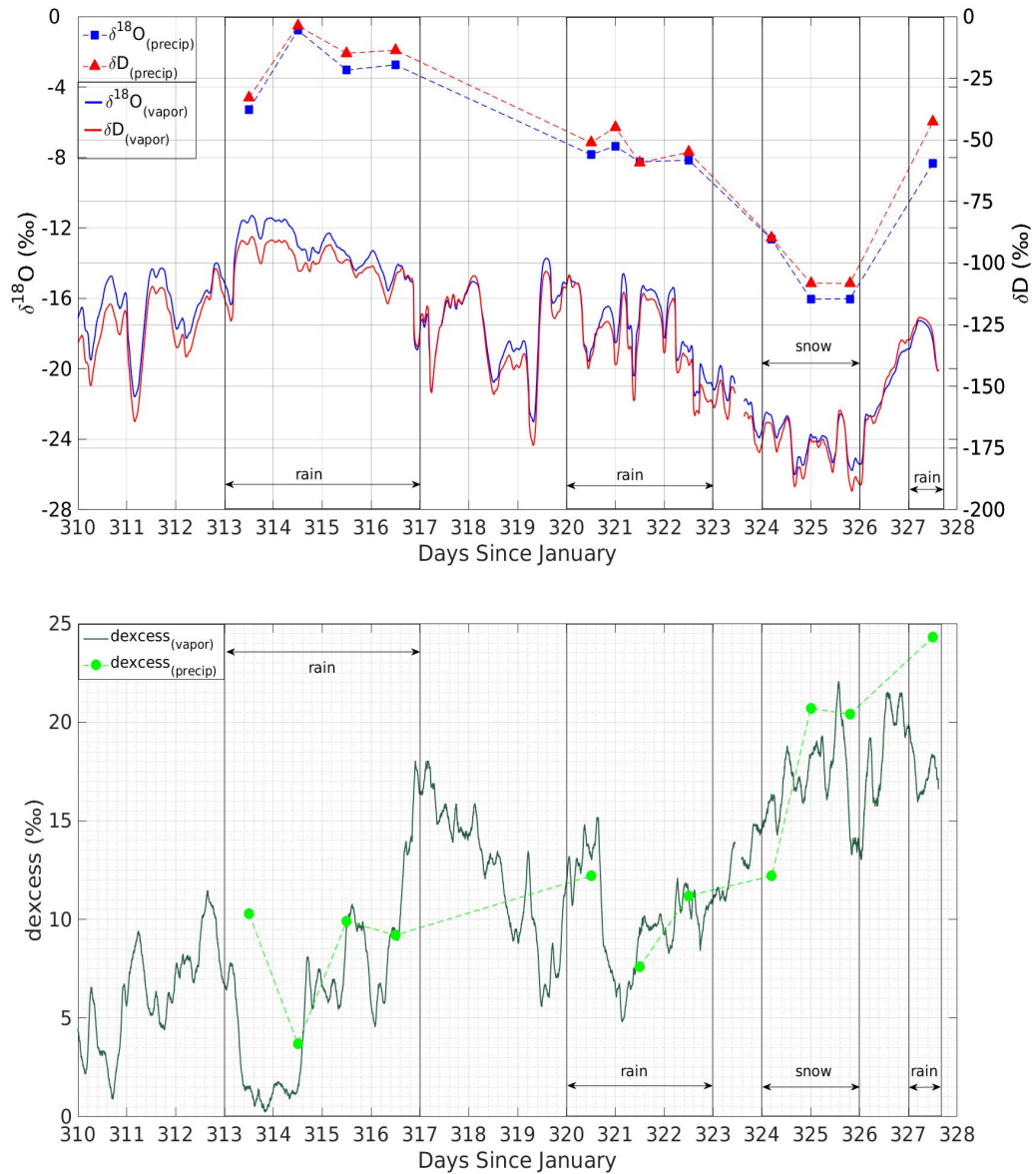


Figure 5.5: Isotopic variability of meteoric water samples and atmospheric water vapor for November. Vapor data shown in the plots correspond to measurements from Odo.

6

Discussion-Conclusions

6.1 Discussion

The last chapter of this study aims to focus on the most important aspects and conclusions after the experimental set-up, the data processing and the results have been presented and shown in the previous chapters. Some modifications-improvements are also proposed and ideas for further interpretation of the acquired data series are given.

Collection of meteoric water samples took place throughout the whole period according to principles that sufficiently eliminate fractionation effects. Samples were immediately stored in KAUTEX plastic bottles and sealed with parafilm before being stored in the freezer ($\approx -35^{\circ}\text{C}$), ensuring no phase change that could alter their isotopic synthesis. Extra effort, when this was possible, was put to collect meteoric water samples directly after precipitation stopped to reduce the waiting time inside the rain collector. The plastic sampling bottle was replaced after every collection attempt and placed inside an oven for several hours (depending on the needs for sampling since there were only two units of plastic sampling bottles) in order to vaporize any residuals left from the previous sampling.

The two different mathematical approaches used to calculate the humidity correction factors and correct our data for possible drifts due to varying humidity levels reveal the importance of fitting our data with a 3rd order polynomial fit and not with a regression fitting curve; in that case only the linear section of the higher water concentrations is taken into account, underestimating the non-linearity of the lower water vapor concentrations and especially the non-linearity for δD . This is supported by the $\delta^{18}\text{O}_{\text{rms}}$ and $\delta\text{D}_{\text{rms}}$ values calculated for the two approaches. Fitting with higher order polynomial showed signs of over-fitting, probably because it takes into account the noise existing in our data and not the true distribution itself.

One of the basic drawbacks and possible source of uncertainties for the quality of the data lies in the limited number of calibrations with respect to the VSMOW-SLAP scale. During the 5-months period of vapor sampling there was only one calibration performed using locally produced standards. It is generally accepted that frequent calibrations using water samples of known isotopic composition contribute to increased confidence regarding the quality of the measurements. VSMOW-SLAP calibration for the second spectrometer (Walter) was indirect since water samples of unknown isotopic composition were used to calibrate this instrument. On the other hand, meteoric water samples were measured and calibrated with respect to the VSMOW-SLAP scale in the Isotope Laboratory of the Center for Ice and Climate, using strict protocols in terms of procedures and materials, ensuring the quality and reliability of our results.

Possible improvements of the experimental set up would be mostly related with the initiation of a system that would make the separation between data acquired from the 3-way valve position 1 (sampling line for atmospheric vapor) and position 2 (sampling line of liquid water samples) easier and more automated. The valve could be connected with a simple electric circuit that produces a digital signal that is 0 and 1, corresponding to the two different valve positions. During data analysis, measured isotopic values that correspond to 0 value of the signal, corresponding to measurements obtained from the valve position 2 (the choice is arbitrary since it could be the opposite way) would be easily discarded. Data separation between valve position 1 and 2 at this study was performed manually, based on notes kept during the period of collection, and this, of course, might have an influence on the number of measurements considered as non-atmospheric vapor measurements due to the manual determination of these segments.

Furthermore, the reliability on our vapor measurements could be further strengthened if the vapor line was insulated and heated in a temperature higher than the ambient temperature. This way possible problems related with water re-condensation inside the copper tube of the vapor sampling line would be eliminated, although we are still pretty confident that the vapor line temperature was even during the warmest months higher than the ambient temperature.

As already mentioned in previous chapters, problems related with the pressure inside the optical cavity were present during the whole period; these problems, seen as fluctuations of the pressure above the desired range, could be likely attributed to minor or more important problems associated with instrumental functionality.

Pressure fluctuations inside the optical cavity and deviations from the desired value of 35 ± 0.1 torr might alter the isotopic measurements due to changes that happen in the absorbing spectra for different pressures.

Measurements of atmospheric water vapor might be strongly affected by local factors such as infrastructure or morphology of the surrounding area, especially for measurements acquired close to the city center. The locality factor combined with the absence of older measurements close to our collection site, makes the comparison and interpretation of the data series more tricky. Various studies around the world pay extra attention to local and regional geomorphology when interpretation of data takes place. Last but not least, examination of seasonality is not possible at this study, since only summer and autumn isotopic behavior was fully captured.

Data processing and implementation was quite demanding due to the high temporal resolution of the two data series. During our data analysis, extra attention was paid to exclude the less data possible in order to have the most detailed image about isotopic variability of atmospheric water vapor. Uncertainties regarding the data might have different source and some of them (i.e. cavity pressure) might have played a cumulative effect. Comparison, though, between the two data series gives us confidence about their degree of agreement.

6.2 Investigating possible time shifts between the data series of the two spectrometers

In order to compare the data series from the two spectrometers and increase our level of confidence, we investigated whether there is any asynchronicity between the two instruments. Possible time shifts could introduce a bias that would make the comparison and interpretation of our results more complicated. In that case, calculation of a time parameter would probably be necessary to correct measurements in terms of time shifts.

A number of randomly chosen periods of time were plotted and checked for possible general trend in time shift between the two instruments. An example is given in Figure 6.1. Time, as recorded by Odo, was tested against Walter's. The plot compares temporal evolution of $\delta^{18}\text{O}$ for a period of almost two days. Various constants (from 0.02-0.05 days) were added to time recorded by Walter to check if this

improves the synchronicity between the two instruments. We observe that when no constant is added in Walter's time the two instruments are not completely in phase (see and compare the peak at around 296.1 days); things seem to improve when fractions of a day are added in Walter's time, especially when adding 0.05 days, which corresponds to 80 minutes. Still, this plot is not representative of the general situation. During the randomly checked periods of time, things could be the other way round and differences in time be even larger or not present at all.

One more thing we should take into account, when examining possible time shifts, is the temporal resolution of our data which is of the order of seconds. Atmospheric isotopic variability and evolution, though, is of higher order, such as hours or even days. From that point of view, time shifts between the two instruments do exist, but without any tendency (towards to one or the other spectrometer) and without affecting our data, when examined for longer periods. This is depicted in Figure 6.2 which investigates isotopic variability in terms of different time spans. In the top sub-plot, $\delta^{18}\text{O}$ isotopic values from the two instruments are plotted against a period of 6 days. We are interested to check what is happening if we zoom in the area characterized as final period of interest; before zooming in at this period, we reduced the time span to 3 days (middle subplot). We see that now time shifts between the instruments become more obvious. Bottom sub-plot depicts the isotopic behavior of the atmosphere for a period of 0.4 days. Various occasions for which the two instruments are in phase or exhibiting a time shift are shown with arrows.

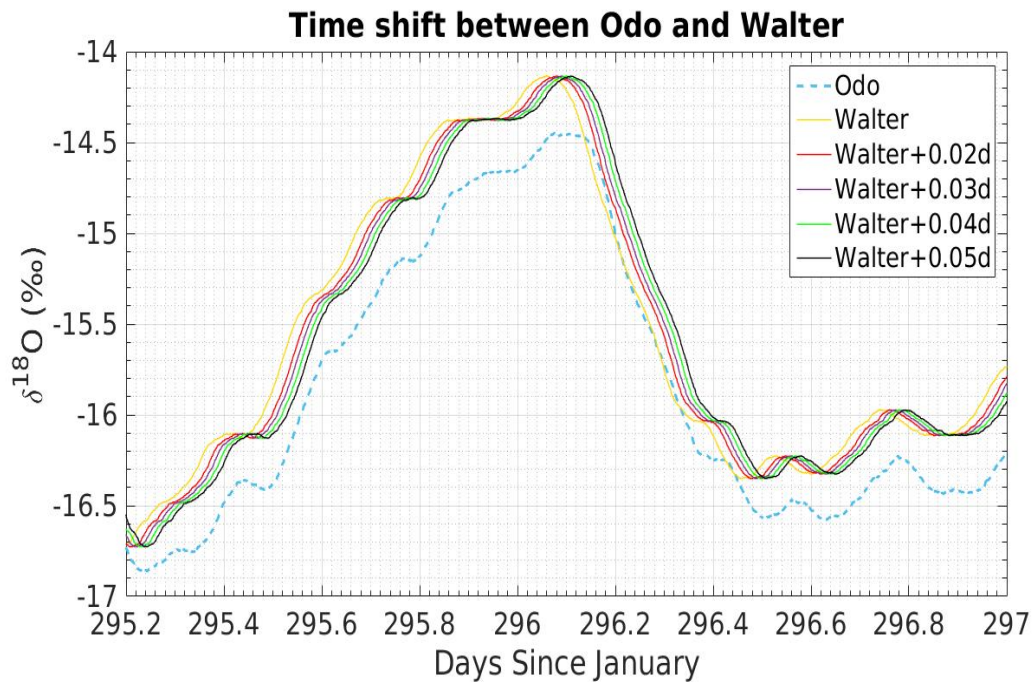


Figure 6.1: Investigation of possible time bias due to time shifts between the two instruments.

Summing up, no significant trend in the time shift between the two instruments was observed; there are sections when Odo is lacking in phase with respect to Walter or the opposite way. Periods in which the two instruments are more or less synchronized can be found. In terms of isotopic variability of atmospheric water vapor in the time span of days, which is under investigation at this project, we conclude that no time bias is introduced to our data.

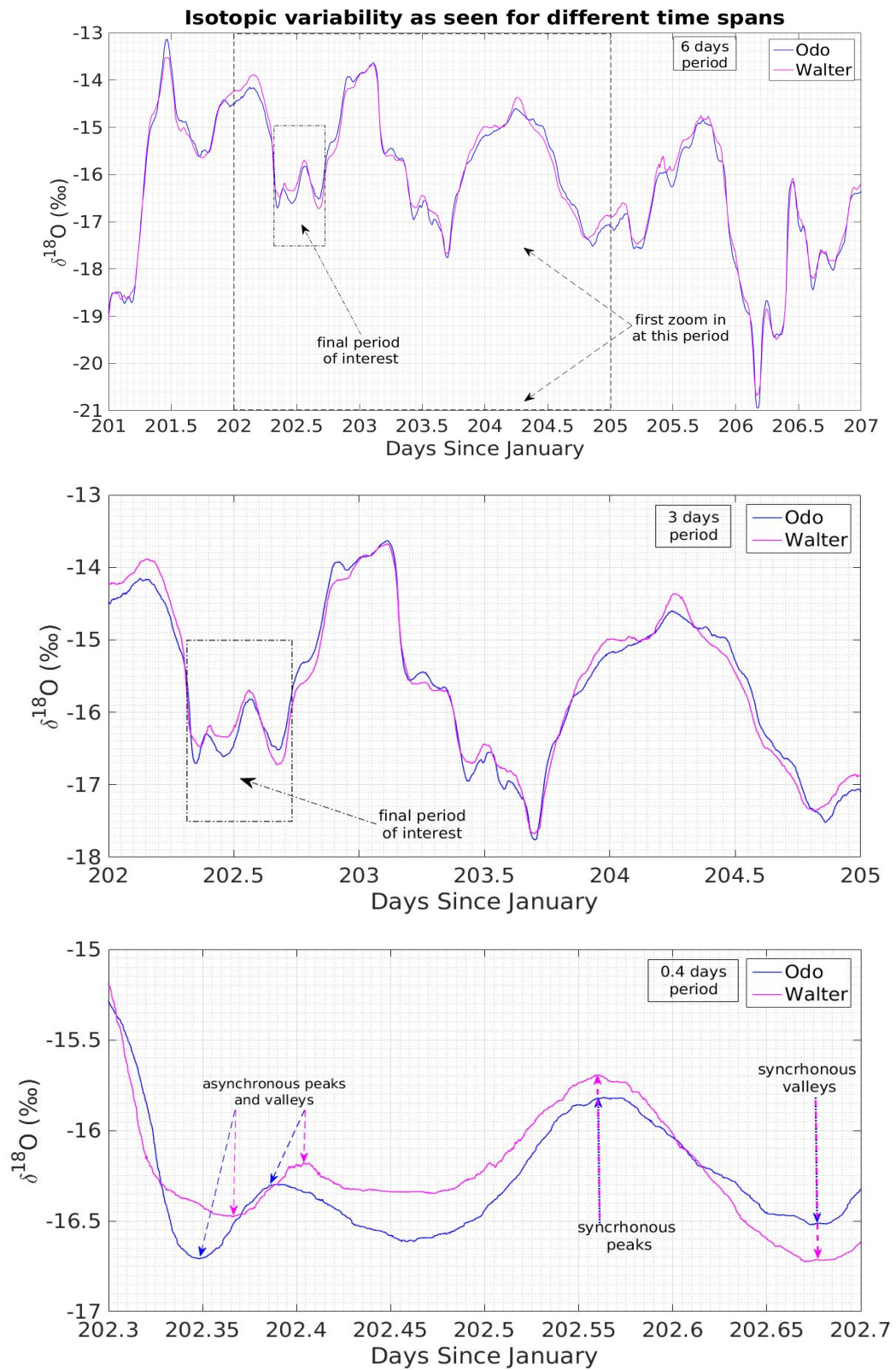


Figure 6.2: Isotopic variability of the two instruments when we focus on different time spans.

6.3 Conclusions

The water stable isotopes H_2^{18}O , HD^{16}O and H_2^{16}O were measured in atmospheric water vapor and precipitation for a 5-months period using two high precision laser spectrometers (Picarro, L1102-i). Natural variability of the liquid-solid and vapor state of water was captured and an effort was made to correlate data between these phases. Isotopic values for $\delta^{18}\text{O}$ and δD measured in atmospheric water vapor and precipitation are realistic since they show the generally accepted behavior of a more depleted, in heavy isotopes, vapor phase. Due to limitations that emanate from the available time for completing this study (corresponding to 1 year), no meteorological data that coincide with the period of vapor and meteoric water sampling were processed and this restricts our capability of interpreting data from a meteorological point of view.

The main result of this study is the acquisition of two data series of high temporal resolution and the confidence that results from the two instruments coincide in a satisfying way, based on the values for the daily mean offset between the two instruments (section 4.4). Including an extra spectrometer in our experimental set-up introduced extra complexity but results can be better evaluated and interpreted with higher confidence.

6.4 Outlook

Interpretation of data acquired from the two instruments can only take place in terms of the physical background of isotopes (i.e. equilibrium and kinetic fractionation, Rayleigh condensation etc). Lack of meteorological data limits our capability to correlate the observed isotopic variability with variables such as temperature, atmospheric pressure, wind direction, relative humidity etc.

Knowledge of wind pattern combined with the isotopic composition of meteoric water samples (deuterium excess) would make it easier, for example, to determine the possible source of evaporation. This way, explaining with arguments about whether the air mass originates from the east (dry and cold air masses) or the west (wet and warm air masses) would be easier and more accurate.

Data referring to atmospheric pressure could be directly related with the observed

natural isotopic behavior of the various weather fronts (i.e. days 238-240, Figure 5.4). Temperature is always one of the most important meteorological variables, informing us about the prevailing weather conditions and of course directly correlated with isotopic variability, in both vapor and precipitation. Furthermore, it should be mentioned that spectrometers measure absolute humidity in the atmosphere and not relative humidity; the latter, along with the constant, k (see equation 2.13), which depends on the location where evaporation takes place is essential if we want to calculate the kinetic fractionation factor.

References

- [1] R.K. Pachauri [Core Writing Team and L.A. Meyer (eds.)]. Ipcc, 2014: Climate change 2014: Synthesis report. contribution of working groups i, ii and iii to the fifth assessment report of the intergovernmental panel on climate change. Technical report, IPCC, Geneva, Switzerland, 151 pp., 2014.
- [2] H. Craig. Isotopic variations in meteoric waters. *Science*, Vol. 133, No. 3465, pages 1702–1703, 1961.
- [3] K. M. Cuffey and W.S.B. Paterson. *The Physics of Glaciers (4th edition)*. Elsevier, 2010.
- [4] W DANSGAARD. Stable isotopes in precipitation. *TELLUS*, 16(4):436–468, 1964.
- [5] Sir Fisher, Ronald Aylmer. *Statistical methods for research workres*. New York : Harper, 13th ed., rev edition, 1958.
- [6] V. Gkinis, T. J. Popp, T. Blunier, M. Bigler, S. Schuepbach, E. Kettner, and S. J. Johnsen. Water isotopic ratios from a continuously melted ice core sample. *Atmospheric Measurement Techniques*, 4(11):2531–2542, 2011.
- [7] Vasileios Gkinis, Trevor J. Popp, Sigfus J. Johnsen, and Thomas Blunier. A continuous stream flash evaporator for the calibration of an ir cavity ring-down spectrometer for the isotopic analysis of water. *Isotopes In Environmental and Health Studies*, 46(4):PII 930869087, 2010.
- [8] M. Groening, H. O. Lutz, Z. Roller-Lutz, M. Kralik, L. Gourcy, and L. Poeltenstein. A simple rain collector preventing water re-evaporation dedicated for delta o-18 and delta h-2 analysis of cumulative precipitation samples. *Journal of Hydrology*, 448:195–200, July 2012.
- [9] J. HORITA and D. J. WESOLOWSKI. Liquid-vapor fractionation of oxygen and hydrogen isotopes of water from the freezing to the critical-temperature. *Geochimica Et Cosmochimica Acta*, 58(16):3425–3437, August 1994.
- [10] J. JOUZEL and L. MERLIVAT. Deuterium and o-18 in precipitation - modeling of the isotopic effects during snow formation. *Journal of Geophysical Research-atmospheres*, 89(ND7):1749–1757, 1984.
- [11] Maurice G. (Maurice George) Kendall, 1922 Stuart, Alan, and 1942 Ord, J. K. (John Keith). *The advanced theory of statistics*. London : C. Griffin, 4th ed

- edition, 1977.
- [12] L. MERLIVAT and G. NIEF. Fractionnement isotopique lors des changements de état solide-vapeur et liquide-vapeur de leau a des temperatures inferieures a 0 degrees c. *Tellus*, 19(1):122–&, 1967.
- [13] W. G. Mook. *Environmental Isotopes In The Hydrological Cycle - Principles and Applications vol.1,2*. International Atomic Energy Agency, 2000.
- [14] Teukolsky S.A. Press, W.H., W.T. Vetterling, and B.P. Flannery. *Numerical Recipes in C*. Cambridge University Press, 2nd ed. edition, 1992.
- [15] V. Salamalikis, A. A. Argiriou, and E. Dotsika. Stable isotopic composition of atmospheric water vapor in patras, greece: A concentration weighted trajectory approach. *Atmospheric Research*, 152:93–104, January 2015.
- [16] Markus Schmidt, Kadmiel Maseyk, Celine Lett, Philippe Biron, Patricia Richard, Thierry Bariac, and Ulli Seibt. Concentration effects on laser-based del o-18 and del h-2 measurements and implications for the calibration of vapour measurements with liquid standards. *Rapid Communications In Mass Spectrometry*, 24(24):3553–3561, December 2010.
- [17] M. Wozniak and J Dera. *Light Absorption in Sea Water*. Springer New York, 2007.

Appendices



A.0.1 Dates of collected meteoric water samples

Table A.1: Dates referring to sampling of precipitation.

Number of sample	Date	Form of precipitation
01	04/08/2015	Rain
02	11/08/2015	Rain
03	24/08/2015	Rain
04	25/08/2015 (morning)	Rain
05	25/08/2015 (afternoon)	Rain
06	27/08/2015	Rain
07	28/08/2015	Rain
08	31/08/2015	Rain
09	04/09/2015	Rain
10	14/10/2015	Rain
11	10/11/2015	Rain
12	11/11/2015	Rain
13	12/11/2015	Rain
14	13/11/2015	Rain
15	17/11/2015 (morning)	Rain
16	17/11/2015 (afternoon)	Rain
17	18/11/2015	Rain
18	19/11/2015	Rain
19	20/11/2015	Rain
20	22/11/2015	Rain
21	23/11/2015	Snow
22	24/11/2015	Snow
23	25/11/2015	Snow
24	11/12/2015	Rain
25	07/01/2016	Snow
26	13/01/2016	Snow
27	25/01/2016	Rain

A.0.2 Full data series acquired from Odo

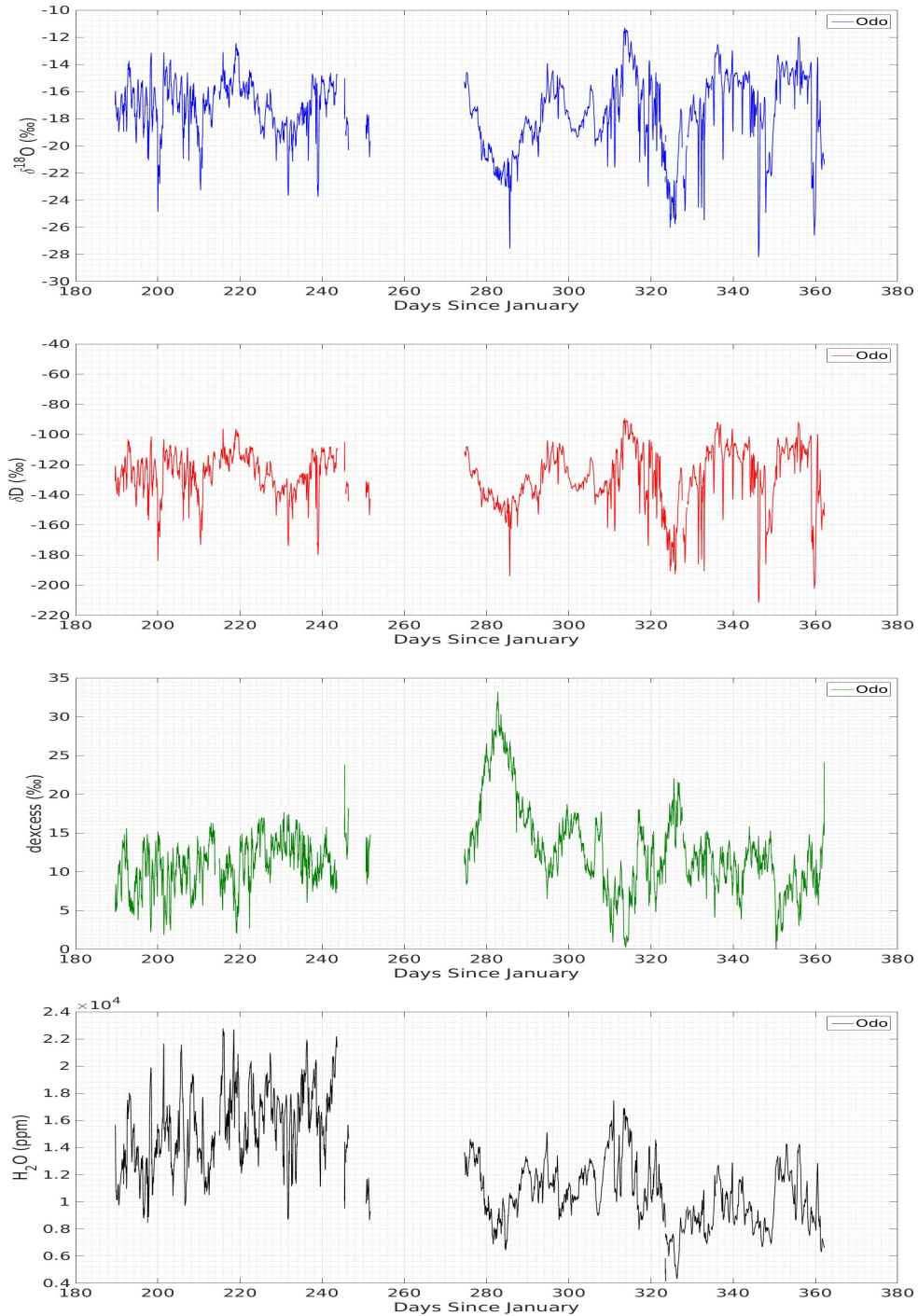


Figure A.1: Full data series acquired from Odo, covering the period 10 July-end of December, 2015. From top to bottom subplots: $\delta^{18}\text{O}$, δD , dexcess and humidity concentration in the atmosphere.